Anomalies within Magnetic Holography

Dissertation

zur Erlangung des akademischen Grades
doctor rerum naturalium (Dr. rer. nat.)

seit 1558

vorgelegt dem Rat der Physikalisch-Astronomischen Fakultät der Friedrich-Schiller-Universität Jena

von M. Sc. Julian Leiber
geboren am 08.09.1989 in Schweinfurt

Gutachter

1. Jun. Prof. Dr. Martin Ammon
   Friedrich-Schiller-Universität Jena
   Theoretisch-Physikalisches-Institut

2. Prof. Dr. Johanna Erdmenger
   Julius-Maximillians-Universität Würzburg
   Institut für Theoretische Physik und Astrophysik Universität Würzburg

3. Prof. Dr. Karl Landsteiner
   Universidad Autónoma de Madrid
   Instituto de Física Teórica

Datum der Disputation: 25.10.2017

Zusammenfassung

Im Rahmen der Dualität zwischen Eich- und Gravitationstheorien untersuchen wir vierdimensionale konforme Feldtheorien mit chiraler Anomalie. Diese Theorien sind dual zu Einstein-Maxwell-Chern-Simons Theorien in fünf dimensionalen Raumzeiten mit negativer kosmologischer Konstante.

Im ersten Teil dieser Dissertation berechnen wir Quasinormal-Moden (QNM) von Metrik- und Eichfeldpertubationen auf dem Hintergrund eines elektrisch und magnetisch geladenen schwarzen Loches. Im Rahmen der „Eichtheorie/Gravitations"-Korrespondenz ist diese Theorie dual zu einer bestimmten Klasse von Feldtheorien mit chiraler Anomalie, welche sich im Zustand eines geladenen Plasma mit externen Magnetfeld B befinden. Diese QNM sind dual zu den Polen der Zwei-Punkt Funktionen des Energie-Impuls-Tensors und des axialen Stromes und enthalten Information über Dissipation und Transport im Plasma. Ergänzend zur Gravitationsrechnung entwickeln wir die hydrodynamische Beschreibung der dualen Feldtheorie mit chiraler Anomalie und konstantem externen Magnetfeld B. Wir finden QNM die ein Verhalten ähnlich zu Landau-Leveln zeigen, nämlich für großes B langlebig werden, vorausgesetzt die Stärke der Anomalie überschreitet einen kritischen Wert. Wir untersuchen chiralen Transport jenseits des hydrodynamischen Limes für die fünf (ehemaligen) hydrodynamischen Moden, eingeschlossen eine chirale magnetische Welle.

Im zweiten Teil betrachten wir das Phasendiagram bei endlicher Temperatur, chemischen Potential und Magnetfeld. Bei hohen Temperaturen ist die Lösung durch das elektrisch und magnetisch geladene AdS Reissner-Nordstroem schwarze Loch gegeben, welche wir im ersten Teil der Dissertation untersucht haben. Für hinreichend große Chern-Simons Kopplung, hinreichend tiefen Temperaturen und kleinen Magnetfeldern finden wir eine neue Phase mit Helixstruktur, welche Translationsinvarianz spontan bricht. Für den Wert der Chern-Simons Kopplung in dieser Dissertation ist der Phasenübergang von zweiter Ordnung. Die kritischen Exponenten stimmen mit „mean field" Exponenten überein. Da die Entropiedichte im Limes niedriger Temperaturen verschwindet sind wir überzeugt, dass es sich um den wahren Grundzustand handelt. Dies ist die holographische Version der „chiralen magnetischen Spirale".

Abstract

Within gauge/gravity duality, we study the class of four dimensional CFTs with chiral anomaly described by Einstein-Maxwell-Chern-Simons theory in five dimensions.

In the first part of this thesis we compute quasinormal modes (QNMs) of the metric and gauge field perturbations about electrically and magnetically charged black branes. By the gauge/gravity correspondence, this theory is dual to a particular class of field theories with a chiral anomaly, in a thermal charged plasma state subjected to a constant external magnetic field B. The QNMs are dual to the poles of the two-point functions of the energy-momentum tensor and axial current operators, and they encode information about the dissipation and transport of charges in the plasma. Complementary to the gravity calculation, we work out the hydrodynamic description of the dual field theory in the presence of a chiral anomaly, and a constant external B. We find QNMs exhibiting Landau level behavior, which become long-lived at large B if the anomaly coefficient exceeds a critical magnitude. Chiral transport is analyzed beyond the hydrodynamic approximation for the five (formerly) hydrodynamic modes, including a chiral magnetic wave.

In the second part we consider the phase diagram at finite temperature T, chemical potential μ and magnetic field B. At high temperatures the solution is given by the electrically and magnetically charged AdS Reissner-Nordstroem black brane, studied in first part of this thesis. For sufficiently large Chern-Simons coupling and at sufficiently low temperatures and small magnetic fields, we find a new phase with helical order, breaking translational invariance spontaneously. For the Chern-Simons couplings studied, the phase transition is second order with mean field exponents. Since the entropy density vanishes in the limit of zero temperature we are confident that this is the true ground state which is the holographic version of a chiral magnetic spiral.

Table of Contents

1. Introduction

Over the last century physicists have made great progress in understanding nature's basic principles. More and more sophisticated theories have been developed and tested to great precision. However, nearly all areas of physics still face unresolved puzzles. Quite often such problems are highly technical and the describing theory it is not amenable for non-experts, for example quantum field theory (QFT).

Black holes play a very important counterexample. The theoretical description of black holes by Einstein's general relativity still requires a profound mathematical background, yet the concept of black holes itself is surprisingly simple. The astrophysicists Chandrasekhar once said about black holes: "The black holes are the most perfect macroscopic objects there are in the universe."

Let us perform an intriguing gedanken-experiment: What if we throw a box into a black hole? Naively we would expect that the black hole grows proportional to the volume of this box. But this proves to be false. A black hole does not simply absorb the box, but rather stores the information on its horizon area, like an optical hologram stores a three dimensional image on a two dimensional photographic plate. This holographic principle questions our very basic interpretation of space and time itself.

Within the theoretical framework of string theory a concrete example of such a holographic description was found, the renowned anti-de Sitter/conformal field theory (AdS/CFT) duality. One of its amazing statements is that certain classical gravity theories are equivalent to certain quantum theories, namely conformal quantum field theories (CFT), living on the boundary of the spacetime. This implies that the CFT is defined in one dimension less than the gravity theory.[1] At first glance this seems very odd, since the realm of classical physics and the realm of quantum physics are rather different.

Despite the fact that the AdS/CFT duality is not proven yet, many non-trivial tests have been performed successfully and a wide area of research has developed.

[1] Note that this is the weak form of the duality. In its strong form it states a duality between $\mathcal{N} = 4$ Super Yang-Mills theory at any rank and any coupling on the one side and quantum string theory on the other side.

This novel idea of holography rendered progress in many areas of physics and even offers new insights into quantum field theory itself. It allows us to explore parts of quantum field theory, which could not be tackled previously. Additionally, it provides a new approach to strongly coupled systems. Remarkably it may also hint how to solve the long-standing problem of quantizing gravity and understanding spacetime at its smallest scales. In this thesis we utilize the AdS/CFT duality to tackle problems in QFT, which are related to anomalies, i.e. symmetries which are present on classical level but broken by quantization and renormalization.

1.1. Symmetries in physics and anomalies

Symmetries play a great role in theoretical physics and are one of the most fundamental concepts. The mathematical concept of symmetries are the foundation of modern theoretical physics. In physics, a symmetry describes the feature of a system to stay unchanged under certain transformation, e.g. a sphere stays unchanged under rotations. In mathematical terms, symmetries act on the configuration space and lead to identical physics. These transformations may be continuous, as the aforementioned rotations, or discrete, e.g. reflections.

The importance of symmetries is strongly tied to the very famous Noether theorem. The Noether theorem states that to every continuous symmetry, there corresponds a constant of motion. Translational symmetry, for example, implies conservation of momentum. Technically speaking each continuous symmetry even gives a local conservation law for a conserved current.

Incorporating these conserved quantities greatly helps to simplify the problem of solving the equations of motion on the one hand. On the other hand symmetries guide to write down a proper theoretical description based on symmetry arguments.

Let us give a historical example: Trying to solve the Schroedinger equation for the hydrogen atom straightforwardly in cartesian coordinates is a very intricate problem. The spherical symmetry of the hydrogen atom tells us to write down the problem rather in spherical coordinates. This gives a way more feasible problem that can be solved in a basic quantum mechanics course.

Beyond that, it is even possible to get the energy levels of the hydrogen atom without knowing the equations of motion just based on symmetry considerations. The hydrogen atom possesses an additional conserved quantity, the Laplace-Runge-Lenz (LRL) vector. In 1926 Wolfgang Pauli predicted the energy levels using the LRL vector without knowing the Schroedinger equation [1].

Over time the concept of symmetries has been further developed in physics. The approximate isospin symmetry helped to classify the zoo of mesonic particles in representations of their symmetry groups. The concept of approximate symmetries was then extended to include corrections to these approximate symmetries. This takes into account the small breaking of the symmetry and allowed to calculate e.g. branching ratios of meson decays. The charge (C), parity (P) and time reversal (T) symmetries in the CPT theorem played a crucial role to develop the interpretation of particles and antiparticles.

Later the theoretical description of symmetry transformations has been extended to allow for local transformations, which are the vital ingredient for the description of interactions by gauge symmetries. The novel idea was to allow for a different transformation at every point in spacetime, in contrast to the former considered global symmetries. These gauge transformation describe interactions via the exchange of gauge bosons, for example the local $U(1)$ symmetry describing electromagnetic interactions by the exchange of photons. Note that gauge symmetries are not symmetries in the conventional physical sense but rather redundancies in our mathematical description.

The Standard Model of particle physics describes the three fundamental forces, strong, weak and electromagnetic force, based on gauge symmetries and classifies the elementary particles according to their symmetry properties. It is the most successful theory in physics up to now and passed dozens of high precision test, for example at particle colliders like the LHC.

The recent discovery of the Higgs boson is another milestone in the utilization of symmetries. The generation of mass and the existence of the Higgs boson is described by a spontaneous breaking of a gauge symmetry in the Standard Model.[2] Yet there are still open problems in the Standard Model. One of the biggest attempts to evolve the Standard Model is based on symmetry considerations, the so called Supersymmetry.

Apart from particle physics and phenomenology symmetries play a crucial role in the description of gravity, where the Einstein equations manifest the symmetry of diffeomorphisms. These diffeomorphisms in gravity describe the freedom to choose a coordinate system, in our case described by a metric for the spacetime.

[2] Technically speaking it is not possible to break a gauge symmetry. Only the global part of the gauge symmetry gets broken [2].

Anomalies

So far we have seen that symmetries play a crucial role in our current description and understanding of physics. Rather unexpectedly physicists found that it is possible to break a classical symmetry when quantizing the theory. A symmetry of the classical action may not be present in the full quantum theory, called anomaly. Technically speaking, the Lagrangian is invariant under symmetry transformations, but the measure of the path integral is not.

In the case of an anomalous global symmetry, anomalies do not indicate any inconsistency of the theory, but quite often have interesting physical consequences. This was first discovered in the anomaly of the axial current, which is important for the description of the pion decay $\pi^0 \to \gamma\gamma$. Let us outline the role of anomalies for the pion decay: Pions can be seen as Nambu-Goldstone bosons of the spontaneous symmetry breaking of the chiral symmetry of QCD $SU(2)_L \times SU(2)_R$. This implies that the relevant $\pi\gamma\gamma$ coupling is a correction to this symmetry and hence is suppressed by powers of m_π^2/m_n^2 with m_n the nucleon mass. This is in contrast to the experimental observation, namely that the Pion decay is not suppressed. Consequently something must be "anomalous" with this symmetry. In 1969 Adler [3], Bell and Jackiw [4] realised that the symmetry, suppressing the decay, is anomalous due to quantum effects such that the suppression mechanism does not take place. They found a violation of the chiral symmetry on the quantum level in the presence of electromagnetism. On the contrary, anomalies in gauge symmetries indicate fundamental inconsistency as the theory is not unitary any more.

We will outline this mechanism in the theory sec. 2.1, where we discuss further technical details regarding anomalies. In general we are concerned with different effects of chiral anomalies in strongly coupled systems in this thesis.

1.2. Anomaly induced effects

Ever since the discovery of anomalies, many anomaly induced effects have been found in very different areas in physics. We already briefly discussed the Pion decay as a microscopic effect of anomalies. On the contrary, we have macroscopic effects, e.g. changes in transport properties and instabilities induced by anomalies. This is a very intriguing case since we are able to directly observe the quantum effect of violation of symmetries by anomalies in macroscopic physics.

Many of these phenomena are observed in strongly coupled system. But studying anomalies in strongly coupled systems inherently poses a problem since most of our

current approaches are based on weak coupling expansions. Furthermore many of the macroscopic anomaly induced effects, e.g. anomalous transport, only show up at finite density (chemical potential), finite temperature and non-vanishing magnetic field[3] where most of the strong coupling methods fail to give reliable results. Apart from that we need to be able to describe real time physics posing additional problems for many methods.

But such systems are widely found, e.g. in condensed matter experiments. Besides condensed matter physics, strongly coupled systems at finite temperature and chemical potential also appear in heavy ion collisions (HIC), e.g. lead–lead at CERN. In such a collision process a strongly coupled plasma with possibly strong magnetic field emerges. Particularly in this context we are concerned with the influence of anomalies on transport properties.

In the following we introduce anomalous transport, the emergence of quantum critical points (QCP) and novel spatially modulated phases in the presence of anomalies.

1.2.1. Transport and hydrodynamics

The presence of anomalies can in principle have an great affect on many properties of a system. This includes equilibrium physics as well as dynamical properties. In the following two subsections we consider the phase diagram of theories with anomalies. Here we discuss the dynamical properties around a given thermodynamic equilibrium state.

Full nonlinear time-dependent dynamics are a very intricate problem. But quite often studying the full dynamics is not only cumbersome but also hard to analyse. Often, a much clearer framework is given by studying small fluctuations around a fixed equilibrium state. Correspondingly we study long lived, long wavelength fluctuations of small energy. The response of the system to these fluctuations and the equilibration by dissipation is given by hydrodynamics. Hydrodynamics describes the coarse grained system as a fluid close to thermal equilibrium and, as an effective theory, does not require knowledge about the microscopic theory. Intriguingly it has been found that anomalies significantly modify hydrodynamics. The holographic framework played a great role in the recent development of anomalous hydrodynamics [5–7]. The special property of anomalous transport is, that it can happen without dissipation.[4]

[3] Being precise, to connect to experiments we mainly consider 1-point functions. This requires external fields for the anomaly to show up.

[4] The transport coefficients are P-odd/T-even in contrast to “usual” dissipative coefficients [7, 8]

Let us discuss one example, namely the interplay of anomalies with a magnetic field at strong coupling. The presence of an external (background) magnetic field $\vec{B}$, for example, can cause an electric current $\vec{J}$ along the magnetic field; the so called chiral magnetic effect (CME) $\vec{J} = \sigma_5 \vec{B}$. The intuitive reasoning is illustrated in fig. 1.1 and can be explained as follows:

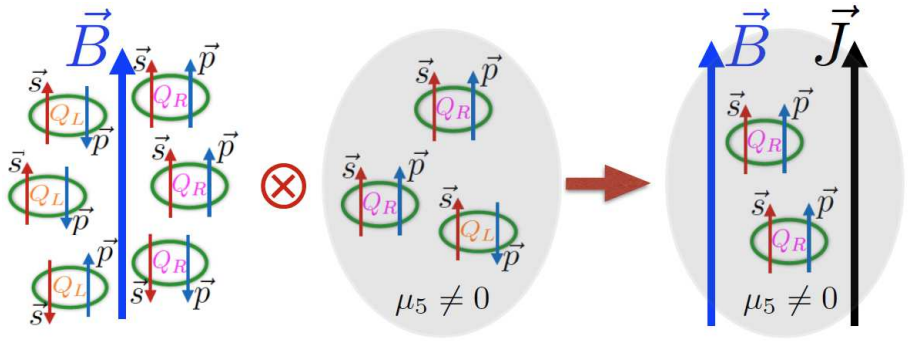

Fig. 1.1.: Explanation of the CME: The magnetic field aligns the spins parallel to the magnetic field such that right handed particles have their momentum in direction of the magnetic field while left handed particles in the opposite direction (left panel). We then put the system at a chirality imbalance $\mu_5 \neq 0$, such that we have more right handed particles (middle panel). Hence the overall momentum of left and right handed particles does not balance any more and results in a net current along the magnetic field $\vec{J} = \sigma_5 \vec{B}$. Figure taken from [9].

First the magnetic field aligns the spins parallel/anti-parallel to the magnetic field. Thus right handed particles will have their momentum aligned parallel to the magnetic field, while left handed particles will have momentum in the opposite direction. For a finite chirality imbalance there are more particles of one species, either right or left handed. The overall momentum thus does not balance and results in a net movement along the magnetic field, the induced current.

In addition, anomalies induce novel collective excitation within hydrodynamics, e.g. the chiral magnetic wave. The chiral magnetic wave consist of an alternating fluctuation between vector and axial density "caused" by the CME and the chiral separation effect (CSE). Experiments with Weyl semimetals report the observation of such chiral transport effects in presence of magnetic fields, namely an anomalous magneto-resistivity [10–14].

1.2.2. Quantum critical behaviour

So far we have considered dynamical effects of anomalies. But the presence of an anomaly can also change the thermodynamic properties, e.g. the phase diagram. One example is given by the presence of a quantum critical point (QCP) in theories with a chiral anomaly. Quantum critical points have recently gathered a lot of attention, as they may be crucial for the understanding of a wide range of materials.

Within holography a QCP was found for theories with anomalies, as we outline in sec. 1.3.2. This is a very interesting point, since there is no field theoretical model that relates anomalies and QCP up to now. Therefore let us briefly introduce the theory of QCP here, for an extensive introduction see [15].

In contrast to thermal phase transitions, driven by thermodynamic fluctuations, there also exist quantum phase transitions, which occur at zero temperature driven by quantum fluctuations. The corresponding critical point is called quantum critical point. Such a quantum phase transition can be accessed by varying the coupling constant g in experiments, which can be exotic, e.g. doping or magnetic field. The latter will be realised in this thesis.

Since we are at zero temperature, we have to consider the ground state properties for a quantum phase transition (QPT). Let us consider quantum mechanics example, namely a Hamiltonian $H(g)$, that depends on a dimensionless coupling g. Generically the ground state energy is a smooth function of g. One counterexample is the case $H(g) = H_0 + g\,H_1$, where $[H_0, H_1] = 0$ commute. In this case H_0 and H_1 can be simultaneously diagonalized and hence the eigenfunctions do not depend on g. But the eigenvalues vary with g. We now tune the H_0 and H_1 in such a way, that the lowest level and the first excited level cross at some g_c. In this case the ground state energy changes non-analytically, see fig. 1.2. For infinite systems an

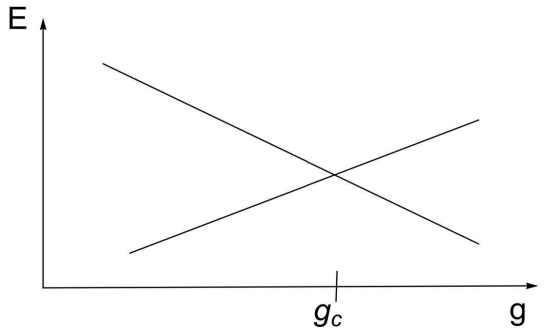

Fig. 1.2.: Level-crossing at a Quantum critical point. The lowest and next to lowest level cross when varying the coupling g at some g_c resulting in a quantum phase transition.

avoided level crossing can also result in a non-analytical behaviour of the ground state energy. We identify the point of non-analyticity in the ground state energy as a quantum phase transition. This is usually accompanied by qualitative changes of correlations, e.g. a change in the resistivities.

As zero temperature is not realisable in experiment, the quantum critical point itself cannot be tested. But the presence of the quantum critical point has great influence on the finite temperature behaviour, the so called quantum critical region, where quantum fluctuations still dominate the finite temperature physics. This is illustrated by the yellow region in fig. 1.3.

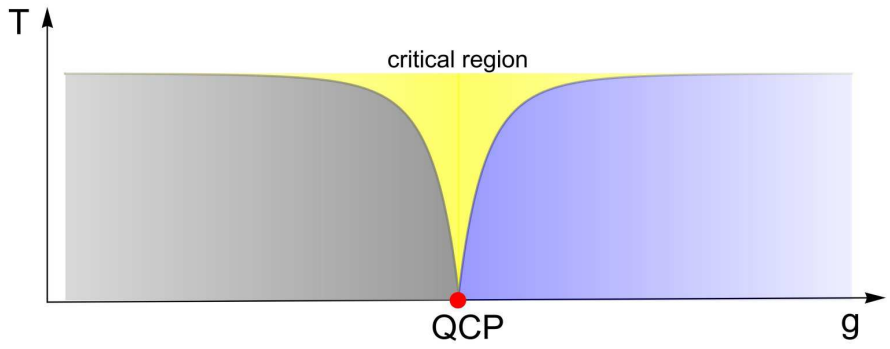

Fig. 1.3.: Example of a phase diagram with a quantum critical point. By varying the coupling g, the system undergoes a phase transition at zero temperature. At finite temperature there are crossovers from the quantum critical region (yellow) to the other regions (blue and grey). In the quantum critical region (yellow) the presence of the QCP (red) still dominates the physics even at finite temperature.

For example metamagnetic materials, e.g. $Sr_3Ru_2O_7$ [16], undergo such a quantum phase transition when varying the external magnetic field. $Sr_3Ru_2O_7$ is a material with layered structure. For large magnetic fields (8 Tesla) perpendicular to the layers a line of first order phase transitions ends in a finite temperature critical point. With a magnetic field in plane of the layers the critical point can be brought to zero temperature.

1.2.3. Spatially modulated phases

We have already seen that anomalies change the physical properties of a system near equilibrium. It is reasonable to assume that these fluctuations might become unstable in certain regions of the phase diagram and lead to new phases, that are

for example spatially modulated. Within field theory it was found that the chiral anomaly can induce spatial modulation, e.g. a spiral dependence [17].[5]

In condensed matter systems a variety of phases, which are spatially modulated appear. These phases spontaneously break translational invariance. This spatial dependence can be very different, such as helical order, striped order or checker-board order. The helical phase considered in this thesis still has a Bianchi VII_0 symmetry [20][6], while for striped order spatial invariance is broken in one direction and for checker-boards in two dimensions respectively, see fig. 1.4. Helical structures for example appear in chiral nematic liquid crystals, where the molecules twist along the direction of the helix, illustrated on the left panel of fig. 1.4.

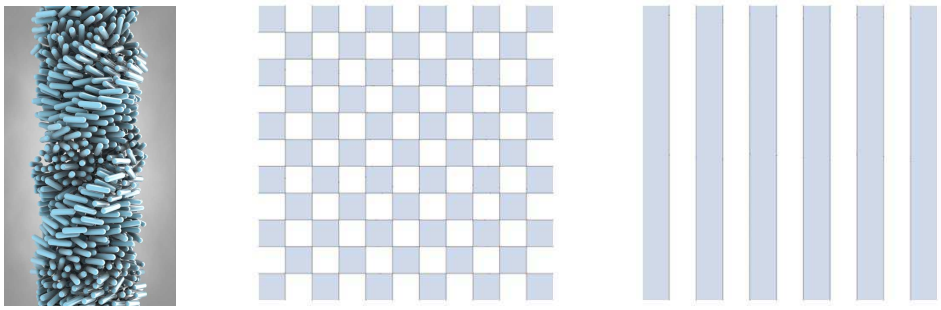

Fig. 1.4.: Illustration of different spatially modulated dependences. On the left we show a helical modulation of a chiral nematic liquid crystal, taken from [21]. The middle panel shows spatial invariance broken in two directions resulting in a checker-board dependence. The right panel shows the case where the spatial invariance is only broken in one direction, giving a striped order.

In experiments with very pure samples of $Sr_3Ru_2O_7$ such a new phase emerges in the low temperature limit. This phase is believed to be a spatially anisotropic nematic phase [22]. Intriguingly the QCP of $Sr_3Ru_2O_7$ is hidden behind this nematic phase, which avoids the problem of finite entropy approaching zero temperature close to the QCP, which we observe also in our holographic model, see sec. 4.4.

1.3. AdS/CFT and anomalies

One of the amazing developments emerging from the research in string theory is the idea of a gauge/gravity duality [23]. Remarkably, the duality relates the strongly coupled regime of gauge theories to the weakly coupled regime of the dual

[5]For other work on holographic chiral spirals see [18, 19].
[6]The helical structure associated with the Bianchi VII_0 symmetry is displayed in fig.4.1.

(super)gravity. Consequently, it has become a powerful tool to study strongly interacting systems by using a dual weakly coupled gravitational theory. At present, holographic descriptions of non-perturbative phenomena include, among other applications, condensed matter physics, high energy physics and quark-gluon plasma. For textbooks see [24–26], for reviews see [27–31]. For example, in the context of condensed matter physics, s-wave [32] and p-wave [33–36] superconductors were studied, as well as Non-Fermi liquids [37, 38], the Kondo effect [39–42], topological insulators [43–45] and Quantum Hall transitions [46].

Using the framework of AdS/CFT it is possible to study strongly coupled conformal field theories at finite temperature and finite charge density. Besides, it is possible to include anomalies within AdS/CFT, where the anomaly on the CFT side corresponds to adding a Chern-Simons action for the gauge field[7] on the gravity side [47], see ch. 2.3.5. These Chern-Simons terms arise naturally in consistent truncation of string theory, see ch. 2.3.6. Indeed plenty of phenomena induced by anomalies have been found in holographic models, such as chiral transport, QCP and spatially modulated phases as we present now.

1.3.1. Transport and quasinormal modes

Within holography information about transport and dissipation of the CFT is encoded in quasinormal modes (QNMs) of the dual gravitational theory [48]. The relation arises as follows: The transport properties can be obtained by studying retarded Greens functions in linear response theory in QFT. The location of the poles of these retarded correlators in the dual field theory correspond to QNM frequencies [49]. Numerous studies have shown that QNMs play an important role in the evolution dynamics of strongly interacting non-equilibrium systems, particularly in the relaxation process [50–55].

In gravity QNMs are small fluctuations around a fixed background, e.g. a black hole. These fluctuations can be gravitational fluctuations, i.e. perturbations of the metric, and electromagnetic fluctuations, i.e. perturbations of the gauge field. Over time these fluctuations may fall into the black hole horizon and equilibrate.

Mathematically, QNM frequencies are (quasi)eigenvalues of the linearised Einstein equations describing fluctuations on a fixed background. Since the operator corresponding to the eigenvalue problem is not self-adjoint, the QNM frequencies are in general complex-valued and therefore called “quasi”-normal modes. In contrast to

[7] The Chern-Simons term corresponds to effects of anomalies induced by the presence of external fields.

real-valued normal modes, complex QNMs implicate dissipation.

For correlators of conserved quantities such as the energy-momentum tensor, the QNM spectrum typically contains an infinite tower of gapped modes that are strongly damped, as well as a set of hydrodynamic modes $\omega = \omega(k)$ such that $\omega(k) \to 0$ as $k \to 0$ [48, 56].

We are interested in the transport properties in the presence of a chiral anomaly [7], see ch. 3. In that vein, a host of papers explored the interplay between external magnetic fields and a chiral anomaly within holographic models of Weyl semimetals [57–61]. Weyl semimetals are an exciting class of material which show exotic electronic properties that mimic Weyl fermions, see e.g. [62] for an introduction.

1.3.2. Quantum critical points in AdS/CFT

A Quantum critical point within holography was discovered in a series of papers [63, 64]. Let us summarise the main results here. The coupling varied in the model is given by an external magnetic field B; a sketch of the phase diagram obtained within holography is shown in fig. 1.5. Note that fig. 1.5 nicely resembles fig. 1.3. At a critical magnetic field B_c a continuous phase transition occurs. Note that there is no change of symmetry, the QCP is determined through thermodynamic quantities.

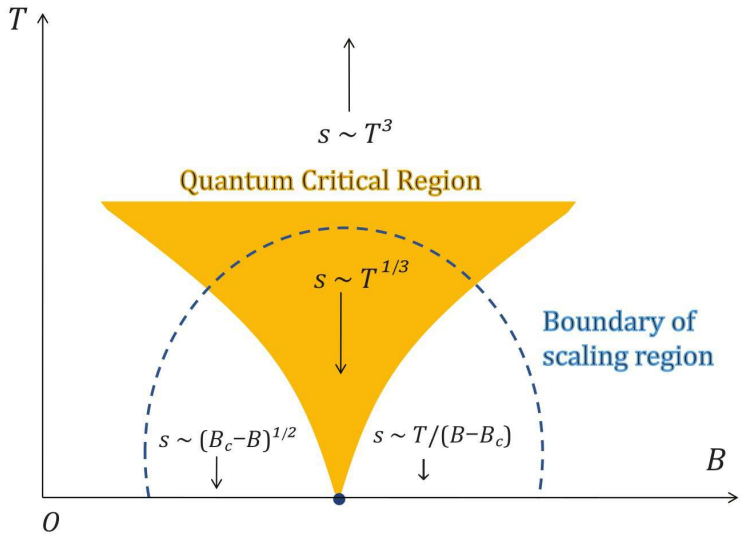

Fig. 1.5.: Sketch of a Phase diagram with a QCP obtained with holography with varying the magnetic field B, taken from [65]. The different scaling regions of the entropy density s indicate two different low Temperature phases separated by a QCP at zero Temperature and a Quantum Critical Region (yellow). For high temperatures the systems shows a universal scaling.

For low temperatures T a Quantum Critical Region emerges (yellow), where the entropy scales with $T^{1/3}$. For high temperatures the entropy scaling changes to its universal T^3 scaling, bounding the Quantum Critical Region. For $B > B_c$ the entropy density s goes linear with the temperature reflecting a Fermi liquid phase. Approaching the critical point from this region the entropy density diverges as $1/(B - B_c)$, indicating a breakdown of Fermi liquid theory. For low magnetic fields $B < B_c$ the entropy is constant, in conflict with the laws of thermodynamics $s \to 0$ with $T \to 0$. We discuss how this problem is solved by the emergence of a spatially modulated phase in ch. 4. We study this system with a QCP in this thesis, particularly we consider transport and the low temperature instability towards a helical phase.

1.3.3. Spatially modulated phases in AdS/CFT

Within holography a spatially modulated phase with helical symmetry at vanishing magnetic field was found in [66]. For sufficiently large Chern-Simons-coupling[8] and finite density the AdS-Reissner-Nordstroem (RN) black brane becomes unstable at low temperatures towards a helical charged black brane. Striped phases have been constructed in a holographic setup in [67] and checkerboards in [68]. Spatially modulated phases in the presence of magnetic fields were also discussed in [69–80].

We generalize this spatially modulated phase with helical symmetry to finite magnetic field in ch. 4. There we study thermal equilibrium states for finite temperature, chemical potential and magnetic field and determine the phase diagram. Depending on the coefficient of the chiral anomaly we find a spatially modulated phase extending the results of [66] to non-zero magnetic fields. In particular, the quantum critical point [63, 64] is hidden within this new phase. In addition the new phase has vanishing entropy at zero temperature, solving the entropy problem of the charged magnetic branes.

1.4. Outline

In this thesis we study both transport properties and the helical instability of the electrically and magnetically charged charged AdS Reissner-Nordstroem black branes. Using the gauge /gravity duality we translate our results to hydrodynamic properties and helically modulated phases of CFTs with a chiral anomaly at finite

[8] The Chern-Simons-coupling corresponds to the anomaly coefficient in the QFT.

charge, magnetic field and temperature. This thesis is based on and heavily draws from [81, 82].

The thesis is structured as follows: First we give a brief introduction to the String theory foundations, e.g. AdS/CFT and illustrate the methods later used, see ch. 2. At this point we also discuss the AdS-RN black brane. We then extend this setup to finite magnetic field and charge density, the charged magnetic brane solution in ch. 3 and study its thermodynamical and hydrodynamical properties using QNMs. Complementary we work out the field theory hydrodynamic description and compare to our gravitational results. Finally we study the helical instability in ch. 4 and the thermodynamic properties of this new phase. The numerics used in this thesis are presented in app. A.

2. Theoretical basics

Within this chapter we work out the theoretical foundations and basic concepts used in this thesis. We start with anomalies and hydrodynamics, thereafter we cover the string theory basics and develop the AdS/CFT tools. We use these to construct the holographic model used in this thesis. In the end we discuss the relevant black hole physics.

2.1. Anomalies and quantum field theory

We have already considered different aspects of anomalies in ch. 1. This section covers the theoretical basics of anomalies. We present the relation of anomalies to regularization and derive the relevant conservation equations for hydrodynamics in the presence of anomalies.

2.1.1. Anomalies and regularization

Let us first consider a toy model of massless QED in two spacetime dimensions, which has an axial anomaly, and show how the anomaly arises.[1] First note that the existence of anomalies is strongly tied to chiral fermions, which do not exist in odd dimensions. We choose to work in two dimensions here to have a simpler structure of Gamma matrices.

The Lagrangian is given by a Maxwell term plus the fermionic term

$$\mathcal{L} = -\frac{1}{4e^2} F_{\mu\nu} F^{\mu\nu} + i\bar{\Psi}\gamma^\mu D_\mu \Psi \,, \tag{2.1}$$

where $\mu = 0, 1$. The gauge invariant derivative $D_\mu = \partial_\mu + i\, e A_\mu$ couples the gauge field with the fermions. We use two component Dirac-spinors

$$\Psi = \begin{pmatrix} \Psi_+ \\ \Psi_- \end{pmatrix} \,, \tag{2.2}$$

[1] We follow the steps of [83].

and choose the Gamma matrices such that

$$\gamma^0 = \begin{pmatrix} 0 & -i \\ i & 0 \end{pmatrix}, \quad \gamma^1 = \begin{pmatrix} 0 & i \\ i & 0 \end{pmatrix}, \quad \gamma^5 = \begin{pmatrix} 1 & 0 \\ 0 & -1 \end{pmatrix}. \tag{2.3}$$

Similar to four dimensions, we can define the projectors onto the chiral representations $\mathcal{P}_\pm = (1 \pm \gamma^5)/2$. On a classical level the theory is invariant under vector $\Psi \mapsto e^{i\alpha}\Psi$ and chiral $\Psi \mapsto e^{i\gamma_5\alpha}\Psi$ transformations. The Noether theorem thus gives us two conserved currents, a vector and an axial current

$$J^V_\mu = \bar{\Psi}\gamma_\mu\Psi\,, \qquad J^A_\mu = \bar{\Psi}\gamma_\mu\gamma_5\Psi\,. \tag{2.4}$$

Note that in two dimensions the currents are actually related by $J^{V\,\mu} = \epsilon^{\mu\nu}J^A_\nu$, where $\epsilon^{\mu\nu}$ is the total antisymmetric tensor in two dimensions with $\epsilon^{01} = 1$.

As the anomaly does not show up on tree level, we have to consider the one-loop correction to the vector current in the presence of a background gauge field a_μ,

$$\langle J^V_\mu(q)\rangle_a = \Pi_{\mu\nu}(q)a^\nu\,. \tag{2.5}$$

Following the standard Feynman rules, the one-loop vacuum polarisation $\Pi_{\mu\nu}(q)$ in momentum space is given by

$$\Pi^{\mu\nu}(q) = \left(q^2\eta^{\mu\nu} - q^\mu q^\nu\right)\Pi(q^2)\,, \qquad \Pi(q^2) = \frac{1}{\pi q^2}\,, \tag{2.6}$$

where we have to use a regularization that maintains gauge invariance, e.g. dimensional regularization. To detect the anomaly we compute the divergence of the current $\partial^\mu\langle J^A_\mu\rangle$ in momentum space. We use (2.6) and the relation between the currents to get

$$q^\mu\langle J^A_\mu\rangle = q_\mu\epsilon^{\mu\nu}\langle J^V_\nu\rangle = \frac{1}{\pi}q_\mu\epsilon^{\mu\nu}a_\nu\,. \tag{2.7}$$

Translating the result into position space and using $\epsilon^{\mu\nu}q_\mu a_\nu \to \epsilon^{\mu\nu}\partial_\mu a_\nu = \frac{1}{2}\epsilon^{\mu\nu}F_{\mu\nu}$ we finally compute the divergence to be

$$\partial^\mu\langle J^A_\mu\rangle = \frac{1}{2\pi}\epsilon^{\mu\nu}F_{\mu\nu}\,. \tag{2.8}$$

We clearly see, that the expectation value of the axial current is not conserved any more in the presence of a background gauge field $\partial^\mu\langle J^A_\mu\rangle \neq 0$.

We have chosen a specific regularization, and the question remains if we can remove the anomaly in any other regularization. Therefore let us now consider the

dependence on the regularization. In any regularization the vacuum polarization can be written as

$$\Pi_{\mu\nu}(q) = \left(F_1(q^2)\eta^{\mu\nu} - F_2(q^2)\frac{q^\mu q^\nu}{q^2} \right) , \tag{2.9}$$

due to Lorentz invariance. The divergences of the currents are then given by

$$q^\mu \langle J^A_\mu \rangle = F_1 \, \epsilon^{\mu\nu} q_\mu a_\nu \, , \quad q^\mu \langle J^V_\mu \rangle = -q^\mu a_\mu \, (F_1 - F_2) \, . \tag{2.10}$$

If we now choose a regulator such that the axial current is conserved, $F_1 = 0$, the vector current (2.10) is not conserved any more . But the vector current is associated with the $U(1)$ QED gauge group, which must not be anomalous. Hence we cannot remove the anomaly in the axial current.

2.1.2. Anomalies in 4d

Let us consider the triangle anomaly to outline further aspects of anomalies. For simplicity, the previous calculation was done in two dimensions. Now we extend the calculation to four dimensions. In QFT Ward identities are the quantum analogue of the classical Noether's theorem. In case of an anomalous symmetry the Ward identities may be modified, and for example read

$$\partial_\mu \langle J^\mu(x_1) J^\nu(x_2) \dots J^\rho(x_n) \rangle \neq 0 \, . \tag{2.11}$$

We are going to consider the three-point function for the following two reasons. First we derive the anomalous current from the three-point function. Second the three-point function is anomalous independent of external fields, whereas the anomaly in the one-point function only shows up for a state with external fields.

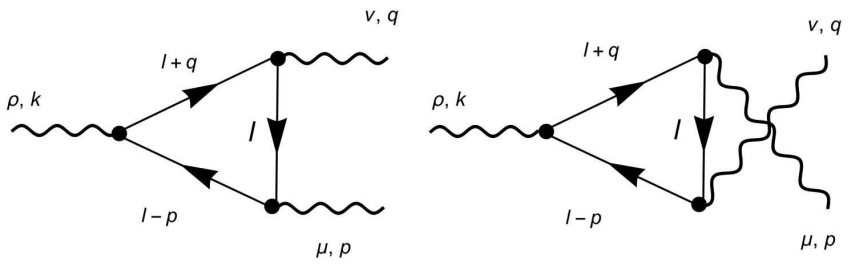

Fig. 2.1.: One loop Feynman diagramms with three external legs contributing to the three-point amplitude $V^{\mu\nu\rho}_{\pm}(p, q, k)$.

The Feynman diagrams contributing to the three-point amplitude $V_{\pm}^{\mu\nu\rho}(p,q,k)$ are depicted in fig. 2.1. The amplitude has three external legs with momenta p, q, k, while the internal momentum in the fermion loop is denoted by l.

Using standard Feynman rules for the sum of the two diagrams we get the following amplitude

$$iV_{\pm}^{\mu\nu\rho}(p,q,k) = \int \frac{d^4l}{(2\pi)^4} \left(\frac{\mathrm{tr}\left[(-\not{l}+\not{p})\gamma^\mu(-\not{l})\gamma^\nu(-\not{l}-\not{p})\gamma^\rho\mathcal{P}_\pm)\right]}{l^2(l-p)^2(l+q)^2} + (\mu\leftrightarrow\nu, p\leftrightarrow q)\right), \tag{2.12}$$

where $\mathcal{P}_\pm$ is the projection operator for the different parities. The trace of the gamma matrices is given by $\mathrm{tr}\left[\gamma^\mu\gamma^\nu\gamma^\rho\gamma^\sigma\gamma_5\right] = -4i\epsilon^{\mu\nu\rho\sigma}$.[2] To evaluate the conservation of the current we contract with one external momentum

$$k_\rho V^{\mu\nu\rho} = 2\int \frac{d^4l}{(2\pi)^4}\left[\frac{l_\alpha(l_\beta - p_\beta)}{l^2(l-p)^2} + \frac{l_\alpha(l_\beta+q_\beta)}{l^2(l+q)^2}\right]\epsilon^{\alpha\nu\beta\mu} + (\mu\leftrightarrow\nu, p\leftrightarrow q)\,. \tag{2.13}$$

Note that the single integrals are linearly divergent. In general we are allowed to shift the internal loop momentum $l \to l + c(p-q) + d(p+q)$ with c, d real numbers. However it turns out, that the finite value of the sum of the integrals depends on the choice of c

$$p_\mu V_{\pm}^{\mu\nu\rho} = \pm\frac{-i}{8\pi^2}(1-c)\epsilon^{\nu\rho\alpha\beta}q_\alpha k_\beta\,, \tag{2.14}$$

$$q_\nu V_{\pm}^{\mu\nu\rho} = \pm\frac{-i}{8\pi^2}(1-c)\epsilon^{\mu\rho\alpha\beta}k_\alpha p_\beta\,, \tag{2.15}$$

$$k_\rho V_{\pm}^{\mu\nu\rho} = \pm\frac{-i}{8\pi^2}2\,c\,\epsilon^{\mu\nu\alpha\beta}q_\alpha p_\beta\,. \tag{2.16}$$

To fix the value of c we have to impose an additional physical constraint on the three-point function. If we impose symmetry on the external legs, such that (2.14)-(2.16) are equal, the so-called consistent choice, we get $c = 1/3$.

To derive the anomalous current we contract the other two legs with external gauge fields $\partial_\mu\langle J_\pm^\mu\rangle = ik_\rho V_\pm^{\mu\nu\rho}A_\mu A_\nu$ and notice that in Fourier space $2\epsilon^{\mu\rho\alpha\beta}q_\alpha A_\rho = \epsilon^{\mu\rho\alpha\beta}F_{\alpha\rho}$. Taking into account the symmetry on the two external legs, we get an additional factor of $1/2$. Finally the result for the consistent chiral anomaly in four dimensions is given by

$$\partial_\mu\langle J_\pm^\mu\rangle = \pm\frac{1}{96\pi^2}\,\epsilon^{\mu\nu\rho\sigma}\,F_{\mu\nu}\,F_{\rho\sigma}\,. \tag{2.17}$$

[2] We choose $\epsilon^{\mu\nu\rho\sigma}$ to be the totally antisymmetric tensor of four dimensional Minkowski spacetime which we normalise such that $\epsilon^{0123} = 1$.

The vector and axial current are defined as $J^\mu = J^\mu_+ + J^\mu_-$ and $J^\mu_5 = J^\mu_+ - J^\mu_-$ and satisfy therefore

$$\partial_\mu \langle J^\mu_5 \rangle = \pm \frac{1}{48\pi^2} \epsilon^{\mu\nu\rho\sigma} F_{\mu\nu} F_{\rho\sigma} \,, \tag{2.18}$$

$$\partial_\mu \langle J^\mu \rangle = 0 \,. \tag{2.19}$$

This is the famous Adler-Bell-Jackiw (ABJ) anomaly [3, 4]. Note that the consistent current can be obtained as a functional derivative of a quantum action, but is not gauge invariant in presence of an anomaly.

If we choose to put the anomaly into a single leg $c = 1$, we get a current which couples covariantly to external gauge fields. This defines the so called covariant current, for an extensive introduction see [84]. The covariant anomaly is then given by

$$\partial_\mu \langle J^\mu_5 \rangle = -\frac{1}{16\pi^2} \epsilon^{\mu\nu\rho\sigma} F_{\mu\nu} F_{\rho\sigma} \,, \tag{2.20}$$

We like to study the effect of anomalies in the presence of external fields. Therefore let us take a closer look at (2.18):

$$\partial_\mu \langle J^\mu_5 \rangle = -\frac{1}{16\pi^2} \epsilon^{\mu\nu\rho\sigma} F_{\mu\nu} F_{\rho\sigma} \sim \vec{E} \cdot \vec{B} \,. \tag{2.21}$$

For the r.h.s. to be non-zero we clearly need in our model an external electric field $\vec{E}$ and a parallel external magnetic field $\vec{B}$. Accordingly we study strongly coupled four-dimensional field theories with such a chiral anomaly in the presence of a constant external magnetic field B in x_3 direction

$$F = dA^{ext} = B\, dx_1 \wedge dx_2 \,, \tag{2.22}$$

using holography, for example also studied in [52]. Consequently we add an axial current J_5 to our model.[3][4]

For a given QFT the anomaly coefficient has a fixed value, as we have seen in the calculation above. In this thesis we study a whole class of theories where the chiral anomaly coefficient is given by γ, which we treat as a free parameter. This is possible within holography for the following reason: We consider $SU(N)$ gauge theories in the large N-limit with N_f flavours. Accordingly the anomaly coefficient

[3] This can also be seen as having only one helicity J_L in the model.

[4] Note that consequently we consider an axial magnetic field in our model. In nature fundamental axial magnetic fields do not appear but they can appear in effective theories, e.g. in the effective description of Weyl semimetals [85].

is proportional to N_f/N, which varies continuously in the large N-limit. For reasons of clarity we drop the subscript "5" from now on,

$$\partial^\mu \langle J_\mu \rangle = \frac{\gamma}{8} \epsilon^{\mu\nu\rho\sigma} F_{\mu\nu} F_{\rho\sigma} \,. \tag{2.23}$$

2.2. Hydrodynamics

In this subsection we develop the hydrodynamical description in presence of anomalies for our system. The results for our system are presented in ch. 3.5.

2.2.1. Equilibrium state

Let us briefly introduce the relevant thermodynamic quantities. The equilibrium state is characterised by temperature T, chemical potential μ, energy density ϵ, pressure p and charge carrier density n.[5]

Below, we will make frequent use of the following thermodynamic relations:

$$d\epsilon = T ds + \mu \, dn \,, \quad dP = s \, dT + n \, d\mu \,, \quad \chi = \left(\frac{\partial n}{\partial \mu}\right)_T \,, \tag{2.24}$$

and

$$\left(\frac{\partial \epsilon}{\partial T}\right)_\mu = T_0 \left(\frac{\partial s}{\partial T}\right)_\mu + \mu_0 \left(\frac{\partial n}{\partial T}\right)_\mu \,, \qquad \left(\frac{\partial \epsilon}{\partial \mu}\right)_T = T_0 \left(\frac{\partial s}{\partial \mu}\right)_T + \mu_0 \left(\frac{\partial n}{\partial \mu}\right)_T \,. \tag{2.25}$$

2.2.2. Anomalous hydrodynamics

Hydrodynamics can be considered as an effective long-distance, long time-scale description, see e.g. [86, 87] for an introduction. The long wavelength deviations from thermal equilibrium are assumed to be small, hence we expand the relevant quantities in powers of derivatives.

We consider a system in the presence of external sources, namely the external gauge field A_ν, and the external metric $g_{\mu\nu}$. We are interested in a non-trivial gauge field background,

$$A_\nu = \left(\mu, \, -x_2 \frac{B}{2}, \, x_1 \frac{B}{2}, \, 0\right) \,, \tag{2.26}$$

with a non-vanishing chemical potential μ, and a magnetic field B in the x_3-direction,

[5] Note that a finite axial charge density corresponds to a difference in the density of left and right handed particles.

plus a first order correction a_μ.[6] For the background metric we take it to be Minkowskian, $\eta_{\mu\nu} = \mathrm{diag}(-1,1,1,1)$, plus a first order correction $h_{\mu\nu}$ which acts as a source for the energy-momentum tensor $T^{\mu\nu}$. First, we consider weak field hydrodynamics. By weak field we refer to a background magnetic field which is of first order in the derivative counting in hydrodynamics, i.e. the field strength is $F \sim B \sim \mathcal{O}(\partial)$. In other words, we consider a background magnetic field which is of the same order as the spatial derivatives, and hence $B \sim k_3 = k$. Second, we study "strong field' thermodynamics, where the background magnetic field is of zeroth order in derivatives.

The defining relations for hydrodynamics are the conservation equations for the energy momentum tensor $T^{\mu\nu}$ and the conserved current(s) J^μ

$$\begin{aligned} \nabla_\mu \langle T^{\mu\nu} \rangle &= F^{\nu\mu} \langle J_\mu \rangle \,, \\ \nabla_\mu \langle J^\mu \rangle &= \frac{\gamma}{8}\, \epsilon^{\mu\nu\rho\sigma}\, F_{\mu\nu}\, F_{\rho\sigma} \,. \end{aligned} \tag{2.27}$$

Note that we are already considering anomalous hydrodynamics here.

Given any timelike vector u^μ, we can decompose the energy-momentum tensor and the current into components which are transverse and longitudinal to u^μ:

$$\langle T^{\mu\nu} \rangle = \epsilon u^\mu u^\nu + P \Delta^{\mu\nu} + u^\mu q^\nu + u^\nu q^\mu + \tau^{\mu\nu} \,, \tag{2.28}$$

$$\langle J^\mu \rangle = n u^\mu + \nu^\mu \,, \tag{2.29}$$

where we defined the projector $\Delta^{\mu\nu} = \eta^{\mu\nu} + u^\mu u^\nu$. Note that $u_\mu \tau^{\mu\nu} = 0$, $u_\mu \nu^\mu = 0$, and $u_\mu q^\mu = 0$.

Now in hydrodynamics we assume that the coefficients ϵ, P, q^μ, $\tau^{\mu\nu}$, n and ν^μ can be expressed in terms of the hydrodynamic variables, namely the local temperature $T(x)$, the local chemical potential(s) $\mu(x)$, and the local fluid velocity $u^\mu(x)$. This allows us to describe the system close to equilibrium, namely it will respond to the fluctuations with corrections to the equilibrium values for all the hydrodynamic variables

$$T(t,x_3) = T_0 + \varepsilon\, T_1(t,x_3) \,, \quad u^\nu(t,x_3) = u_0^\nu + \varepsilon\, u_1^\nu(t,x_3) \,, \quad \mu(t,x_3) = \mu_0 + \varepsilon\, \mu_1(t,x_3) \,, \tag{2.30}$$

where ε is the expansion parameter.[7] Note that here we have chosen the particular case in which the momentum of the response is parallel to the magnetic field $\vec{k} \,||\, \vec{B}$.[8]

[6] Note that we have chosen here to put the magnetic field B in a symmetric way in A_2 and A_3.

[7] Mind the difference between the expansion parameter ε and the energy density ϵ.

[8] Another interesting choice would be to consider the momentum to be perpendicular to the

In addition, we have chosen the magnetic field B to point in the x_3-direction and hence we choose the corrections to depend only on x_3 and t.

These corrections in the hydrodynamic variables will cause corrections in the thermodynamic quantities ϵ, P, n, which we expand as

$$\epsilon(t,x_3) = \epsilon_0 + \varepsilon \frac{\partial \epsilon}{\partial T} T_1(t,x_3) + \varepsilon \frac{\partial \epsilon}{\partial \mu} \mu_1(t,x_3)\,, \tag{2.31}$$

$$P(t,x_3) = P_0 + \varepsilon \frac{\partial P}{\partial T} T_1(t,x_3) + \varepsilon \frac{\partial P}{\partial \mu} \mu_1(t,x_3)\,, \tag{2.32}$$

$$n(t,x_3) = n_0 + \varepsilon \frac{\partial n}{\partial T} T_1(t,x_3) + \varepsilon \frac{\partial n}{\partial \mu} \mu_1(t,x_3)\,, \tag{2.33}$$

where here and in the remainder of this section partial derivatives with respect to T are evaluated at fixed μ and vice versa, unless stated otherwise.

Taking into account the corrections, the corresponding relations, called constitutive equations, in the case of a weak magnetic field to first order in derivatives read

$$\tau^{\mu\nu} = -\eta \Delta^{\mu\alpha}\Delta^{\nu\beta}\left(\nabla_\alpha u_\beta + \nabla_\beta u_\alpha - \frac{2}{3}\nabla_\lambda u^\lambda g_{\alpha\beta}\right) - \zeta \Delta^{\mu\nu}\nabla_\lambda u^\lambda\,, \tag{2.34}$$

$$\nu^\mu = -\sigma T \Delta^{\mu\nu}\nabla_\nu\left(\frac{\mu}{T}\right) + \sigma E^\mu + \xi_B B^\mu + \xi_V \omega^\mu\,, \tag{2.35}$$

$$q^\mu = \xi_V B^\mu + \xi_3 \omega^\mu\,, \tag{2.36}$$

where E^μ is the electric field, B^μ is the magnetic field and ω^μ the vorticity

$$E^\mu = F^{\mu\nu}u_\nu\,, \quad B^\mu = \frac{1}{2}\epsilon^{\mu\nu\rho\lambda}u_\nu F_{\rho\lambda}\,, \quad \omega^\mu = \epsilon^{\mu\nu\rho\lambda}u_\nu \nabla_\rho u_\lambda\,. \tag{2.37}$$

The so called transport coefficients η, ζ, σ, ξ_B, ξ_V and ξ_3 parametrize the microscopic properties of the theory and in principle cannot be determined within hydrodynamics.

Frame choice

So far we have not mentioned the freedom of choosing a frame. The hydrodynamic variables can be considered as fields in hydrodynamics when considered as an effective field theory. As such, they are only defined modulo field redefinitions leaving the physical quantities invariant. Also note that the parameters like the local temperature $T(x)$ has no first-principle definition out of equilibrium. Fixing this freedom of

magnetic field, see [88] for such a choice in a system with an axial and a vector current.

redefinitions is fixing a "hydrodynamic frame". A well known example is the Landau frame in which the heat current vanishes $q^\mu = 0$, while we mostly work in the thermodynamic frame [89, 90]. In the thermodynamic frame, the temperature T, the chemical potential μ and the velocity u^μ remain unchanged from their equilibrium definition when solving the hydrodynamic equations. In particular, this frame is implicitly chosen by the dual description in AdS/CFT.

Hydrodynamic calculation

In order to determine the location of the poles of the hydrodynamic correlation functions, we insert the constitutive equations (2.28) into the conservation equations (2.27). After linearizing in ε, we solve the system of linear equations for the corrections to the hydrodynamic variables, namely for T_1, μ_1, and for the three spatial components of u_1^μ. Thereby, the time component of u_1^μ is fixed due to the normalization $u^\mu u_\mu = -1$. We provide the results in sec. 3.5 sorted according to the helicity of the corrections and sources with respect to the $SO(2)$ rotation symmetry in the (x_1, x_2)-plane.[9]

Note that the chiral transport coefficients, related to the anomaly, are analytically known in the thermodynamic frame to be

$$\xi_V = -\frac{\gamma}{2}\mu^2 + \tilde{C}T^2, \quad \xi_B = -\gamma\mu, \quad \xi_3 = -\frac{\gamma}{3}\mu^3 + 2\tilde{C}\mu T^2, \tag{2.38}$$

where the T^2 terms can be neglected in the large N limit as they originate from suppressed gauge-gravitational anomalies [47, 91–93].

2.2.3. Strong field thermodynamics

In this subsection, we consider strong magnetic field thermodynamics, more precisely zeroth order in derivatives hydrodynamics for time-independent quantities. A full hydrodynamic treatment of the strong magnetic field case would be interesting but is beyond the scope of this work.[10]

By strong field we mean a background magnetic field of zeroth order in derivatives, i.e. the field strength $F \sim B \sim \mathcal{O}(1)$, with B being the magnitude of the magnetic field. When a system is placed in a strong external field, strong field effects need to be taken into account, for example the polarization or magnetization of the medium [95, 96]. Such polarization effects to zeroth order in a derivative

[9] There are no hydrodynamic poles in the helicity-2 sector.
[10] For an attempt at this, see [94].

expansion can be parametrized using a polarization tensor $M^{\mu\nu} = 2\partial P/\partial F_{\mu\nu}$. Furthermore, effects of the chiral anomaly can contribute to thermodynamic quantities at zeroth order in derivatives [97].

Together, these effects can be expressed in terms of equilibrium constitutive equations for the energy momentum tensor and the axial current

$$\begin{aligned}\langle T^{\mu\nu}\rangle &= \epsilon_0 u^\mu u^\nu + P_0\Delta^{\mu\nu} + q^\mu u^\nu + q^\nu u^\mu \\ &\quad + M^{\mu\alpha}g_{\alpha\beta}F^{\beta\nu} + u^\mu u^\alpha\left(M_{\alpha\beta}F^{\beta\nu} - F_{\alpha\beta}M^{\beta\nu}\right) + \mathcal{O}(\partial)\,, \qquad (2.39)\\ \langle J^\mu\rangle &= n_0 u^\mu + \xi_B B^\mu + \mathcal{O}(\partial)\,, \qquad (2.40)\end{aligned}$$

where

$$q^\mu = \xi_V B^\mu\,, \qquad M^{\mu\nu} = \chi_{BB}\epsilon^{\mu\nu\alpha\beta}B_\alpha u_\beta\,. \qquad (2.41)$$

Note that all quantities above have to be evaluated at zeroth order in derivatives, e.g. $u^\mu = (1,0,0,0)$. When the magnetic field is chosen to point in the x_3-direction, these relations directly reduce to the equilibrium energy momentum tensor (2.42) and the equilibrium axial current (2.43).

Note that in the Landau frame the heat current vanishes, $q^\mu = 0$, hence all the off-diagonal components in the energy momentum tensor vanish. Therefore the observer is travelling with the heat within the fluid. The interesting point is that such a heat current exists in equilibrium at strong magnetic fields and in the presence of an anomaly.

Field theory energy momentum tensor and current

From a completely field theoretical analysis in thermodynamic equilibrium, taking into account a strong background magnetic field of $\mathcal{O}(\partial^0)$ in the derivative expansion [96], and a chiral anomaly [97] (see sec. 3.5 for more details), the energy-momentum tensor and the axial current are given by

$$\langle T^{\mu\nu}\rangle = \begin{pmatrix} \epsilon_0 & 0 & 0 & \xi_V^{(0)}B \\ 0 & P_0 - \chi_{BB}B^2 & 0 & 0 \\ 0 & 0 & P_0 - \chi_{BB}B^2 & 0 \\ \xi_V^{(0)}B & 0 & 0 & P_0 \end{pmatrix} + \mathcal{O}(\partial)\,, \qquad (2.42)$$

$$\langle J^\mu\rangle = \left(n_0,\, 0,\, 0,\, \xi_B^{(0)}B\right) + \mathcal{O}(\partial)\,, \qquad (2.43)$$

where a subscript "0" indicates that the quantity is evaluated in the thermodynamic equilibrium state. Similarly, the superscript "(0)" on the chiral transport coefficients,

$\xi_{V,B} = \xi_{V,B}(\mu, T)$, indicates that all thermodynamic quantities involved are evaluated in the thermodynamic equilibrium.

Note that, at strong magnetic fields, the equilibrium partition function can depend on T, μ and on B^2 [96]. Therefore, also the equilibrium quantities ϵ_0, P_0, and n_0 are in general functions of T, μ, and B^2.

Note also that the trace of the energy momentum tensor is in general given by $\langle T_\mu{}^\mu \rangle = \alpha_0 B^2$ for any conformal field theory (such as ours) in an external B field in flat spacetime. The contribution on the right-hand side is the standard trace anomaly arising from the external field, with a coefficient α_0, see e.g. [52]. For (2.42) we have $\langle T_\mu{}^\mu \rangle = -\epsilon_0 + 3P_0 - 2\chi_{BB} B^2$. In principle, the expression for the energy momentum tensor (2.42) receives derivative corrections. However, in our case T, μ, and B, as well as the field theory metric are all constant in space and time. Hence, derivative corrections vanish [96] in this particular equilibrium state.

2.3. String theory foundations

In string theory fundamental particles are replaced by extended strings of length l_s, which can be either open or closed. In addition to these 1-dimensional strings the theory also contains higher dimensional extended objects, called Dp-branes with p being the spatial dimension of the brane. The Dp-branes are extended in spacetime and hence are $p+1$ dimensional hypersurfaces.

A full understanding of string theory is not needed here. Thus we refer to the literature for an introduction, e.g. [98, 99]. String theory provides a concrete realisation of the holographic principle and hence allows to develop precise relations.[11] Throughout this chapter we will present the relevant string theory basics where needed. To start we now introduce the best known example of holography, namely AdS/CFT and briefly discuss its origin in string theory.[12] For a complementary introduction to AdS/CFT, see e.g [24, 100].

The AdS/CFT correspondence states precise relations and directly shows how to translate the boundary values of the gravitational fields to the expectation values of the dual field theory operators; the so called AdS/CFT dictionary. Later on we will use these relations to read off the field theory results from our gravity computation.

[11] Note however, that holography may be general and hence independent of string theory.
[12] In some sections we follow the lines of [100].

2.3.1. D3 brane AdS/CFT

Originally AdS/CFT was discovered in the context of string theory [23], where the Dp-branes played a crucial role. A Dp-brane is a $(p+1)$-dimensional object embedded in 10 dimensional spacetime. The Dp-branes are hypersurfaces, on which the string endpoints can end, where "D" stands for Dirichlet boundary conditions, illustrated in fig. 2.2.

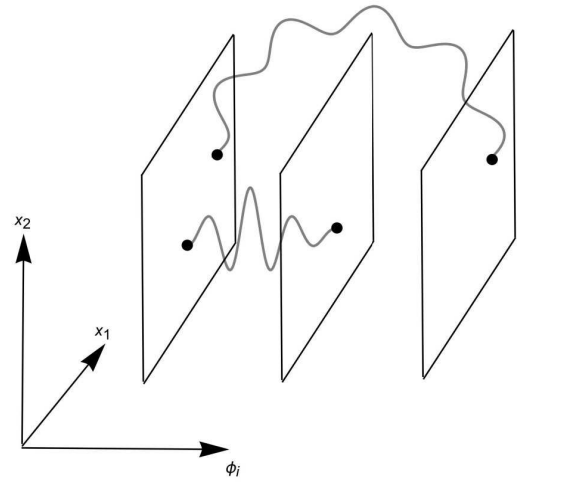

Fig. 2.2.: Two dimensional D-branes extended in $\{x_1, x_2\}$ directions and seven transverse directions ϕ_i embedded in 9 dimensional space. Strings ending on the different D2-branes.

In particular Dp-branes can be described from two different viewpoints, the perspective of gauge fields living on the brane and the gravity perspective. The effective description in these two limits gives rise to the two sides of the AdS/CFT duality.

Gauge fields living on the brane

The Dp-Branes are non-perturbative soliton-like solutions of string theory that are dynamical, e.g. they can move and be excited. The excitations are of two different types, namely deformations of their shape, which can be parametrized by the $9-p$ coordinates ϕ_i transverse to the brane and internal excitations, which are described by open string endpoints on the brane. These endpoints carry charge, which sources a gauge field on the brane. The action describing the massless open string excitations is given by the so-called Dirac-Born-Infeld action

$$S_{DBI} = -T_{Dp} \int \mathrm{d}^{p+1}x \sqrt{-\det(g_{\mu\nu} + 2\pi l_s^2 F_{\mu\nu})}\,, \tag{2.44}$$

where $g_{\mu\nu}$ is the induced metric on the worldvolume of the brane, $F_{\mu\nu}$ is the field strength of a gauge field A_μ, l_s is the characteristic string length and T_{Dp} is the tension of the brane.

For simplicity let us consider the Dp-brane in flat spacetime $\eta_{\mu\nu}$

$$g_{\mu\nu} = \eta_{\mu\nu} + (2\pi l_s^2)^2 \partial_\mu \phi^i \partial_\nu \phi^i \,, \tag{2.45}$$

where the ϕ^i are the coordinates transverse to the brane describing the embedding in the 10d spacetime. Here we consider the open strings as perturbations on fixed branes. For this picture to hold the backreaction of the strings given by the string coupling constant has to be small $g_s \ll 1$ and hence the tension of the Dp-brane $T_{Dp} \sim 1/g_s$ is large. Expanding the square root in the action (2.44) in powers of small field strength $F_{\mu\nu}$ and small derivatives $\partial_\mu \phi$, we obtain to second order

$$S_{DBI} \approx -\frac{2\pi T_{Dp}}{l_s^2} \int \mathrm{d}x^{p+1} \left(\frac{1}{4} F_{\mu\nu} F^{\mu\nu} + \frac{1}{2} \partial_\mu \phi^i \partial^\mu \phi^i \right) . \tag{2.46}$$

Clearly, this is the action of a $U(1)$ gauge field and $9-p$ scalar fields. Higher order terms, describing non-local interactions corresponding to extended strings, are suppressed by powers of L^2/l_s^2, where L is the radius of curvature. In the case of $D3$-branes the Yang-Mills coupling of the gauge theory can be identified to be

$$g_{YM}^2 = 4\pi g_s \,. \tag{2.47}$$

For open strings ending on N different branes we can describe all possibilities of the endpoints in a $N \times N$ matrix representations. In this case we get a non-abelian $U(N)$ gauge theory. For the case of $D3$-branes we have a 3+1 dimensional worldvolume of the branes and 6 scalar fields, see the left panel of fig. 2.3.

In addition, we know from the quantisation condition for D3-branes how to relate the constants

$$L^4 = 4\pi g_s N l_s^4 \,. \tag{2.48}$$

Consequently, the two limits $g_s \ll 1$ and $L/l_s \ll 1$ correspond to

$$\lambda = 4\pi g_s N \ll 1 \,, \tag{2.49}$$

where we describe a stack of non-gravitating branes. The effective description in the low energy limit $l_s \to 0$ is given by $\mathcal{N} = 4$ supersymmetric Yang-Mills (SYM) theory in 3+1 dimensions with gauge group $SU(N)$.[13]

[13]The $U(1)$ component of $U(N)$ can be decoupled, giving a $SU(N)$ gauge theory.

Gravity solution

We can also view the Dp-branes from a different viewpoint: In the low energy limit of string theory, namely supergravity, branes can be viewed as gravitational objects curving the spacetime. For supergravity to be a good description we need weak curvature $L/l_s \gg 1$. Taking into account (2.48), this limit corresponds to the opposite limit given in the previous discussion (2.49),

$$\lambda = 4\pi g_s N \gg 1\,. \tag{2.50}$$

Let us now derive the effective description in the weak curvature limit. The stack of N coincident D3-branes can be described as solution of 10d supergravity. We choose the D3-branes to be extended in the $\vec{x}_3 = \{x_1, x_2, x_3\}$ directions and $\{r^2, \Omega_5\}$ to be the coordinates perpendicular to the brane. Accordingly, this solution is given by

$$\mathrm{d}s^2 = H^{-1/2}\left(-\mathrm{d}t^2 + \mathrm{d}\vec{x}_3^2\right) + H^{1/2}\left(\mathrm{d}r^2 + r^2\mathrm{d}\Omega_5^2\right)\,. \tag{2.51}$$

The warp factor $H(r)$ is determined by the equations of motion yielding

$$H(r) = 1 + \frac{L^4}{r^4}\,. \tag{2.52}$$

In the so called near-horizon region $r \to 0$ we may approximate the warp factor by $H(r) = \frac{L^4}{r^4}$ and get

$$\mathrm{d}s^2 = \frac{r^2}{L^2}\left(-\mathrm{d}t^2 + \mathrm{d}\vec{x}_3^2\right) + \frac{L^2}{r^2}\mathrm{d}r^2 + L^2\mathrm{d}\Omega_5^2\,. \tag{2.53}$$

Equivalently, we can introduce z-coordinates $z = L^2/r$ to obtain

$$\mathrm{d}s^2 = \frac{L^2}{z^2}\left(-\mathrm{d}t^2 + \mathrm{d}\vec{x}_3^2 + \mathrm{d}z^2\right) + L^2\mathrm{d}\Omega_5^2\,. \tag{2.54}$$

This is the line element of $AdS_5 \times S^5$ in Poincare coordinates. The near-horizon limit $r \to 0$ corresponds to a low energy limit. The low energy excitations are described by classical gravitational perturbations around this background, which is illustrated on the right panel of fig. 2.3.

The Correspondence

So far we found two different descriptions of the D3-branes, either as a gauge theory or as a classical gravitational perturbations on $AdS_5 \times S_5$. Maldacena conjectured that these two theories are actually dual to each other [23].

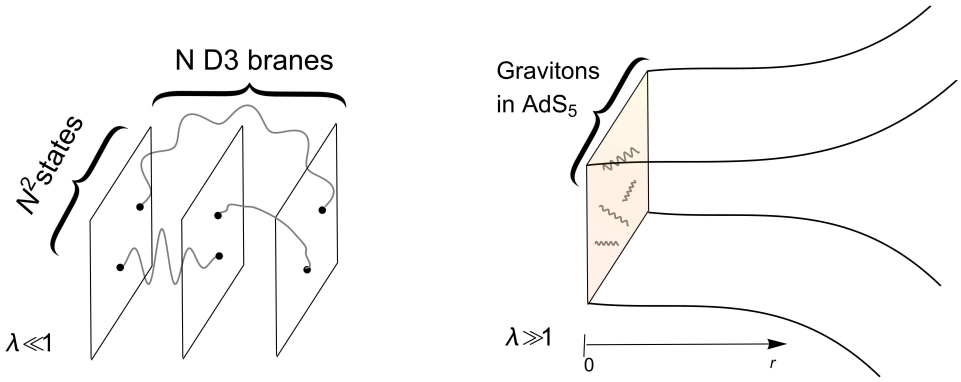

Fig. 2.3.: Opposite limits of D3-branes and corresponding low energy excitations. On the left, we display N coincident D3-branes and N^2 different string ending on the D3-branes in the limit $\lambda \ll 1$, which are described by a $SU(N)$ gauge theory. On the right, we display the black brane build out of N coincident branes in the opposite limit $\lambda \ll 1$, where the low energy description is given by gravity on AdS_5 in the near horizon region $r \to 0$.

One side of the duality is SYM theory with gauge group $SU(N)$ of rank N and coupling constant g_{YM} in 3+1 dimensions. Taking into account (2.48) and (2.47) we relate the couplings via

$$\frac{L^4}{l_s^4} = N g_{YM}^2 \,. \tag{2.55}$$

The gravity theory on the other side contains the AdS-radius L and Newtons constant in 10 dimensions $G_{10} = l_P^8$, where we introduced the Planck length l_P. The constants are given by

$$\frac{l_P^8}{L^8} = \frac{\pi^4}{2N^2} \,. \tag{2.56}$$

In order to have classical gravity we have to suppress quantum gravity corrections $l_P/L \ll 1$, which implies $N \gg 1$. Moreover we like to suppress higher string states and impose therefore $l_s/L \ll 1$.

The conjecture now states that $\mathcal{N} = 4$ SYM theory with gauge group $SU(N)$ in 3+1 dimensions is dynamically equivalent to 5d gravity theory on AdS_5.[14] This is

[14] Any field on $AdS_5 \times S_5$ can be reduced to a tower of Kaluza-Klein modes on AdS_5.

the weakest form of the conjecture, which holds in the limit

$$N \to \infty\,, \qquad \lambda \to \infty\,, \tag{2.57}$$

where we first perform the large N-limit while keeping $\lambda = N g_{YM}^2$ fixed and second the limit $\lambda \to \infty$. The duality maps the dynamics governed by the action, the degrees of freedom given by operators and the symmetries of both theories onto each other.

2.3.2. Scales and symmetries

Let us now discuss the relevant scales and symmetries and revisit the two limits introduced in the previous section.

Scales

To get an interpretation of the holographic coordinate z let us relate the scales on both theories. The conformal factor $(L/z)^2$ in (2.54) changes the proper distance d if we move away from the boundary into the bulk. The proper distance d_{QFT} at the boundary $z = 0$ and the proper distance inside the bulk d are related by the conformal factor

$$d = \frac{L}{z} d_{QFT}\,. \tag{2.58}$$

Consequently the energies scale inversely

$$E = \frac{z}{L} E_{QFT}\,. \tag{2.59}$$

Thus the near boundary region $z = 0$ corresponds to high energies in the dual QFT while dynamics in the far bulk describe low energy physics, illustrated in fig. 2.4.

In order to break conformal invariance we can introduce a minimal scale, that acts as a low energy cutoff. In the case of the AdS-spacetime one possibility is to introduce a black hole horizon at some finite radial coordinate z_h. This corresponds to introducing a temperature in the field theory. As a result the field theory temperature is equal to the black hole Hawking temperature.

Comparison of symmetries

For the duality to hold, both the symmetries and the degrees of freedom have to match. The symmetries itself can then be used to classify the relevant fields/operators

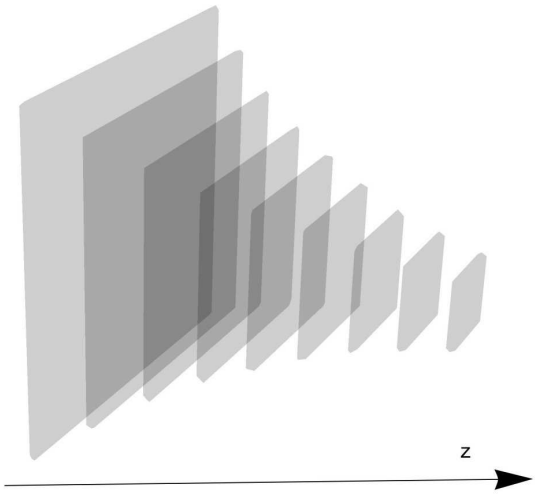

Fig. 2.4.: Holographic coordinate illustrated as energy scale. The bulk is sliced into copies (grey) of the QFT at a different length/energy scales along the holographic coordinate z.

according to their transformation.

The $\mathcal{N} = 4$ SYM theory in $4d$ is invariant under conformal transformations, including dilatations and special conformal transformations, see e.g. [101, 102] for an introduction to conformal field theory. The conformal group in four dimensions is $SO(4,2)$. The AdS_5 space on the other side is maximally symmetric with isometry group $SO(4,2)$.

In addition the $\mathcal{N} = 4$ SYM is a maximally supersymmetric theory with 32 supercharges, that can be grouped in 4 sets of complex Majorana generators Q^A_α, $\bar{Q}^A_{\dot{\alpha}}$ with $A \in \{1,2,3,4\}$ and $\alpha, \dot{\alpha} \in \{0,1\}$. This generators can be internally rotated, the so called R-symmetry, which gives an $SU(4)$ symmetry group. The six scalar fields ϕ_i transform in the fundamental representation of $SO(6)$. Note the Lie algebra isomorphism $\mathfrak{su}(4) \cong \mathfrak{so}(6)$.

On the gravity side, the maximally symmetric five-sphere S_5 is invariant under rotations $SO(6)$. The scalar fields are interpreted as the coordinates of the S_5 and the isometries of the S_5 are identified with the internal rotations of the scalar fields and supercharges. Hence the symmetry generators indeed agree on both sides. In general, the global part of the gauge symmetries in the bulk on the gravity side corresponds to global symmetries in the dual QFT.

2.3.3. Scalar field in AdS

Let us illustrate how the duality works by studying the simplest subsector, a scalar field ϕ in AdS_5 and its dual scalar operator $\mathcal{O}$ in the QFT.

Equations of motion

We want to study a scalar field ϕ on the gravity side of the duality. The background spacetime is AdS_5 in Poincare coordinates with line element in Euclidean signature

$$\mathrm{d}s^2 = \frac{1}{z^2}\left(dz^2 + \delta_{\mu\nu}\mathrm{d}x^\mu \mathrm{d}x^\nu\right) , \tag{2.60}$$

where we set the radius $L = 1$. As a reminder, the conformal boundary is located at $z = 0$. We are using coordinates $(x^m) = (x^\mu, z)$, where $m \in \{0, 4\}$ and $\mu \in \{0, 3\}$ respectively. The coordinates x^μ may be identified with the field theory coordinates, where $x^0 = t$, x^i are the spatial coordinates of the field theory and z is the radial coordinate of AdS_5.

A minimal action for a scalar field with mass m_s in curved space is given by

$$S = -\frac{1}{2}\int \mathrm{d}x^5 \sqrt{g}\left(g^{mn}\partial_m\phi\,\partial_n\phi + m_s^2\phi^2\right) , \tag{2.61}$$

where $g = \det g_{mn}$. Varying the action (2.61) with respect to ϕ gives the equations of motion (EOM)

$$\frac{1}{\sqrt{g}}\partial_m\left(\sqrt{g}\, g^{mn}\partial_n\phi\right) - m_s^2\phi = 0\,. \tag{2.62}$$

Using the explicit form for the metric g_{mn} and performing a Fourier transform in x^μ direction $\phi(x^\mu, z) = \int \frac{\mathrm{d}^4k}{(2\pi)^4}\exp(ikx)\,\phi_k(z)$, we finally obtain

$$z^5\partial_z\left(z^{-3}\partial_z\phi(z)\right) + z^2k^2\phi(z) - m_s^2\phi(z) = 0\,, \tag{2.63}$$

where we omit the subscript "k". The duality relates the scalar field at the conformal boundary to a scalar operator in the field theory. To gain more insight let us first perform a boundary analysis at the conformal boundary for the scalar field. We plug the near boundary expansion $\phi \sim z^\beta$ into the EOM (2.63) and solve for β:

$$\beta(\beta - 4) - m_s^2 = 0\,, \qquad \beta_\pm = 2 \pm \sqrt{2 + m_s^2}\,. \tag{2.64}$$

For the sake of completeness, let us do the following calculation for general dimen-

sions d and also give the result (2.64) for general AdS_{d+1}

$$\beta(\beta - d) - m_s^2 = 0\,, \qquad \beta_\pm = \frac{d}{2} \pm \sqrt{\frac{d^2}{4} + m_s^2}\,. \tag{2.65}$$

For later convenience we define $\Delta = \beta_+$ and $(d - \Delta) = \beta_-$. After Fourier transforming back the final result for the near boundary behaviour is

$$\phi(x, z) \approx A(x) z^{d-\Delta} + \cdots + B(x) z^{\Delta} + \dots\,, \tag{2.66}$$

where $\dots$ stand for subleading terms in z. Note that in AdS the mass for a scalar field can be negative and is bound from below by the so called Breitenlohner-Freedman (BF) bound [103]

$$m_s^2 \geq -\left(\frac{d}{2L}\right)^2\,. \tag{2.67}$$

We notice that Δ is real if the mass satisfies the BF bound. If we choose $m^2 > 0$, the exponent of the leading term in (2.66) is negative $d - \Delta < 0$. Hence in this case ϕ is divergent at the conformal boundary $z = \epsilon \to 0$:

$$\phi(x, z = \epsilon) \approx \epsilon^{d-\Delta} A(x)\,. \tag{2.68}$$

In order to relate the boundary value of the scalar field to a source φ for the QFT operator $\mathcal{O}$ we have to remove this divergence:

$$\varphi(x) = \lim_{z \to 0} z^{\Delta - d} \phi(x, z)\,, \tag{2.69}$$

where $\varphi(x)$ is now finite at the conformal boundary. The non-normalisable[15] mode $A(x)$ is the source for the dual operator in the QFT, while $B(x)$ can be identified with the vacuum expectation value (VEV) of the scalar operator, illustrated in fig. 2.5.

Scaling dimension

We still need to identify the role of Δ on the CFT side. Therefore let us consider the general action for a source coupled to a dual operator $\mathcal{O}$ at the boundary $z = \epsilon$

$$S_{bdy} \sim \int \mathrm{d}^d x \sqrt{\det(\gamma_\epsilon)}\, \phi(x, \epsilon) \mathcal{O}(x, \epsilon)\,. \tag{2.70}$$

[15] We introduce normalisable and non-normalisable modes on the next page, sec. 2.3.3.

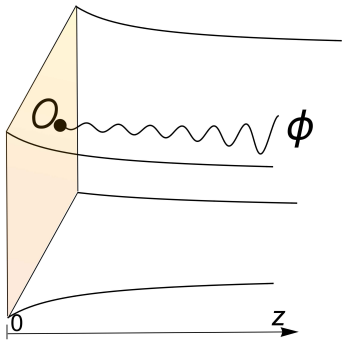

Fig. 2.5.: The boundary asymptotics of a scalar-field ϕ at the conformal boundary $z = 0$ in gravity corresponds to source and VEV of a scalar operator $\mathcal{O}$ in the QFT living on the boundary $z = 0$ (shaded region).

The determinant of the induced metric γ_ϵ close to the boundary scales as $\sqrt{\det(\gamma_\epsilon)} \sim (1/\epsilon)^d$. We now plug in the boundary behaviour for the scalar field (2.68):

$$S_{bdy} \sim \int \mathrm{d}^d x \, \varphi(x) \mathcal{O}(x, \epsilon) \epsilon^{-\Delta} \,. \tag{2.71}$$

For S_{bdy} to be finite and independent of ϵ we have to require that

$$\mathcal{O}(x, \epsilon) = \mathcal{O}(x) \epsilon^{\Delta} \,. \tag{2.72}$$

This is just the mass scaling dimension of the operator $\mathcal{O}$, if we keep in mind that going from the boundary $z = 0$ to $z = \epsilon$ is equivalent to a scale transformation in the dual QFT.

Normalisable mode

The natural norm for a solution of the Klein-Gordon equation on curved space in Euclidean signature is given by [100]

$$||\phi||^2 = -i \int_{\Sigma_t} \mathrm{d}z \, \mathrm{d}^d x \sqrt{g} \, g^{tt} (\phi^* \partial_t \phi - \phi \partial_t \phi^*) \,, \tag{2.73}$$

where Σ_t is a slice of constant time. We are interested in the near boundary $z \to 0$ behaviour of the two solutions (2.66). In case of AdS_{d+1} we have $(\sqrt{g} \, g^{tt}) \sim z^{1-d}$. The scalar field scales as $\phi \sim z^\beta$ and the derivative scales as $(\phi^* \partial_t \phi) \sim z^{2\beta}$. As a result the norm (2.73) is convergent for

$$2\beta - d + 2 > 0 \,. \tag{2.74}$$

The subleading solution $B(x)z^{\Delta}$ is hence always normalisable provided the BF bound holds. The leading solution $A(x)z^{d-\Delta}$ is non-normalisable for

$$m_s^2 \geq -\frac{d^2}{4} + 1\,, \tag{2.75}$$

which corresponds to a source. If the mass is below this bound, but above the BF bound

$$-\frac{d^2}{4} \leq m_s^2 \leq -\frac{d^2}{4} + 1 \tag{2.76}$$

both modes are normalisable and different quantisations are possible, identifying one or the other as source and VEV respectively.

2.3.4. Correlation functions

Dynamics

So far we have only considered non-dynamical properties of the duality. But the AdS/CFT dictionary also relates the dynamics of both theories. On the QFT side we like to calculate Euclidean correlators between different operators

$$\langle \mathcal{O}(x_1)....\mathcal{O}(x_n)\rangle\,. \tag{2.77}$$

Therefore we add source terms $J(x)\mathcal{O}(x)$ to the Lagrangian leading to the generating functional

$$Z_{QFT}[J] = \langle \exp(\int J(x)\mathcal{O}(x))\rangle\,. \tag{2.78}$$

As usual the connected correlators can then be obtained by functional derivatives with respect to the sources

$$\frac{\partial}{\partial J_{x_1}}...\frac{\partial}{\partial J_{x_n}} \log(Z_{QFT}[J])\bigg|_{J=0} = \langle \mathcal{O}(x_1)....\mathcal{O}(x_n)\rangle\,, \tag{2.79}$$

where we set the source J to zero after taking the functional derivatives.

On the gravity side we have to consider the partition function Z_G, which is the path integral over all field configurations, which asymptote to the right boundary value $\phi \to \varphi$ at the conformal boundary

$$Z_{grav}[\phi \to \varphi] = \int\limits_{\phi\to\varphi} \mathcal{D}\phi\, e^{S_{grav}[\phi]}\,. \tag{2.80}$$

In the classical limit the path integral is dominated by the classical solution and we

can use a saddle point approximation. Thus the path integral (2.80) is approximated by the exponential of the action, with the solution of the classical equations of motion inserted, the so called on-shell action $S^{o.s.}$:

$$Z_{grav}[\phi \to \varphi] \approx e^{S^{o.s.}_{grav}[\phi \to \varphi]} \,. \tag{2.81}$$

The classical on-shell gravity action is typically divergent and needs to be renormalized. This can be achieved by adding proper counterterms to the action, as we discuss for the gravity setup used in this thesis in sec. 2.4.2.

We are now at the point to formulate the dynamical equality stated in the AdS/CFT dictionary. The duality translates the generating functional $Z_{QFT}[J]$ of the QFT to the gravity on-shell action evaluated on the classical solution, which asymptotes the correct boundary value φ,

$$Z_{QFT}[\varphi] = \langle \exp[\int \varphi \, \mathcal{O}] \rangle = e^{S^{o.s.}_{grav}[\phi \to \varphi]} \,, \tag{2.82}$$

where φ is identified with the source in the QFT $J = \varphi$. This dynamical equality is a remarkable statement, since it relates a classical theory with a quantum theory. In addition, let us stress again that the two theories are defined for a different number of dimensions.

One-point function

Now we are able to calculate correlation functions on the QFT side, i.e. one- and two-point functions with the AdS/CFT dictionary. The knowledge of such correlation functions becomes relevant for the study of hydrodynamics within AdS/CFT.

Using the AdS/CFT dictionary (2.82), we derive the one-point function of an operator $\mathcal{O}$ in presence of a source φ

$$\langle \mathcal{O}(x) \rangle_\varphi = \frac{\delta S_{grav}[\phi]}{\delta \varphi(x)} \,, \tag{2.83}$$

where $\varphi(x)$ again denotes the finite part at the boundary $\varphi(x) = \lim_{z \to 0} z^{\Delta - d} \phi(x, z)$, see (2.69). This gives

$$\langle \mathcal{O}(x) \rangle_\varphi = \lim_{z \to 0} z^{\Delta - d} \frac{\delta S_{grav}[\phi]}{\delta \phi(z, x)} \,, \tag{2.84}$$

which can be explicitly calculated within gravity, when we have obtained the classical solution of the gravity equations of motion. At this point we are able to calculate the one-point function within the gravity side of the duality.

Let us now study the one-point function on the QFT side, which is given by the path integral

$$\langle \mathcal{O}(x) \rangle_\varphi = \int \mathcal{D}\Phi \, \mathcal{O}(x) \, e^{S[\Phi] + \int \mathrm{d}y \, \varphi(y) \mathcal{O}(y)} \, . \tag{2.85}$$

Doing linear response theory, this gives to linear order in φ

$$\langle \mathcal{O}(x) \rangle_\varphi = \langle \mathcal{O}(x) \rangle_{\varphi=0} + \int \mathrm{d}y \, G_E(x-y) \varphi(y) \, , \tag{2.86}$$

with $G_E(x-y) = \langle \mathcal{O}(x) \mathcal{O}(y) \rangle$ the Euclidean two-point function. For normal-ordered operators the relation $0 = \langle \mathcal{O}(x) \rangle_{\varphi=0}$ holds, such that (2.86) measures the linear response around its expectation value. The convolution is simply given by a product in momentum space, resulting in

$$G_E(k) = \frac{\langle \mathcal{O}(k) \rangle_\varphi}{\varphi(k)} \, . \tag{2.87}$$

This equation will become important for the hydrodynamic calculations. Note that we have calculated Euclidean correlation functions. The corresponding retarded correlation functions can be obtained via analytical continuation.

2.3.5. Field-operator map

So far we have considered the case of a scalar field ϕ dual to a scalar operator $\mathcal{O}$. But the holographic dictionary can be extended to include additional operators and fields. We can utilize the fact that the symmetries coincide in both theories and relate operators and fields in the same representation. We give the operators and fields relevant for this thesis and refer the reader to the literature for a complete discussion, e.g. [24].

As outlined in ch. 1.3 we study the dual description of 4d field theories with an external magnetic field at finite temperature and chemical potential. We use μ, ν for 4d field theory coordinates and m, n as indices for the 5d gravity coordinates. The energy-momentum tensor $T_{\mu\nu}$ of the field theory is dual to metric fluctuations on the gravity side g_{mn}, whereas the current J_μ is dual to a gauge field A_m.

field theory operator			supergravity field
scalar operator	$\mathcal{O}$	ϕ	scalar field
energy-momentum Tensor	$T_{\mu\nu}$	g_{mn}	metric
conserved current	J_μ	A_m	gauge field

Table 2.1.: Field theory operators and dual gravity fields.

Finite density ρ and finite chemical potential μ on the 4d field theory side can then be realised by suitable boundary conditions for the temporal component of the gauge field A_t on the 5d gravity side at the conformal boundary $z = 0$:

$$A_t(z) = \mu - \frac{\rho}{2} z^2 + \mathcal{O}(z^3) \,. \tag{2.88}$$

A finite magnetic field on the 4d field theory side, e.g. in x_3 direction, is introduced by a background magnetic field for the gauge field in the 5d gravity theory

$$A = A_m \mathrm{d}x^m = \frac{B}{2} \left(-x_2 \, \mathrm{d}x_1 + x_1 \, \mathrm{d}x_2 \right) \,. \tag{2.89}$$

The non-conservation of currents due to background fields in the presence of an anomaly in the QFT is related to the existence of gauge non-invariant boundary terms in the dual gravitational description [104]. Since we identify the QFT and the gravity action, the classical gravity action must not be gauge invariant in the presence of an anomaly in the dual QFT. This is realised by adding a Chern-Simons-term (CS) for the gauge field to the action on the 5d gravity side

$$S_{CS} \sim \gamma \int_{\mathcal{M}} \left(A \wedge F \wedge F \right) \,, \tag{2.90}$$

which is dual to the chiral anomaly with anomaly coefficient γ, as we discuss in sec. 2.4 for the specific model used in this thesis. Note that the CS-term explicitly depends on A and hence the action is not gauge invariant upon a boundary term.

2.3.6. Consistent truncations

We have not put much attention to the truncation from string theory to supergravity and the difference between supergravity and gravity in the AdS/CFT dictionary so far. In a top-down approach we have to start with a string theory model and consistently truncate it down to supergravity and gravity. In applied AdS/CFT we usually rely on a bottom-up approach, where we collect the phenomenological ingredients needed without having a consistent truncation.

So far we used the spirit of a bottum-up approach to AdS/CFT. The holographic model, that we introduce in the next section 2.3.6, is a such bottom-up model that remarkably has a consistent top-down truncation. For $\gamma = 2/\sqrt{3}$, the action of this minimal model, given in (2.93), coincides with the bosonic part of minimal gauged supergravity in five dimensions. Hence it is a consistent truncation of the most

general class of type IIB supergravity in ten dimensions or supergravity in eleven dimensions which are dual to $\mathcal{N} = 1$ superconformal field theories, see e.g. [105–108]. As the consistent truncation leads to the Einstein-Maxwell-Chern-Simons (EMCS) theory our approach is intriguingly general, but minimal and simple.

2.4. Holographic setup

Our goal is to study gravity solutions within AdS/CFT to get new results regarding anomalies in strongly coupled field theories. With the AdS/CFT dictionary at hand let us now collect the minimal features of the gravity model needed within the framework of gauge/gravity duality. On the QFT side we describe a theory with chiral anomaly at finite temperature and finite density with a background magnetic field.

2.4.1. Minimal model

First, the model has to contain a metric g_{mn}, which is dual to the energy-momentum tensor $T^{cft}_{\mu\nu}$ of the corresponding four-dimensional CFT, see sec. 2.3.5. The action for the metric is given by the Einstein-Hilbert action plus a negative cosmological constant Λ

$$S_{EH} = \frac{1}{2\kappa^2}\left[\int_{\mathcal{M}} \mathrm{d}^5x\,\sqrt{-g}\,(R - 2\Lambda)\right], \tag{2.91}$$

where $g = \det g_{mn}$ and $2\kappa^2 \equiv 16\pi G_5$ with the five-dimensional gravitational constant G_5. To describe asymptotic AdS_5 solutions the cosmological constant has to be $\Lambda = -(d-1)(d-2)/(2L^2) = -6/L^2$ for $d = 5$. We introduce finite temperature by imposing a black hole horizon in our gravity model.

Secondly we need a U(1) gauge field $A = A_m\,\mathrm{d}x^m$, which is dual to the current J^{cft}_μ on the field theory side, see sec. 2.3.5. Moreover, $F = \mathrm{d}A$ is the field strength tensor of the U(1) gauge field A. The gauge field "contains" the background magnetic field and allows us to switch on finite density. The action for the gauge field is given by the Maxwell action on curved space. In addition we add a Chern-Simons-term on the gravity side that is dual to the chiral anomaly with anomaly coefficient γ. This is another vital ingredient of the gravitational toy model,

$$S_{MCS} = \frac{1}{2\kappa^2}\left[\int_{\mathcal{M}} \mathrm{d}^5x\,\sqrt{-g}\left(-\frac{L^2}{4}F_{mn}F^{mn}\right) - \frac{\gamma}{6}\int_{\mathcal{M}} A\wedge F\wedge F\right]. \tag{2.92}$$

This is the holographic implementation of the axial $U(1)$ anomaly in covariant form [47]. Also note that the Chern-Simons-term is topological, i.e. it does not include the metric $\sqrt{-g}$, and hence does not contribute to the stress-energy tensor in the Einstein equations.

To summarize, the action of the gravitational toy model reads

$$S_{grav} = \frac{1}{2\kappa^2}\left[\int_{\mathcal{M}} \mathrm{d}^5x\,\sqrt{-g}\left(R + \frac{12}{L^2} - \frac{L^2}{4}F_{mn}F^{mn}\right) - \frac{\gamma}{6}\int_{\mathcal{M}} A\wedge F\wedge F\right]. \tag{2.93}$$

To keep notation compact we set $2\kappa^2 = 1$ as well as $L = 1$ from now on.

As mentioned before for $\gamma = 2/\sqrt{3}$, the action (2.93) is a consistent truncation of type IIB supergravity in ten dimensions, see sec. 2.3.6. However, in this thesis γ is treated as a free parameter[16] and we study the phase diagram as a function of γ. This action has to be supplemented by boundary terms to treat divergences, as we discuss in sec. 2.4.2.

Equations of motion

The equations of motion associated with the action (2.93) read in the trace-reduced form

$$R_{mn} = -4g_{mn} + \frac{1}{2}\left(F_{mo}F_n{}^o - \frac{1}{6}g_{mn}F_{op}F^{op}\right) \tag{2.94}$$

for the metric. The right-hand side corresponds to the cosmological constant term plus the stress-energy tensor of the electromagnetic field. Let us stress again that the Chern-Simons term does not contribute to the stress-energy tensor. Furthermore, the equations for the gauge field are given by

$$\mathrm{d}\star F + \frac{\gamma}{2}F\wedge F = 0\,. \tag{2.95}$$

In addition, the field strength tensor has to satisfy the Bianchi identitiy

$$\mathrm{d}F = 0\,. \tag{2.96}$$

Note that the Chern-Simons term appears explicitly only in the Maxwell equations. Equivalently, we can rewrite (2.95) as

$$\nabla_m F^{mn} + \frac{\gamma}{8\sqrt{-g}}\,\tilde{\epsilon}^{nmopq}F_{mo}F_{pq} = 0\,, \tag{2.97}$$

[16] See the discussion at the end of sec. 2.1.2.

where $\tilde{\epsilon}^{mnopq}$ is the totally antisymmetric Levi-Civita symbol in five spacetime dimensions with $\tilde{\epsilon}^{t123z} = 1$.

2.4.2. Divergencies and counterterms

We have already encountered divergences in the study of the scalar field, sec. 2.3.3. Let us now perform a systematic treatment of divergences, the general method within AdS/CFT is called holographic renormalisation [109], see [110] for an introduction. The large scale divergences at the conformal boundary correspond to UV-divergences in the field theory. Cutting off the radial coordinate at some finite z_h by a black hole horizon corresponds to introducing a low energy cutoff by a temperature.

Counterterms

The action (2.93) has to be supplemented by boundary terms [111–113] of the form

$$S_{bdy} = \frac{1}{\kappa^2} \int_{\partial\mathcal{M}} \mathrm{d}^4x \sqrt{-h} \left(K - \frac{3}{L} + \frac{L}{4} R(h) + \frac{L}{8} \ln\left(\frac{z}{L}\right) F_{\mu\nu} F^{\mu\nu} \right) , \tag{2.98}$$

where we display L and κ for completeness.[17] Here, $h_{\mu\nu}$ is the metric induced by g_{mn} on the conformal boundary of AdS_5. The extrinsic curvature K_{mn} is given by

$$K_{mn} = \mathcal{P}_m{}^o \, \mathcal{P}_n{}^p \, \nabla_o n_p \, , \qquad \text{with} \quad \mathcal{P}_m{}^o = \delta_m{}^o - n_m n^o \, , \tag{2.99}$$

where ∇ is the covariant derivative and n_m are the components of the outward pointing normal vector of the boundary $\partial\mathcal{M}$. Moreover, K is the trace of the extrinsic curvature with respect to the metric at the boundary.

The first term in (2.98) is the standard Gibbons-Hawking term which is needed for well-posedness of the variational principle. The Einstein-Hilbert action (2.91) in general contains second derivatives of the metric, while usually field theory Lagrangians contain only first order derivatives. Due to the second derivatives, we pick up an additional boundary term in the variation of the action, which is exactly cancelled by the the Gibbons-Hawking term resulting in the desired Einstein equations.

If we require the stress-energy tensor to be finite, the counterterms in (2.98) are uniquely fixed [112, 113]. The divergences correspond to ultraviolet divergences of quantum field theory, and thus may be removed by adding local counterterms to

[17] Note that we set $2\kappa^2 = 1$ as well as $L = 1$.

the action.

In our case, the conformal boundary of AdS_5 is flat Minkowski space and hence the Ricci scalar associated with the boundary metric, $R(h)$, vanishes. Note that the last term in (2.98) is not invariant under diffeomorphisms. As we will see explicitly, this term in the boundary action is needed to remove the divergence associated with the trace anomaly on the field theory side

$$\eta^{\mu\nu}\left\langle T^{cft}_{\mu\nu}\right\rangle = -\frac{1}{4}F_{\mu\nu}F^{\mu\nu}\,. \tag{2.100}$$

2.4.3. Energy momentum tensor and current

With the proper counterterms in our action we can read off the energy momentum tensor and current in our dual field theory. Making use of standard recipes of AdS/CFT correspondence, in particular the relation [112]

$$\langle T_{\mu\nu}\rangle = \lim_{z\to 0}\frac{1}{z^2}\left(-2K_{\mu\nu}+2(K-3)\,h_{\mu\nu}+\ln(z)\left(F_{\mu}{}^{\alpha}F_{\nu\alpha}-\frac{1}{4}\,h_{\mu\nu}F^{\alpha\beta}F_{\alpha\beta}\right)\right)\,, \tag{2.101}$$

we can extract the energy-momentum tensor of the dual conformal field theory. Similarly, from the relation [114]

$$\langle J^{\mu}\rangle = \lim_{z\to 0}\left(\frac{1}{z^3}h^{\mu\alpha}\partial_z A_\alpha+\frac{\gamma}{6}\epsilon^{\alpha\beta\gamma\mu}A_\alpha F_{\beta\gamma}\right)\,, \tag{2.102}$$

we can obtain the expectation value of the current in the dual field theory.

To illustrate the divergences we use the following metric

$$\begin{aligned} \mathrm{d}s^2 &= \frac{1}{z^2}\left[\frac{\mathrm{d}z^2}{u(z)}-u(z)\,\mathrm{d}t^2+v(z)^2\,\left(\mathrm{d}x_1^2+\mathrm{d}x_2^2\right)+w(z)^2\,\left(\mathrm{d}x_3+c(z)\mathrm{d}t\right)^2\right]\,,\\ F &= A_t'(z)\,\mathrm{d}z\wedge\mathrm{d}t+B\,\mathrm{d}x_1\wedge\mathrm{d}x_2+P'(z)\,\mathrm{d}z\wedge\mathrm{d}x_3\,, \end{aligned} \tag{2.103}$$

which is the ansatz of ch. 3 in Poincare coordinates $z\in[0,1]$. This describes a charged magnetic black hole solution, where B is the magnetic field, $z=0$ the conformal boundary and $z=1$ the horizon. Let us exemplary show the non-vanishing

contributions to T_{tt}:

$$\begin{aligned}
\frac{1}{z^2}\left(-2K_{tt}\right) &= \left(-\frac{1}{6}B^2\ln(z) - \frac{B^2}{6} - u_4 + \frac{2}{z^4}\right), \\
\frac{1}{z^2}\left(2K\, h_{tt}\right) &= \left(-\frac{4}{3}B^2\ln(z) + \frac{B^2}{6} - 8u_4 - \frac{8}{z^4}\right), \\
\frac{1}{z^2}\left(-6\, h_{tt}\right) &= \left(B^2\ln(z) + 6u_4 + \frac{6}{z^4}\right), \\
\frac{1}{z^2}\left(-\frac{\ln(z)}{4}\, h_{tt}F^{\alpha\beta}F_{\alpha\beta}\right) &= \frac{1}{2}B^2\ln(z)\,,
\end{aligned} \tag{2.104}$$

where u_4 appears in expansion of $u(z) = 1 + z^4u_4 + z^4\ln(z)\frac{B^2}{6} + \ldots$, see (3.4). In the sum of (2.104) all divergences cancel and hence we obtain the finite result

$$\langle T_{tt}\rangle = -3u_4\,. \tag{2.105}$$

2.5. Black holes

So far we have discussed the field theoretical basics and the AdS/CFT dictionary. In the end our approach boils down to finding and studying asymptotic AdS black hole solutions. Let us therefore first discuss the Einstein-Maxwell equations and second cover the thermodynamic properties of black holes required for the later discussion.

2.5.1. Reissner-Nordstroem black brane

We consider black hole solutions to the Einstein-Maxwell-Chern-Simons equations (2.94) and (2.95). The black holes studied in this thesis are only obtainable on a numerical level. Yet these black holes generalize the analytical AdS_5 Reissner-Nordstroem (RN) black brane, in our case to magnetic field and spatial modulation. Let us therefore first study the analytical RN solution.

We want to describe an electrically charged, asymptotic AdS_5 black hole. Accordingly we choose the following ansatz for the metric $g_{mn}\mathrm{d}x^m\mathrm{d}x^n = \mathrm{d}s^2$ and the gauge field $A_m\mathrm{d}x^m = A$ in Poincare coordinates

$$\mathrm{d}s^2 = \frac{L^2}{z^2}\left(\frac{\mathrm{d}z^2}{u(z)} - u(z)\,\mathrm{d}t^2 + \sum_{i=1}^{3}\mathrm{d}x^i\,\mathrm{d}x^i\right), \qquad A = -E(z)\mathrm{d}t\,, \tag{2.106}$$

where we switch on a blackening function $u(z)$ in g_{tt} and g_{zz}. The conformal boundary is located at $z = 0$ and we fix the horizon to be at $z = 1$. Note that the ansatz

is isotropic in the x_i directions. We again fix the AdS radius $L = 1$. We get from (2.106) the corresponding field strength tensor

$$F = e(z)\,\mathrm{d}t \wedge \mathrm{d}z, \quad \text{with} \quad e(z) = \frac{d}{dz}E(z). \tag{2.107}$$

Plugging the ansatz (2.106) into the Einstein equations (2.94) gives

$$\mathrm{E}_1 : \qquad 24 = 2z^4 e(z)^2 - 24u(z) + 15z\,u'(z) - 3z^2 u''(z)\,, \tag{2.108}$$

$$\mathrm{CON} : \qquad 24 = -z^4 e(z)^2 - 24u(z) + 6z\,u'(z)\,. \tag{2.109}$$

Equation (2.108) is an ordinary second order differential equation, while (2.109) is a first order constraint equation. The left-hand side of (2.108) and (2.109) corresponds to the cosmological constant $24 = -4\Lambda$. The Maxwell equation (2.95) is given by

$$\mathrm{M}_1 : \qquad 0 = e(z) - ze'(z)\,. \tag{2.110}$$

Let us explicitly check the consistency of the constraint. Using the equation of motion of the metric (2.108), denoted by $\mathrm{E}_1(z)$, and the equation of motion for the gauge field (2.110), denoted by $\mathrm{M}_1(z)$, we have to show that the constraint (2.109), denoted by $\mathrm{CON}(z)$, satisfies on-shell the following differential equation

$$\partial_z \mathrm{CON}(z) + f(z)\,\mathrm{CON}(z) = 0\,, \tag{2.111}$$

for some function $f(z)$. We are able to show consistency and obtain the following combination:

$$z\,\partial_z \mathrm{CON}(z) - 2\,\mathrm{CON}(z) - 2\,\mathrm{E}_1(z) - z^4 \mathrm{M}_1(z) = 0\,. \tag{2.112}$$

The differential equation (2.111) for $\mathrm{CON}(z)$ can be formally solved in terms of exponential functions. Hence, solving the constraints $\mathrm{CON}(z_0) = 0$ for some $z = z_0$ guarantees that the constraint is satisfied for all z.

Let us now obtain the solution to (2.108)–(2.110). The Maxwell equation (2.110) is solved by

$$e(z) = \rho\, z\,, \tag{2.113}$$

where ρ is a free parameter. Additionally we have to demand regularity for the gauge field at the horizon $A_t(1) = 0$. This fixes the integration constant for $E(z)$

and thus we obtain for the gauge field

$$A_t(z) = -E(z) = \frac{\rho}{2}(1 - z^2)\,. \tag{2.114}$$

After plugging this solution into the Einstein equation (2.108) we solve for $u(z)$:

$$u(z) = 1 + c_1 z^2 + c_2 z^4 + \frac{1}{12}\rho^2 z^6\,. \tag{2.115}$$

The solution has two free integration parameters c_1 and c_2. In order to describe a black hole we need a horizon. With the horizon condition at $z = 1$ we impose:

$$u(1) = 0\,. \tag{2.116}$$

This allows to eliminate c_2 leading to

$$u(z) = 1 + c_1 z^2 + z^4\left(-c_1 - \frac{\rho^2}{12} - 1\right) + \frac{\rho^2 z^6}{12}\,. \tag{2.117}$$

We still have to satisfy the constraint equation (2.109). Plugging in (2.117) forces $c_1 = 0$. Finally we obtain the RN black brane solution

$$u(z) = 1 - z^4\left(1 + \frac{1}{3}\left(\frac{\rho}{2}\right)^2(1 - z^2)\right)\,, \tag{2.118}$$

$$e(z) = \rho\, z\,, \qquad A_t(z) = -E(z) = \frac{\rho}{2}(1 - z^2)\,. \tag{2.119}$$

The parameter ρ is related to the density of the dual field theory, $\langle J_t^{cft}\rangle = -\rho$, while $\mu = A_t(0) = \rho/2$ is identified with the chemical potential of the dual field theory. Note that we have fixed $u(1) = 0$ to be the location of the horizon. Furthermore we have chosen $u(0) = 1$ to be the location of the conformal boundary. At the conformal boundary (2.106) asymptotes to AdS_5 in Poincare-coordinates

$$\mathrm{d}s^2 = \frac{1}{z^2}\left(\mathrm{d}z^2 - \mathrm{d}t^2 + \sum_{i=1}^{3}\mathrm{d}x^i\,\mathrm{d}x^i\right)\,. \tag{2.120}$$

In the limiting case of zero density $\rho = 0$ the RN-solution (2.106) reduces to the AdS-Schwarzschild black hole solution

$$u(z) = 1 - z^4\,. \tag{2.121}$$

2.5.2. Black hole thermodynamics

Black holes arise as solutions of gravity, given by Einsteins equations. Surprisingly black holes also encode thermodynamic and dissipative processes of systems with a large number of degrees of freedom. Consequently we can assign a temperature T, the so called Hawking temperature and an entropy s to a black hole. Being a thermal object, Black holes have to emit thermal (black body) radiation, the famous Hawking radiation [115].

Temperature

The Hawking temperature and entropy of the black hole can be calculated using gravity in Euclidean signature. After a Wick-rotation of the time direction $\tau = it$ in the metric (2.106) and Taylor-expanding $u(z) \approx u'(1)(1-z)$ around the horizon $z = 1$ we get

$$\mathrm{d}s^2 \approx \left(\frac{\mathrm{d}z^2}{u'(1)(1-z)} + (1-z)u'(1)\,\mathrm{d}\tau^2 + \mathrm{d}\vec{x}^2 \right) . \tag{2.122}$$

To identify the line element (2.122) we perform the following coordinate transformations

$$\rho^2 = \frac{4}{u'(1)}(1-z)\,, \quad \mathrm{d}z = -\frac{1}{2}\,u'(1)\rho\,\mathrm{d}\rho\,, \tag{2.123}$$

$$\mathrm{d}s^2 \approx \mathrm{d}\rho^2 + \frac{u'(1)^2}{4}\rho^2\,\mathrm{d}\tau^2 + \mathrm{d}\vec{x}^2\,. \tag{2.124}$$

Performing another transformation

$$\phi = \frac{|u'(1)|}{2}\tau\,, \tag{2.125}$$

finally results in

$$\mathrm{d}s^2 \approx \mathrm{d}\rho^2 + \rho^2\,\mathrm{d}\phi^2 + \mathrm{d}\vec{x}^2\,. \tag{2.126}$$

We have successfully transformed the coordinates to polar coordinates (ρ, ϕ). To avoid a conical singularity at $\rho = 0$ we have to require $\phi \sim \phi + 2\pi$. In Poincare coordinates this corresponds to a period of $\Delta\tau = \frac{4\pi}{|u'(1)|}$. In Euclidean QFT the period of the time circle $\Delta\tau$ is identified with the field theory temperature $\Delta\tau = \frac{1}{k_B T}$. Therefore we finally obtain

$$T = \frac{|u'(1)|}{4\pi}\,, \tag{2.127}$$

where we have set $k_B = 1$.[18] Accordingly, the temperature of the RN solution (2.118) is given by

$$T = \frac{|\bar{u}_1|}{4\pi} = \frac{1}{\pi}\left(1 - \frac{\mu^2}{6}\right) . \tag{2.128}$$

For $\mu = \sqrt{6}$ this solutions describes an extremal black hole, $u''(0) = 0$, with zero temperature.

Entropy

The entropy density s can be found from the Bekenstein-Hawking [116] entropy formula $S_{BH} = 4\pi\frac{A}{2\kappa^2}$.[19] Remarkably it states that the entropy is proportional to the area of the horizon. In the following we choose to set $2\kappa^2 = 1$.

If we allow for anisotropic black holes, i.e. introducing the functions $v(z)$, $w(z)$ and $l(z)$, the line element reads

$$\mathrm{d}s^2 = \frac{1}{z^2}\left(\frac{\mathrm{d}z^2}{u(z)} - u(z)\,\mathrm{d}t^2 + v(z)^2\mathrm{d}x_1^2 + w(z)^2\mathrm{d}x_2^2 + l(z)^2\mathrm{d}x_3^2\right) . \tag{2.129}$$

For anisotropic black holes the area A of the horizon $z = 1$ is given by

$$A = v(1)w(1)l(1) \cdot \mathrm{vol}(\mathbb{R}^3) . \tag{2.130}$$

Due to the infinite area it is more convenient to work with the entropy density

$$s = 4\pi\, v(1)w(1)l(1) \tag{2.131}$$

Hence the entropy density of the RN solution (2.106) and the Schwarzschild solution (2.121) is given by $s = 4\pi$.

[18] Note that for the Schwarzschild black hole (2.121) the temperature appears to be constant $T = 1/\pi$. This is due to the fact that we have chosen to work in relative coordinates with the horizon fixed at $z_h = 1$. Without this choice the temperature is given by $T = |u'(z_h)|/(4\pi) = 1/(z_h\pi)$.

[19] This entropy density can be also deduced from the grand canonical potential Ω. In AdS/CFT, the grand canonical potential is identified with T times the on-shell bulk action in Euclidean signature, see sec. 4.2 and sec. 4.3.

Energy momentum tensor and current

With the analytical RN solution at hand we can have a closer look at the energy momentum tensor and the current of the dual field theory. The energy momentum tensor $T^{\mu\nu}$, (2.101), and the current J^{μ}, (2.102), are given by

$$\langle T^{\mu\nu} \rangle = \begin{pmatrix} 24\,(3+\mu^2) & 0 & 0 & 0 \\ 0 & 8\,(3+\mu^2) & 0 & 0 \\ 0 & 0 & 8\,(3+\mu^2) & 0 \\ 0 & 0 & 0 & 8\,(3+\mu^2) \end{pmatrix}, \tag{2.132}$$

$$\langle J^{\mu} \rangle = (\rho,\, 0,\, 0, 0)\ . \tag{2.133}$$

We now see explicitly that the charge density of the dual field theory is given by $\langle J^t \rangle = \rho$ and the energy density by $U = \langle T^{tt} \rangle = 24(3+\mu^2)$. Note that the trace of the energy momentum tensor is $\langle T_{\mu}{}^{\mu} \rangle = 0$.

2.5.3. Normalisation

Since all metrics in this thesis are invariant under scale transformations $\hat{x}^m = \lambda\, x^m$, we express the results in terms of dimensionless quantities, normalised by μ. Since under scale transformations we have $\hat{\mu} = \mu/\lambda$, the relevant physical observables are

$$\begin{aligned} &\bar{k} = \frac{k}{\mu}, \qquad \bar{T} = \frac{T}{\mu}, \qquad \bar{B} = \frac{B}{\mu^2}, \qquad \bar{s} = \frac{s}{\mu^3}, \\ &\left\langle \bar{J}_{\mu} \right\rangle = \frac{\langle J_{\mu} \rangle}{\mu^3}, \qquad \bar{\Omega} = \frac{\Omega}{\mu^4}, \qquad \left\langle \bar{T}_{\mu\nu} \right\rangle = \frac{\langle T_{\mu\nu} \rangle}{\mu^4}. \end{aligned} \tag{2.134}$$

In the limit of uncharged branes $\mu \to 0$, it is more convenient to normalize μ, k and B to appropriate powers of temperature, i.e.

$$\tilde{k} = \frac{k}{T}, \qquad \tilde{\mu} = \frac{\mu}{T}, \qquad \tilde{B} = \frac{B}{T^2}\,. \tag{2.135}$$

3. Charged magnetic branes

Our goal is to study quantum field theories with a chiral anomaly at strong coupling, finite temperature, finite density, and in the presence of a (strong) magnetic background field now. In order to obtain results, we use the gauge/gravity correspondence and perform the relevant calculations in the dual gravitational description, which is given by an Einstein-Maxwell-Chern-Simons (EMCS) theory with an external magnetic field. This chapter is based on and heavily draws from [81].

In a series of papers [63, 64, 114, 117, 118] (see [65] for a review) the electrically charged Reissner-Nordström black brane in asymptotically AdS_5 spacetime was generalized to allow for a constant non-vanishing magnetic field B. Without loss of generality, we can assume that the constant magnetic field B is aligned in x_3 direction. As reviewed in the introduction, and as explicitly reproduced in sec. 3.3, the solution exhibits interesting features, such as a quantum critical point.

Previously, the QNM spectrum of this model with only the magnetic field has been studied [53], while [119, 120] computed two shear viscosities in this anisotropic system (see also [94]). Here, we shall analyze the QNM spectrum of the latter system. We solve for the background numerically using spectral methods, which we then use as input to compute the QNMs. We investigate the effects of changing external parameters: the temperature T, chemical potential μ, and the strength of the magnetic field B.

We find interesting phenomena such as the appearance of Landau levels in some cases and various other gapped modes. In the hydrodynamic regime, we compare to our field theoretical calculations provided in sec. 3.5. In particular, we provide dispersion relations for five modes in (3.23) and (3.20). Following the modes for increasing B (also beyond the hydrodynamic regime), we describe the evolution of the shear modes, see fig. 3.4, of two formerly hydrodynamic modes developing a (complex) gap, see fig. 3.5, and of three hydrodynamic modes, see fig. 3.9.

Field theory results

On the field theory side, some results were previously obtained for plasmas which are anisotropic due to a magnetic field. Anomaly-driven effects such as CME and chiral vortical effect (CVE) reveal themselves in the transport properties of a system outside of equilibrium. Hydrodynamically, chiral transport in weak magnetic fields has been considered systematically for one axial current and the energy momentum tensor in [121]. In that work, the authors provide only part of the hydrodynamic modes and impose certain restrictions. In an independent calculation we confirm a subset of their relations and amend their result as discussed in sec. 3.5. Recently, a hydrodynamic analysis similar to [121] was performed for a system containing in addition a conserved vector current [88]. The latter paper additionally considers plasma excitations propagating perpendicular to the magnetic field, while [121] and our present work focus on propagation parallel to the magnetic field. In the weak field case the chiral magnetic wave [94] appears in a certain form, as is evident from [88, 121] and from our result in sec. 3.5.

Fewer reliable hydrodynamic results are available for plasmas in strong external magnetic fields. One exception is [96] considering polarization effects in equilibria with strong external (electro)magnetic fields, generalizing [95]. An attempt at hydrodynamic constitutive relations in presence of a strong external magnetic field has been performed in [94]. The striking finding of that latter paper are the five "shear viscosities" and the two "bulk viscosities" which appear because of the broken rotational symmetry due to the magnetic field. A strong claim was conjectured in [122], where the authors argue for the chiral magnetic wave velocity to be of a particular form for any strength of the magnetic field and without taking the hydrodynamic limit. The authors also find that this velocity approaches the speed of light in the limit of large magnetic field (at weak and at strong coupling), and relate this limit behavior to Landau level physics using a weak coupling argument. In our work, we find evidence for the relation between Landau level physics and the chiral magnetic wave velocity at strong coupling.

3.1. Holographic setup

We use the holographic dictionary of sec. 2.3.5 and collect the minimal ingredients to model a charged fluid at finite temperature with AdS/CFT.

The charged magnetic black brane solutions of the EMCS equations, (2.94) and (2.95), are dual to the charged plasma of interest in a particular class of quantum field the-

ories with a chiral anomaly at strong coupling, and in the presence of a magnetic background field of any strength. Due to the presence of various scales including the temperature, the chemical potential, and the magnetic field, conformal symmetry is broken by the state of such field theories.

3.1.1. Charged magnetic black brane solutions

As we shall see below, when studying the fluctuations, it is convenient to use Eddington-Finkelstein coordinates. Working in units where the horizon of the black brane is located at $z = 1$ and the conformal boundary at $z = 0$, the metric for the charged magnetic black brane can be expressed as

$$\begin{aligned} \mathrm{d}s^2 &= \frac{1}{z^2}\left[\left(-u(z)+c(z)^2\,w(z)^2\right)\,\mathrm{d}v^2 - 2\,\mathrm{d}z\,\mathrm{d}v + 2\,c(z)\,w(z)^2\mathrm{d}x_3\,\mathrm{d}v\right. \\ &\quad \left. +v(z)^2\,\left(\mathrm{d}x_1^2+\mathrm{d}x_2^2\right)+w(z)^2\,\mathrm{d}x_3^2\right]\,, \qquad (3.1) \\ F &= A_v'(z)\,\mathrm{d}z\wedge\mathrm{d}v + B\,\mathrm{d}x_1\wedge\mathrm{d}x_2 + P'(z)\,\mathrm{d}z\wedge\mathrm{d}x_3\,. \qquad (3.2) \end{aligned}$$

The field strength tensor (3.2) may be obtained from a gauge field A of the form

$$A = A_v(z)\,\mathrm{d}v + \frac{B}{2}\,(-x_2\,\mathrm{d}x_1 + x_1\,\mathrm{d}x_2) + P(z)\,\mathrm{d}x_3\,, \qquad (3.3)$$

which is symmetric in x_1 and x_2, and points to the $SO(2)$ rotational symmetry in the (x_1, x_2)-plane.

Introducing a mangetic field B requires to extend the ansatz (2.106) of sec. 2.5. The magnetic field breaks the $SO(3)$ invariance, hence we need to allow for different functions $v(z)$ and $w(z)$ for the spatial coordinates x_1, x_2 and x_3 respectively.

Additionally we have to allow for a function $c(z)$ for the following reason: Without the function $c(z)$ it is not possible to show consistency of the constraint, as presented in sec. 2.5.1. Because of that, we have to allow for further functions in the ansatz. First we add a small contribution of order ϵ to all metric entries and study the EOM in orders of ϵ. It turns out that the EOM require $g_{v\,x_3}$ to be non zero, hence the function $c(z)$ is necessary for a consistent ansatz.

Equations of motion

Inserting the ansatz (3.1) and (3.3) into Einstein's equations (2.94), we obtain five differential equations, i.e. four second order differential equations for the metric functions $u(z)$, $v(z)$, $w(z)$ and $c(z)$ as well as one constraint, which contains only first

derivatives of the metric fields. Moreover, there are two independent equations of motion (2.95) for the gauge fields.[1] The full solution of the functions u, c, w, v, A_v, and P has to be obtained numerically. We use spectral methods in this chapter to obtain these solutions, see app. A.3 for further details.

Asymptotic Expansions

In order to solve the equations of motion for the background, we first consider the asymptotic expansion of the metric and gauge fields close to the horizon and the conformal boundary of the spacetime.[1]

Near the conformal boundary at $z = 0$, the functions appearing in (3.1) and (3.2) may be expanded as

$$\begin{aligned}
u(z) &= 1 + z^4 \left[u_4 + \mathcal{O}(z^2)\right] + z^4 \ln(z) \left[\frac{B^2}{6} + \mathcal{O}(z^2)\right] , \\
v(z) &= 1 + z^4 \left[-\frac{w_4}{2} + \mathcal{O}(z^2)\right] + z^4 \ln(z) \left[-\frac{B^2}{24} + \mathcal{O}(z^2)\right] , \\
w(z) &= 1 + z^4 \left[w_4 + \mathcal{O}(z^2)\right] + z^4 \ln(z) \left[\frac{B^2}{12} + \mathcal{O}(z^2)\right] , \\
c(z) &= z^4 \left(c_4 + \mathcal{O}(z^2) + z^4 \ln(z) \left[-\frac{B^2}{12} c_4 + \mathcal{O}(z^2)\right]\right) , \\
A_v(z) &= \mu - \frac{\rho}{2} z^2 - \frac{\gamma B p_1}{8} z^4 + \mathcal{O}(z^6) , \\
P(z) &= z^2 \left(\frac{p_1}{2} + \frac{\gamma B \rho}{8} z^2 + \mathcal{O}(z^4)\right) ,
\end{aligned} \tag{3.4}$$

where u_4, w_4, c_4, ρ, p_1 are undetermined coefficients, while B and μ are parameters determining the background solution. We have chosen the expansion at the conformal boundary such that the charged magnetic black brane is asymptotically AdS_5. Note that the leading term in $P(z)$ has been fixed such that no explicit source for a persistent current in the x_3-direction appears.

Near the horizon at $z = 1$, expansion of the same functions yields

$$\begin{aligned}
u(z) &= (1-z)\left[\bar{u}_1 + \mathcal{O}(1-z)\right] , & c(z) &= (1-z)\left[\bar{c}_1 + \mathcal{O}(1-z)\right] , \\
v(z) &= \bar{v}_0 + \mathcal{O}(1-z), & A_v(z) &= (1-z)\left[\bar{A}_{v\,0} + \mathcal{O}(1-z)\right] , \\
w(z) &= \bar{w}_0 + \mathcal{O}(1-z), & P(z) &= \bar{P}_0 + \mathcal{O}(1-z) ,
\end{aligned} \tag{3.5}$$

[1] The discussion in app. A.1 shows how to treat the more general setup of ch. 4 in Poincare-coordinates, which includes the ansatz (3.1)–(3.3) as a limiting case.

where $\bar{u}_1$, $\bar{c}_1$, $\bar{w}_0$, $\bar{v}_0$, $\bar{A}_{v0}$ and $\bar{P}_0$ are undetermined coefficients analogous to those in the near boundary expansion (3.4). Note that regularity at the horizon fixes the leading coefficients of $u(z)$, $c(z)$, and $A_v(z)$.

3.2. Thermodynamics

With the ansatz (3.1)–(3.3) at hand we can calculate the thermodynamic properties of our dual field theory, as outlined in sec. 2.5.2. Given our ansatz, the the field theory temperature T and the entropy density s read

$$T = \frac{|\bar{u}_1|}{4\pi}\,, \qquad s = 4\pi \bar{v}_0^2 \bar{w}_0\,. \tag{3.6}$$

Consequently the energy momentum tensor (2.101), and the current (2.102) are given by

$$\langle T^{\mu\nu}\rangle = \begin{pmatrix} -3\,u_4 & 0 & 0 & -4\,c_4 \\ 0 & -\frac{B^2}{4} - u_4 - 4\,w_4 & 0 & 0 \\ 0 & 0 & -\frac{B^2}{4} - u_4 - 4\,w_4 & 0 \\ -4\,c_4 & 0 & 0 & 8\,w_4 - u_4 \end{pmatrix}, \tag{3.7}$$

$$\langle J^\mu\rangle = (\rho,\, 0,\, 0,\, p_1)\ . \tag{3.8}$$

Comparing the holographic result (3.7) and (3.8) with the field theoretical expectation (2.42) and (2.43), we conclude that

$$\chi_{BB} B^2 = \langle T^{33}\rangle - \langle T^{11}\rangle = \frac{1}{4} B^2 + 12 w_4(T, \mu, B^2)\,, \tag{3.9}$$

which can be understood as a defining relation for the magnetic susceptibility coefficient χ_{BB}. This allows us to read off the charge density, the energy density and the pressure:

$$\left\langle J^t \right\rangle = \rho\,, \quad U = \left\langle T^{tt} \right\rangle = -3u_4\,, \quad P_0 = \left\langle T^{11} \right\rangle - \chi_{BB} B^2 = -u_4 + 8w_4\,. \tag{3.10}$$

Note that the trace of the energy momentum tensor is non zero

$$\langle T^\mu{}_\mu\rangle = -\frac{1}{4}\, F_{\mu\nu}\, F^{\mu\nu} = -\frac{B^2}{2}\,. \tag{3.11}$$

Moreover, combining (3.8) and (4.16)[2], we obtain a relation between $\langle J_{x_3} \rangle$ and μ of the form

$$\langle J_{x_3} \rangle = -B\,\gamma\,\mu\,. \tag{3.12}$$

This is precisely the chiral magnetic effect. Due to the chiral anomaly we also expect to find [93]

$$\langle T_{tx_3} \rangle = \frac{\gamma}{2}\,B\,\mu^2\,. \tag{3.13}$$

3.3. Quantum critical point

We now turn our attention to the charged magnetic solution constructed by D'Hoker and Kraus (DK) [63]. One must be careful with the definition of F and A within the action. Our S_{grav}, given by (2.93), coincides with Donos and Gauntlett [66], which in turn differs from the one used by D'Hoker and Kraus [63]. It is crucial to keep in mind that $F_{\text{here}} = 2F_{\text{DK}}$ and $A_{\text{here}} = 2A_{\text{DK}}$. The relevant quantities μ, ρ and B pick up this factor of 2 accordingly.

Moreover, note that D'Hoker and Kraus normalise all their dimensionful quantities by the charge density $\rho = e'(0)$. For example, the dimensionless magnetic field $\hat{B}$ is given by $\hat{B} = \dfrac{B}{\rho^{2/3}}$, whereas we consider the dimensionless magnetic field $\bar{B}$ given by $\bar{B} = \dfrac{B}{\mu^2}$. As usual, the charge density ρ and the chemical potential μ are thermodynamically conjugate. In other words, one may consider the chemical potential to be a function of the charge density or vice-versa. The choice of perspective, i.e. canonical ensemble versus grand canonical ensemble, does not affect the dynamics of the field theory.

Due to different normalisations used we have to be careful when using results from [64]. For example, we first have to translate the location $\hat{B}_{\text{C}}$ of the quantum critical point quoted in [64]. The corresponding value of $\bar{B}_{\text{C}}$ in our notation is related to $\hat{B}_{\text{C}}$ by $\bar{B}_{\text{C}} = \gamma^2 \hat{B}_{\text{C}}^3$.

For instance, for $\gamma = 1.7$ the quantum critical point is located at $\hat{B}_C \approx 0.400$ which corresponds to $\bar{B}_C \approx 0.185$ in our notation. For $\gamma = 1.5$ one obtains $\hat{B}_C \approx 0.461$ or $\bar{B}_C \approx 0.220$, respectively. The location of the quantum critical point is shown in the phase diagram fig. 4.5. In order to check our numerics and the correct normalisation we determine the behaviour of the entropy density $\bar{s}$ as a function of $\bar{T}$ close to the quantum critical point $\bar{B} \approx \bar{B}_C$. We display in fig. 3.1 the entropy $\bar{s}$ as a function

[2] This relation is obtained for the more general setup of ch. 4, which includes the charged magnetic brane solutions discussed here and thus still holds

of $\bar{T}$ for $\gamma = 1.5$. Needless to say that we reproduce the results from [63].

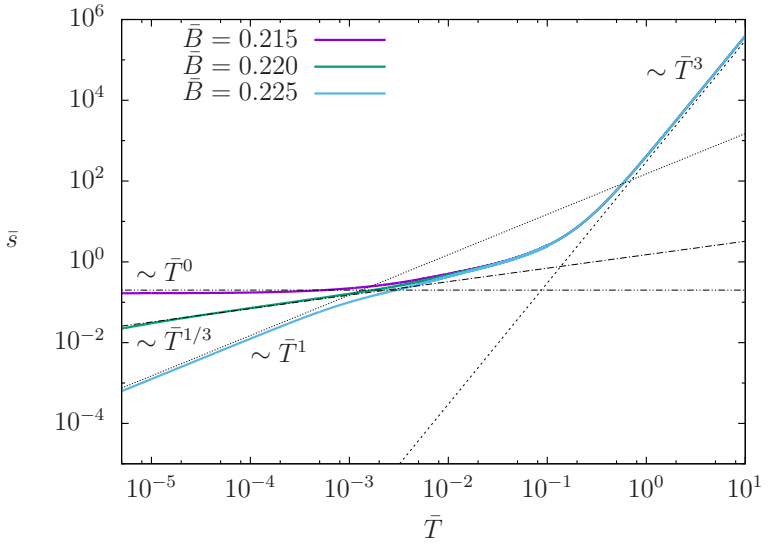

Fig. 3.1.: Entropy $\bar{s}$ as a function of the temperature $\bar{T}$ for the charged magnetic brane. For $\gamma = 1.5$ the quantum critical point is located at $\bar{B}_C \approx 0.220$ and the entropy decays as $\bar{s} \sim \bar{T}^{1/3}$. For $\bar{B} = 0.215 < \bar{B}_C$ the entropy goes to a constant in the low temperature regime, whereas for $\bar{B} = 0.225 > \bar{B}_C$ one has $\bar{s} \sim \bar{T}$. For high temperatures we find the expected behaviour $\bar{s} \sim \bar{T}^3$. All results are in agreement with [63].

A final comment concerning the behaviour of $\langle T_{tx_3} \rangle$ given the different normalisations. As numerically checked along $\bar{B} =$ constant, $\left\langle \bar{T}_{tx_3} \right\rangle = \dfrac{\langle T_{tx_3} \rangle}{\mu^4} = \dfrac{\gamma \bar{B}}{2}$ is also a constant. However, along $\hat{B}$, the left panel of fig. 3.2 shows that neither $\left\langle \bar{T}_{tx_3} \right\rangle$ nor $\left\langle \hat{T}_{tx_3} \right\rangle = \dfrac{\langle T_{tx_3} \rangle}{\rho^{4/3}}$ are constant. Yet, according to (3.7) and (3.13) the relation

$$\langle T_{tx_3} \rangle = 4\, c_4 = \frac{\gamma B}{2}\, \mu^2 \tag{3.14}$$

should still hold. We explicitly checked the validity of this expression in the right panel of fig. 3.2 for $\gamma = 1.5$ along the critical value $\hat{B} = 0.461$. In particular, the inset displays the difference $\left| 1 - \dfrac{8\, c_4}{\gamma\, B\, \mu^2} \right|$, which is limited only by the numerical round-off error.

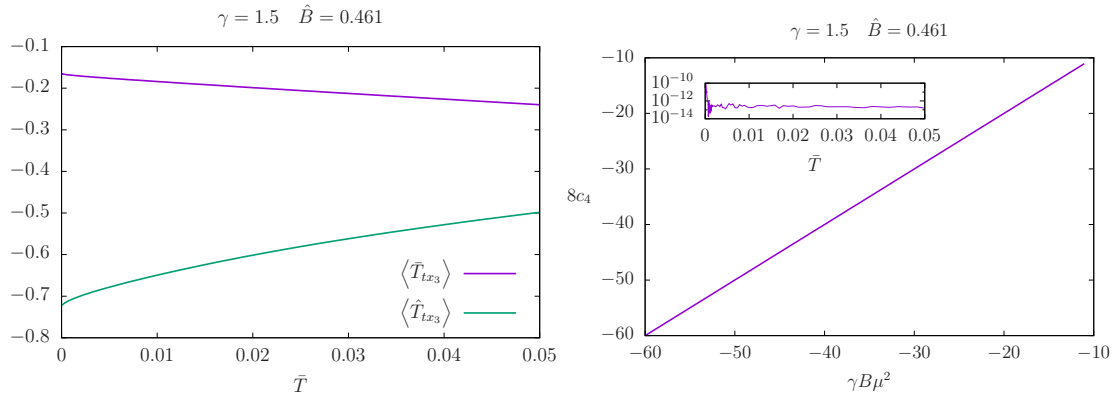

Fig. 3.2.: Component $\langle T_{tx_3} \rangle$ of the energy momentum tensor for constant dimensionless magnetic field $\hat{B}$ normalised by $\hat{B} = B/\rho^{2/3}$. Contrary to the results obtained for constant $\bar{B} = B/\mu^2$, neither $\left\langle \hat{T}_{tx_3} \right\rangle$ nor $\left\langle \bar{T}_{tx_3} \right\rangle$ are constant (left panel). Yet, the relation (3.14) is still valid (right panel).

3.4. Quasinormal modes

The dual description of transport in holography is given by QNMs, see sec. 1.3.1. At vanishing magnetic field, QNMs of charged black branes have been calculated, see [53], references and the discussion therein. Those references worked either at vanishing momentum for the fluctuations or did not consider a Chern-Simons term, i.e. in those cases effects of the anomaly remained unknown. Fluctuations about a charged black brane in presence of a Chern-Simons term but at vanishing magnetic field were considered holographically in [123, 124] in the hydrodynamic limit. Previously, that system was studied holographically in the hydrodynamic limit without the Chern-Simons term [125, 126].

In the present work, we are closing the gaps in the gravitational calculations and present a systematic study of all metric and gauge field fluctuations with nonzero momentum along the external magnetic field in a background of charged magnetic black branes in presence of a Chern-Simons term.

3.4.1. Fluctuations

We consider fluctuations of the metric, $g_{mn}(z, x^\mu)$, and the gauge field, $A_m(z, x^\mu)$, on a fixed background solution, which we denote by $\bar{g}_{mn}(z)$ and $\bar{A}_m(z)$ respectively. To derive the fluctuation equations, we write the metric and the gauge field as sums

of a background and a fluctuation part:

$$g_{mn} = \bar{g}_{mn} + \varepsilon\, h_{mn}\,, \qquad A_m = \bar{A}_m + \varepsilon\, a_m\,, \tag{3.15}$$

and we expand the equations of motion to first order in ε. It is more convenient to work in momentum space, and so we perform a Fourier transformation on the fluctuations, h_{mn} and a_m, along the spacetime coordinates of the dual field theory:

$$h_{mn}(z, x^\mu) = \int \mathrm{d}^4k\, e^{ik_\mu x^\mu}\, \tilde{h}_{mn}(z, k^\mu)\,, \qquad a_m(z, x^\mu) = \int \mathrm{d}^4k\, e^{ik_\mu x^\mu}\, \tilde{a}_m(z, k^\mu)\,, \tag{3.16}$$

where $k_\mu x^\mu = -\omega t + \vec{k}\cdot\vec{x}$. For notation simplicity, we will drop the tilde on the Fourier transformed fields from now on.

The presence of the magnetic field B defines a preferred direction. For simplicity, we shall consider only the case of the momentum k being aligned with B. We can then choose a coordinate system in which k is orthogonal to the (x_1, x_2)-plane, and the $SO(2)$ symmetry of the background is preserved. If k was not aligned with B, the $SO(2)$ would be broken by the fluctuations, and they would all be coupled together in the fluctuation equations.

Given that the $SO(2)$ stays unbroken, fluctuations may be classfied in accordance to their transformation under rotations about the x_3-axis:

Helicity	Fluctuation modes
2	h_{12}, $h_{11} - h_{22}$
1	h_{t1}, h_{13}, a_1, h_{z1}
	h_{t2}, h_{23}, a_2, h_{z2}
0	h_{tt}, h_{t3}, h_{33}, $h_{11} + h_{22}$, h_{zt}, h_{z3}, h_{zz}, a_t, a_3, a_z

The equation of motions for modes of different helicities decouple, thus each helicity sector can be treated independently.

In order to consider only the physical modes of the system, we have to fix the gauge freedom. To do so, we choose a gauge where $a_z = 0$ and $h_{mz} = 0$. The equations of motion for these fields then correspond to constraints, which are first order ordinary differential equations (ODEs). We then expect constraints to arise from the following modes:

Helicity	Constraint modes
2	none
1	h_{z1}, h_{z2}
0	h_{zt}, h_{z3}, h_{zz}, a_z

Let us consider the helicity-2 sector. The two fluctuations h_{12} and $h_{11} - h_{22}$ are decoupled from each other, and their equations of motion are identical. Next, the fluctuations within the helicity-1 sector can be further decoupled. In particular, the physical modes split into helicity-$1^{\pm}$ subsectors consisting of modes

$$a_{\pm} = a_1 \pm i a_2 \,, \quad h_{t\pm} = h_{t1} \pm i h_{t2} \,, \quad h_{3\pm} = h_{31} \pm i h_{32} \,. \tag{3.17}$$

The $\pm$ subsectors are decoupled from each other, and fluctuations of each subsector satisfy three second-order differential equations and one constraint equation. Lastly, there are six physical modes, h_{tt}, h_{t3}, h_{33}, $h_{11} + h_{22}$, a_t, a_3, in the helicity-0 sector, which satisfy six second order differential equations and four constraint equations.

In each of the three helicity sectors, the set of fluctuations is invariant under the following two transformations:

$$\mathcal{R}_1 : \begin{cases} B \mapsto -B \\ \gamma \mapsto -\gamma \end{cases} \,, \qquad \mathcal{R}_2 : \begin{cases} B \mapsto -B \\ k \mapsto -k \end{cases} \,. \tag{3.18}$$

Under the transformation $\mathcal{R}_1$, all other parameters such as μ, T, and k, as well as the background fields remain unchanged. The equations of the helicity-2 and helicity-0 sectors are invariant under $\mathcal{R}_1$, while the equations of the helicity-$1^{\pm}$ subsectors are mapped into each other.

Under $\mathcal{R}_2$, the sign flips in the background functions $c(z)$ and $P(z)$ as can be seen from their near boundary expansions in (3.4) given (3.12) and (3.13); all fluctuations with one leg in the x_3-direction also flip their signs. The equations of the helicity-2 and helicity-0 sectors then stay invariant under $\mathcal{R}_2$ (up to an overall sign flip), while the helicity-$1^{\pm}$ subsectors are again mapped into each other.

3.4.2. Quasinormal modes and numerical details

Since we consider QNM corresponding to retarded Greens functions we impose incoming boundary conditions at the horizon of the brane. With the black brane solution written in Eddington-Finkelstein coordinates, incoming boundary conditions are imposed by requiring regularity at the horizon. Because QNMs do not source any dual operators, at the conformal boundary we have to set the non-normalizable modes to zero.

In order to find the QNMs, we have to find the QNM frequency ω for which there is a non-trivial regular solution to the fluctuation equations, subject to the

boundary conditions mentioned above. This problem can be recast into a generalized eigenvalue problem for ω.[3,4] In particular, in each helicity sector the resulting second order differential equations may be schematically written as

$$\Big(A[\bar{g}_{mn}, \bar{A}_m, \partial_z, k] + \omega\, B[\bar{g}_{mn}, \bar{A}_m, \partial_z, k]\Big) \begin{pmatrix} h_{mn}(z) \\ a_m(z) \end{pmatrix} = 0\,, \tag{3.19}$$

where A and B are differential operators involving the background fields, $\bar{g}_{mn}$ and $\bar{a}_m$, derivatives with respect to z, and the momentum k.

The generalized eigenvalue problem can be solved numerically by using spectral methods, in which the differential operators, A and B, are represented by matrices, $\hat{A}$ and $\hat{B}$. The QNM frequencies are then the generalized eigenvalues associated with these differential matrices, and the QNM functions the corresponding eigenvectors. Below, we will use the QNM functions to check explicitly whether the constraint equations are satisfied in the helicity-1 and helicity-0 sectors. For more details, we refer to app. A.3.

3.5. Hydrodynamic results

In this section, we present expressions for the location of the poles of retarded correlation functions of the energy momentum tensor $T^{\alpha\beta}$, and the axial current J^μ, in the hydrodynamic approximation. These poles are identified with the lowest lying QNMs of the corresponding gravitational fields via the gauge/gravity correspondence. Hence, this section will serve to predict the QNM frequencies at small frequency values and small momenta.

Poles in helicity-1 sector

There are two poles in the correlation functions of the helicity-1 components of the energy momentum tensor $T^{\mu\nu}$ and the axial current J^μ, located at

$$\begin{aligned} \omega \;=\; & \mp\frac{Bn_0}{\epsilon_0+P_0} - ik^2\frac{\eta}{\epsilon_0+P_0} + k\frac{Bn_0\xi_3}{(\epsilon_0+P_0)^2} - \frac{iB^2\sigma}{\epsilon_0+P_0} \\ & \pm k^3\frac{i\eta\xi_3}{(\epsilon_0+P_0)^2} \mp k^2B\frac{n_0\xi_3^2}{(\epsilon_0+P_0)^3} \pm kB^2\frac{i\sigma\xi_3}{(\epsilon_0+P_0)^2} + \mathcal{O}(\partial^3)\,, \end{aligned} \tag{3.20}$$

[3] For a method to compute the residues using spectral methods see [127].

[4] In the helicity-zero sector, there are terms quadratic in ω in the fluctuation equations. However, as explained in app. A.3, by introducing auxiliary fields we can still transform the problem into the linear form shown in (3.19).

which originates from the two solutions

$$\omega = -\frac{\pm B n_0 + i k^2 \eta + i B^2 \sigma}{\epsilon_0 + P_0 \pm k \xi_3}\,, \tag{3.21}$$

when expanded in k and B. The second line in (3.20) is third order in B and k, and it will receive corrections from second order contributions to the constitutive equations. It is remarkable that in the limit of $B = 0$, explicit numerical checks confirm that the k^3-term in the pole does not appear to receive any corrections from terms of second order in the constitutive relations in the RN case. In that case (3.20) reduces to

$$\omega \;=\; -ik^2 \frac{\eta}{\epsilon_0 + P_0} \pm k^3 \frac{i\eta\xi_3}{(\epsilon_0 + P_0)^2} + \mathcal{O}(\partial^3)\,, \tag{3.22}$$

which is the standard charge diffusion k^2 term plus a contribution from the anomaly. This expression is in agreement with the holographic result [123, 124]. Note that this k^3-term in equation (3.20) is not present in Landau frame at first order in the derivative expansion as it originates from the heat current contribution q^μ in the energy momentum tensor in the thermodynamic frame.

Poles in helicity-0 sector

For convenience, we define first some useful notation: $w_0 = \epsilon_0 + P_0$ is the enthalpy density, $\mathfrak{s}_0 = s_0/n_0$ is the entropy per particle, $c_s^2 = (\partial P/\partial \epsilon)_{\mathfrak{s}}$ is the speed of sound, $\tilde{c}_n = T_0(\partial \mathfrak{s}/\partial T)_n$ and $\tilde{c}_P = T_0(\partial \mathfrak{s}/\partial T)_P$ are the specific heats at constant density and pressure respectively[5], and $\alpha_P = -(1/n_0)(\partial n/\partial T)_P$ is the thermal expansivity at constant pressure.

There are three poles in the helicity-0 sector:

$$\omega_0 = v_0\, k - i D_0\, k^2 + \mathcal{O}(\partial^3)\,, \tag{3.23}$$

$$\omega_+ = v_+\, k - i \Gamma_+\, k^2 + \mathcal{O}(\partial^3)\,, \tag{3.24}$$

$$\omega_- = v_-\, k - i \Gamma_-\, k^2 + \mathcal{O}(\partial^3)\,. \tag{3.25}$$

For the generalized diffusion pole, which we refer to as a chiral magnetic wave pole

[5]Note that this definition of the specific heat at constant pressure is different from that in [121] by a factor of the charge density n_0.

from now on, we have

$$v_0 = \frac{2B\,T_0}{\tilde{c}_P n_0}\left(\tilde{C} - \frac{\gamma}{2}\mathfrak{s}_0^2\right), \qquad D_0 = \frac{w_0^2\,\sigma}{\tilde{c}_P n_0^3 T_0}, \tag{3.26}$$

where D_0 is the generalized diffusion coefficient. For the generalized sound poles, we have

$$v_\pm = \pm c_s - B\,\frac{c_s^2}{n_0}\left(1 - \frac{\alpha_P w_0}{\tilde{c}_P n_0}\right)\left[\frac{\gamma}{2}T_0\mathfrak{s}_0 + \frac{\alpha_P T_0^2}{\tilde{c}_P}(\tilde{C} - \frac{\gamma}{2}\mathfrak{s}_0^2) + \frac{1}{2}\xi_B^{(0)} - \frac{n_0}{w_0}\xi_V^{(0)}\right] + B\,\frac{1-c_s^2}{w_0}\,\xi_V^{(0)}, \tag{3.27}$$

$$\Gamma_\pm = \frac{3\zeta + 4\eta}{6w_0} + c_s^2\,\frac{w_0\,\sigma}{2n_0^2}\left(1 - \frac{\alpha_P w_0}{\tilde{c}_P n_0}\right)^2. \tag{3.28}$$

In the limit of vanishing magnetic field $B = 0$, the RN-limit, we have $\zeta = 0$ [6] and thus obtain

$$v_0 = 0\,, \qquad D_0 = \frac{w_0^2\,\sigma}{\tilde{c}_P n_0^3 T_0}\,, \qquad v_\pm = \pm c_s\,, \qquad \Gamma_\pm = \frac{2\eta}{3w_0}\,. \tag{3.29}$$

In the limit of vanishing charge density, $n_0 = 0$, the generalized diffusion and sound poles are given by

$$v_0 = -\frac{B\gamma}{\chi}\,, \qquad D_0 = \frac{\sigma}{\chi}\,, \qquad v_\pm = \pm c_s + B\,\frac{1-c_s^2}{w_0}\,\xi_V^{(0)}\,, \qquad \Gamma_\pm = \frac{3\zeta+4\eta}{6w_0}\,. \tag{3.30}$$

Note that in the case $n_0 = 0$, we have $d\epsilon = Tds$ and $dP = sdT$, and hence the speed of sound is given by $c_s^2 = \partial P/\partial\epsilon = (\partial P/\partial T)/(\partial\epsilon/\partial T)$.

3.6. Quasinormal mode results

We determine the frequencies $\omega(k)$ for the QNMs in all three helicity sectors. Of particular interest are QNMs corresponding to hydrodynamic modes which satisfy $\omega(k) \to 0$ for $k \to 0$ and modes corresponding to long-lived quasi-particles with $\mathrm{Im}(\omega)$ being small.

As discussed above, the sets of fluctuation equations are invariant under the transformations $\mathcal{R}_{1,2}$, (3.18). We can use these two transformations to restrict ourselves to positive values of γ and B. The momentum k of the QNM is taken to be real.

[6] Conformal symmetry is not broken explicitly in the dual field theory. It is only broken at the level of the state.

3.6.1. Helicity-2 sector

First, let us consider the helicity-2 sector. In order to find the QNM frequencies, we rewrite the ordinary differential equation for h_{12} in terms of a generalized eigenvalue problem and represent the derivatives and background fields using spectral methods. To obtain a good convergence of the QNM frequencies, we had to use of order $N = 100$ Chebyshev polynomials.[7] of the QNM frequencies. The number of QNMs we can trust depends highly on the values $\tilde{B}$ and $\tilde{\mu}$ characterizing the background as well as $\tilde{k}$ which specifies the momentum of the QNM.

For example, in fig. 3.3 we show the lowest lying QNMs for $\tilde{\mu} = 10$ and $\tilde{B} = 65$ (corresponding to $\bar{T} = 0.1$ and $\bar{B} = 0.65$). The momentum varies from $\tilde{k} \in [0, 20]$ and we have chosen equidistant values for $\tilde{k}$ in the figure. The convergence plots for

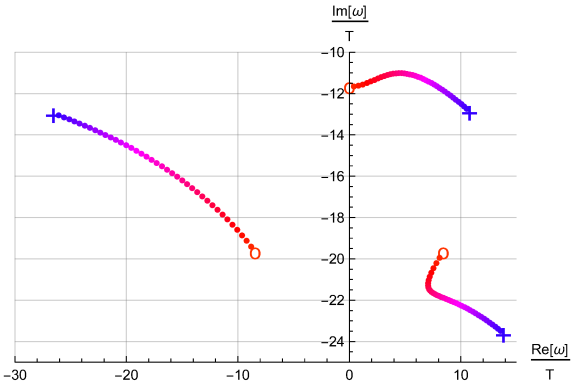

Fig. 3.3.: Three lowest helicity-2 QNMs for $\tilde{\mu} = 10, \tilde{B} = 65$ and $\gamma = 3/2$. The momentum $\tilde{k}$ varies from $\tilde{k} = 0$ (denoted by a circle) to $\tilde{k} = 20$ (denoted by a cross).

these QNMs are shown in app. A.3. In particular, we conclude that we can trust the values of the QNM frequencies up to 10^{-7}.

For large magnetic fields, the QNMs are more sensitive to $\tilde{k}$, and some of them approach the real frequency axis. Moreover, we see that in the extremal limit $T \to 0$, the QNMs coalesce along the imaginary axis, presumably forming a branch cut for the exact extremal case, as was discussed already in [53]. This would be analogous to the near-extremal AdS_4 case studied thoroughly in [128, 129].

[7] The convergence is discussed in app. A.3. In order to improve accuracy, we use a mapping $z \mapsto z^2$. This mapping improves the convergence of the QNM frequencies and avoids the observed oscillatory behavior of the QNM frequency as a function of N. See app. A.3 for more details.

Moreover, we observe that some of the QNMs approach the imaginary axis for very large magnetic fields $\tilde{B}$. This holds at zero as well as at finite chemical potential μ. In fig. 3.4 we show two of these modes for magnetic branes,[8] i.e. with $\mu = 0$.

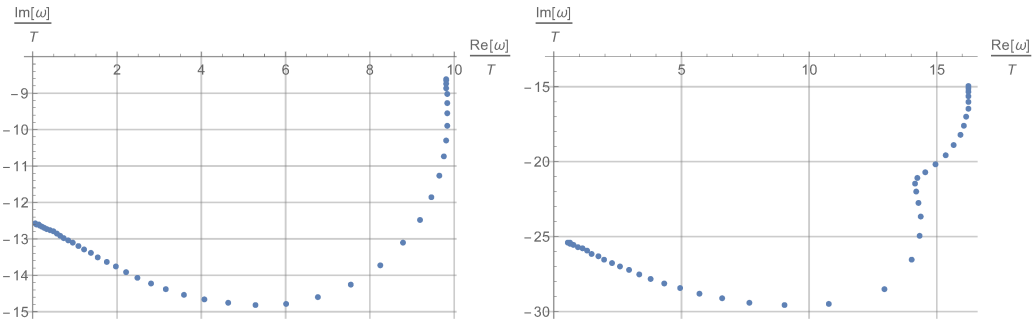

Fig. 3.4.: Two helicity-2 QNMs of the magnetic black brane, i.e. with $\mu = 0$, $\tilde{k} = 0$, for B from 0 to 9 in equidistant steps of $\Delta B = 0.2$. The value $B = 9$ corresponds to $\tilde{B} \sim 3 \cdot 10^4$.

3.6.2. Helicity-1 sector

Next we consider the helicity-1 sector which is of particular interest since the Chern-Simons coupling constant enters explicitly in the fluctuation equations. As explained above, the helicity-1 sector contains two decoupled subsectors, denoted by helicity-1^+ and helicity-1^-. Both sectors consists of three second order ordinary differential equations as well as one constraint. We reformulate the three second order equations in terms of a generalized eigenvalue problem.

We show in fig. 3.5 the lowest lying QNMs for $\tilde{\mu} = 10$ and $\tilde{B} = 65$ (corresponding to $\bar{T} = 0.1$ and $\bar{B} = 0.65$). The momentum varies over $\tilde{k} \in [0, 20]$ and we have chosen equidistant values for $\tilde{k}$. In fig. 3.5 we find in each sector one QNM which does not move with $\tilde{k}$ and is located at $\omega = -2\pi i n T$ with $n \in \mathbb{N}$. These are fake QNMs satisfying the three coupled second order differential equations, but not the constraint. See app. A.3 for a discussion of fake QNMs. From now on, we will discard these modes.

[8] This result is in agreement with [53], in particular fig. 12, where their numerical results were inconclusive at those large magnetic field values.

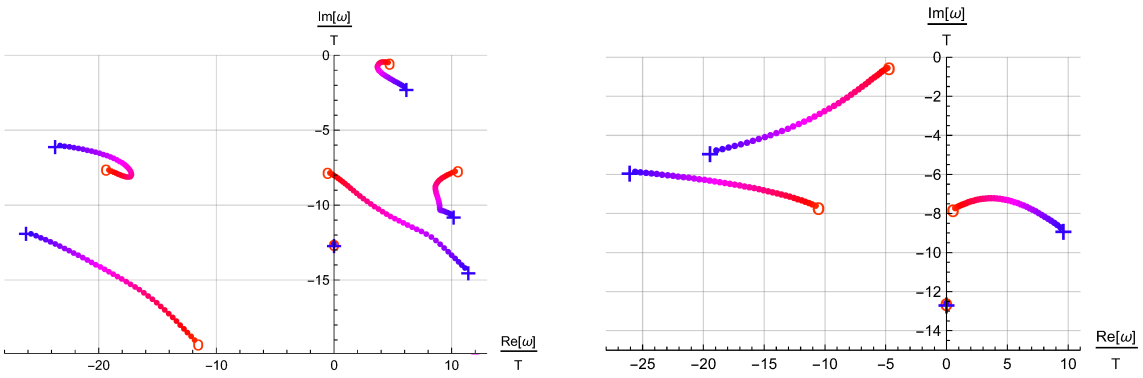

Fig. 3.5.: Lowest QNMs in the helicity-1^+ (left) and helicity-1^- (right) sector. In particular, we find two fake QNMs which do not depend on $\tilde{k}$. The momentum varies from $\tilde{k} = 0$ (denoted by a circle) to $\tilde{k} = 20$ (denoted by a cross). The remaining parameters are chosen like in fig. 3.3.

Hydrodynamic modes

Let us first discuss the hydrodynamic modes in the helicity-1 sector. For vanishing magnetic field, $B = 0$, we find two ungapped hydrodynamic QNMs, which can be identified as the momentum diffusion modes. In presence of the anomaly a term of third order in momentum k affects the momentum diffusion as was already discovered in holographic models [123, 124], whereas we clarify the field theoretical origin of this term in sec. 3.5. In the case of $B \neq 0$, the QNMs are gapped, i.e. their dispersion relations satisfy $\omega(k) \neq 0$ for $k \to 0$. However, it is remarkable that we are still able to find agreement with hydrodynamics, at least for small magnetic fields B, as we explain below. In particular, analyzing the numerical QNMs for small $k \ll 1$, we can fit our results to the hydrodynamic predictions.

For the numerical data, we use backgrounds with fixed temperature $\bar{T} = 0.2$ and magnetic field B and scan the momentum k from zero to one. We then perform a polynomial fit to the real- and imaginary part of the QNMs respectively. The upper limit for the fit range of k, denoted by k_{max}, is chosen such that the coefficients of the fit polynomials do not change when lowering k_{max}.

We take the helicity-1^- sector to be exemplary for helicity-1. We split our analysis in real and imaginary part of the hydrodynamics and numerical results for QNMs, respectively. In fig. 3.6 we show an example for a polynomial fit to the imaginary part of the dispersion relation of the lowest QNM in the helicity-1^- sector for $\bar{T} = 0.2$ and $B = 1$. For small k, the imaginary part of the dispersion relation is fitted by the polynomial $\mathrm{Im}(\omega) = -0.054 - 0.0034k - 0.18k^2 - 0.031k^3$. The coefficients of the fit are also displayed in Table 3.1. For larger k, the third-order polynomial fit

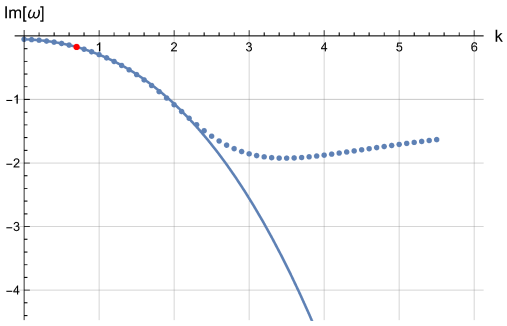

Fig. 3.6.: Comparison of a polynomial fit to the imaginary part of the dispersion relation of the lowest QNM in the helicty-1^- sector for $\bar{T} = 0.2$, $B = 1$ and $\gamma = 3/2$.

highly deviates from the imaginary part of the QNM dispersion relation, see fig. 3.6. We compare the coefficients of the fit polynomial to the hydrodynamic prediction of the dispersion relation at weak B

$$\begin{aligned}\omega \;=\; & \mp\frac{Bn_0}{\epsilon_0+P_0} - ik^2\frac{\eta}{\epsilon_0+P_0} + k\frac{Bn_0\xi_3}{(\epsilon_0+P_0)^2} - \frac{iB^2\sigma}{\epsilon_0+P_0} \\ & \pm k^3\frac{i\eta\xi_3}{(\epsilon_0+P_0)^2} \mp k^2B\frac{n_0\xi_3^2}{(\epsilon_0+P_0)^3} \pm kB^2\frac{i\sigma\xi_3}{(\epsilon_0+P_0)^2} + \mathcal{O}(\partial^3)\,, \end{aligned} \tag{3.31}$$

as discussed in sec. 3.5. In (3.31) we have included some terms of third order, but not all of them, as indicated by $\mathcal{O}(\partial^3)$. Note that the energy density ϵ_0, the pressure P_0, the charge density n_0 as well as transport coefficients such as the shear viscosity η and the conductivity σ enter the prediction from hydrodynamics. While the energy density and the pressure can be determined from the numerical background solutions, the transport coefficients are not known explicity for our setup. Hence, we approximate the transport coefficients for the charged magnetic brane by its values for zero magnetic field, i.e. for RN black brane. In particular, we use $\eta/s = 1/(4\pi)$ and $\sigma = (\mu^2-6)^2/(4(\mu^2+3)^2)$ [123, 126]. This additional approximation is justified for small enough magnetic field B.

With increasing magnetic field B we can clearly track the disagreement between hydrodynamic prediction and numerics. The breakdown for increasing B shows the limits of both of our assumptions: weak field hydrodynamics and the RN approximation for the transport coefficients.

First, we show the imaginary part of the dispersion relation in Table 3.1. We display the fit coefficients and the corresponding hydrodynamic predictions for different B, comparing order by order in k. In particular, we find good agreement for the zeroth, second and third order in k up to surprisingly large B. Also at nonzero

B, the aforementioned k^3-term arises in presence of the anomaly and is approximating the numerical data surprisingly well. The first order in k does not fit as expected, because we have not taken into account all contributions of $\mathcal{O}(\partial^3)$ in our hydrodynamic expansion.

B	$-\frac{B^2\sigma}{P_0+\epsilon_0}$	fit_{QNM}	$\frac{B^2 k\xi_3\sigma}{(P_0+\epsilon_0)^2}$	fit_{QNM}	$-\frac{\eta k^2}{P_0+\epsilon_0}$	fit_{QNM}	$\frac{\eta k^3\xi_3}{(P_0+\epsilon_0)^2}$	fit_{QNM}
0	0	$3.8\cdot10^{-6}$	0	−0.000071	−0.17	−0.17	−0.025	−0.024
0.1	−0.00044	−0.00044	−0.000065	−0.00040	−0.17	−0.17	−0.025	−0.024
0.2	−0.0018	−0.0018	−0.00026	−0.0014	−0.17	−0.17	−0.025	−0.024
0.3	−0.0040	−0.0040	−0.00058	−0.0030	−0.17	−0.17	−0.025	−0.025
0.4	−0.0070	−0.0073	−0.0010	−0.0053	−0.17	−0.17	−0.025	−0.025
0.5	−0.011	−0.012	−0.0016	−0.0084	−0.17	−0.17	−0.025	−0.026
0.6	−0.016	−0.017	−0.0024	−0.012	−0.17	−0.17	−0.025	−0.027
0.7	−0.022	−0.024	−0.0032	−0.017	−0.17	−0.17	−0.025	−0.028
0.8	−0.029	−0.032	−0.0042	−0.022	−0.17	−0.17	−0.025	−0.029
0.9	−0.036	−0.042	−0.0054	−0.028	−0.17	−0.17	−0.025	−0.030
1.0	−0.045	−0.054	−0.0067	−0.034	−0.17	−0.18	−0.025	−0.031

Table 3.1.: Imaginary part of the dispersion relation of the hydrodynamic mode in the helicity-1^- sector for $\bar{T} = 0.2$ and $\gamma = 3/2$. Here we display the coefficients expected from hydrodynamics and from the polynomial fit to the imaginary part of the dispersion relation of the lowest QNM.

Second, we consider the real part of the dispersion relation of the lowest QNM in Table 3.2. The zeroth and first order coefficients in k are well described by our prediction from hydrodynamics. Note that these coefficients can be calculated exactly with the numerical background without approximating transport coefficients, and hence tests only the weak field approximation within our hydrodynamics. Both give very good agreement with the data up to relatively large B. The second order in k does not fit the data, again due to unknown $\mathcal{O}(\partial^3)$ contributions in the hydrodynamic approximation. The third order in k is predicted to be zero in $\mathcal{O}(\partial^2)$ hydrodynamics, while our numerical data indicates a k^3-term increasing monotonically with the magnetic field B.

Long-lived modes

Besides the hydrodynamic modes, it is important to characterize other long-lived modes with a small imaginary part in the dispersion relation for large magnetic fields.

B	$\frac{-Bn_0}{P_0+\epsilon_0}$	fit_{QNM}	$\frac{Bkn_0\xi_3}{(P_0+\epsilon_0)^2}$	fit_{QNM}	$\frac{-Bk^2n_0\xi_3^2}{(P_0+\epsilon_0)^3}$	fit_{QNM}	k^3	fit_{QNM}
0	0	0	0	0	0	0	0	0
0.1	−0.041	−0.041	−0.0060	−0.0060	−0.00089	−0.0044	0	−0.00039
0.2	−0.081	−0.081	−0.012	−0.012	−0.0018	−0.0089	0	−0.00081
0.3	−0.12	−0.12	−0.018	−0.018	−0.0027	−0.014	0	−0.0013
0.4	−0.16	−0.16	−0.024	−0.024	−0.0036	−0.018	0	−0.0019
0.5	−0.20	−0.20	−0.030	−0.030	−0.0045	−0.023	0	−0.0027
0.6	−0.25	−0.24	−0.036	−0.035	−0.0054	−0.029	0	−0.0037
0.7	−0.29	−0.28	−0.043	−0.041	−0.0063	−0.035	0	−0.0049
0.8	−0.33	−0.32	−0.049	−0.047	−0.0073	−0.041	0	−0.0066
0.9	−0.37	−0.36	−0.055	−0.053	−0.0082	−0.048	0	−0.0088
1.0	−0.41	−0.40	−0.062	−0.059	−0.0092	−0.055	0	−0.012

Table 3.2.: Real part of dispersion relation versus polynomial fit to the lowest QNM for $\bar{T} = 0.2$ and $\gamma = 3/2$.

For $\gamma > \gamma_c \approx 4$, we find long-lived modes in the limit of large magnetic fields.[9] In particular, we find that the real part of the QNM dispersion relation is proportional to $\sqrt{B}$ for large magnetic fields, see fig. 3.7. Moreover, for $\gamma > \gamma_c$, the imaginary part of these QNMs stays small for large B. Hence these QNMs are alongside the hydrodynamic modes the longest-lived modes. For example, for $\gamma = 5 > \gamma_c$, the imaginary part of this QNM at $\tilde{B} \approx 5 \cdot 10^3$ is smaller than $|\text{Im}\,(\tilde{\omega})| < 10$, while the imaginary part of all other QNMs is much larger.

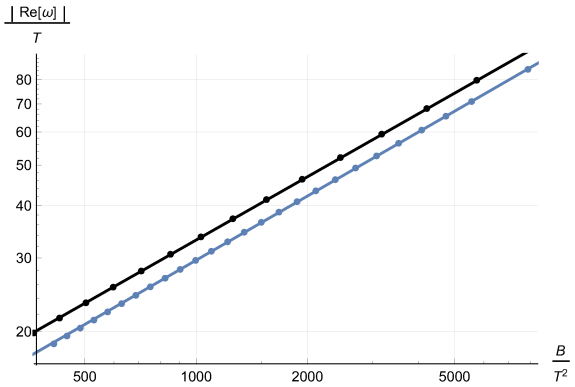

Fig. 3.7.: Real part of a QNM versus the magnetic field for $\mu = 1$, $\tilde{k} = 0$, and $\gamma = 3/2$ (blue line) as well as $\gamma = 5$ (black line), respectively. In particular, we find that $\text{Re}(\omega) \propto \sqrt{B}$ for both values of γ.

[9] In [127], with a different convention for the Chern-Simons coupling $\kappa = \gamma/8$, the critical value of κ was determined numerically to be $1/2$ for helicity-0 QNMs; consistently, we have $\gamma_c = 4$ for $\mu = 0$.

In contrast to that, for $\gamma < \gamma_c$, the imaginary part of the QNMs for these modes diverges for large B and they are not the longest lived modes in our system. However, the real part of the dispersion relation is still proportional to $\sqrt{B}$ for large magnetic fields B.

3.6.3. Helicity-0 sector

Finally, we discuss the helicity-0 QNMs and their frequencies. Note that like in the helicity-1 sector, the Chern-Simons coupling γ also appears explicitly in the equations of motion of the helicity-0 sector.

In fig. 3.8 we display the four lowest QNMs in the helicity-0 sector for $\tilde{\mu} = 10$ and $\tilde{B} = 65$. The momentum varies from $\tilde{k} = 0$ to $\tilde{k} = 20$, while the Chern-Simons coupling is $\gamma = 3/2$. In particular, we identify three hydrodynamic modes and one fake mode. Two of these modes originate from the well-known sound modes and the third one originates from the charge diffusion mode. Note that these three modes stay hydrodynamic modes at $B \neq 0$, i.e. they remain gapless.

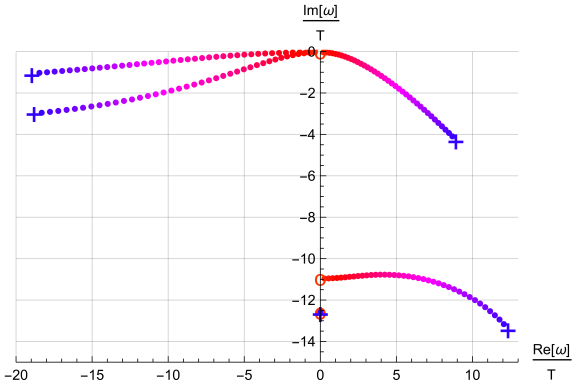

Fig. 3.8.: Lowest four QNMs in the helicity-0 sector as well as one fake mode. The momentum $\tilde{k}$ varies from $\tilde{k} = 0$ (denoted by a circle) to $\tilde{k} = 20$ (denoted by a cross). The remaining parameters are chosen like in fig. 3.3.

Hydrodynamic modes

For the three hydrodynamic QNMs identified, we perform again a fit in k to the numerical results for the QNM dispersion relation of the form

$$\omega_0 = v_0\, k - i D_0\, k^2\,, \qquad \omega_\pm = v_\pm\, k - i\Gamma_\pm\, k^2\,. \tag{3.32}$$

In particular, we find that one of the modes, e.g. ω_0, is purely diffusive for $B = 0$, in agreement with analytical results for the RN case and with the hydrodynamic

predictions summarized in sec. 3.5. This agreement with hydrodynamics holds even for small magnetic fields B as we discuss now. Taking the hydrodynamic prediction for the diffusion constant D_0 and sound velocity v_0, see (3.26), together with the RN approximation for the thermodynamic quantities such as entropy density and the enthalpy, as well as for the conductivity we get

$$v_0 = -\frac{B\gamma}{4}\frac{6+\mu^2}{3+\mu^2}\,, \qquad D_0 = \frac{6+\mu^2}{12+4\mu^2}\,. \tag{3.33}$$

We compare this hydrodynamic prediction, approximated by RN thermodynamics, to the fit data of the dispersion relation of the QNM and obtain very good agreement up to $B = 0.3$ as it is evident from the table:

B	0.	0.1	0.2	0.3	0.4	0.5	0.6	0.7	0.8	0.9
D_0	0.418	0.418	0.418	0.418	0.418	0.418	0.418	0.418	0.419	0.419
fit	0.418	0.415	0.407	0.393	0.375	0.353	0.328	0.302	0.275	0.248
$-v_0$	0.	0.063	0.126	0.188	0.251	0.314	0.377	0.439	0.502	0.565
$-$fit	0.	0.063	0.126	0.187	0.246	0.303	0.356	0.406	0.451	0.491

The same computation can be done for the hydrodynamic modes $\omega_\pm$. Using the hydrodynamic prediction (3.27), and again approximating by thermodynamic expressions of RN black branes, we get

$$v_\pm = \pm\frac{1}{\sqrt{3}} + B\frac{\xi_V}{6+2\mu^2}\,, \qquad \Gamma_\pm = \frac{1}{6+2\mu^2}\,. \tag{3.34}$$

Comparing this to the real part of the first order in k fit coefficient yields

B	0.	0.1	0.2	0.3	0.4	0.5	0.6	0.7	0.8	0.9
$-v_-$	0.577	0.59	0.602	0.614	0.626	0.639	0.651	0.663	0.675	0.687
$-$fit	0.577	0.59	0.603	0.616	0.629	0.643	0.657	0.672	0.687	0.704
v_+	0.577	0.565	0.553	0.541	0.528	0.516	0.504	0.492	0.48	0.467
fit	0.577	0.565	0.554	0.543	0.533	0.523	0.515	0.507	0.501	0.497
$\Gamma_\pm$	0.112	0.112	0.112	0.112	0.112	0.112	0.112	0.112	0.112	0.112
fit$_-$	0.112	0.112	0.112	0.113	0.113	0.113	0.113	0.114	0.114	0.114
fit$_+$	0.112	0.112	0.112	0.113	0.113	0.113	0.114	0.114	0.113	0.112

which is again in good agreement up to $B = 0.3$.

The holographic calculation reveals also some interesting properties for hydro-

dynamics at strong magnetic fields. For any value of the magnetic field, we find three hydrodynamic modes ω_0 and $\omega_\pm$. Let us first consider the imaginary part of each dispersion relation, i.e. $\Gamma_\pm$ and D_0. At weak B we conclude in (3.27) that the attenuations are the same for the sound modes $\omega_\pm$, i.e. $\Gamma_+ = \Gamma_-$. This, however, is not true for strong B, as can be seen in fig. 3.9. For $B \gtrsim 1$, we see that $\Gamma_+ \neq \Gamma_-$. In particular, the figure suggests that Γ_+ approaches zero for large enough magnetic fields, while Γ_- first approaches D_0, before both approach zero together. From the real part of the dispersion relation we can read off the sound velocities $v_\pm$ and v_0. If we treat the magnetic field of order derivative, the velocities v_+ and v_- satisfy $v_+ - v_- = 2c_s = 2/\sqrt{3}$. This is indeed the case as we can see from fig. 3.9. However, for magnetic fields $B \gtrsim 1$, we clearly see deviations from it. It appears that v_- approaches v_0 in the limit of large magnetic fields. While performing the fit, we noticed that a term linear in k is sufficient to fit the real part of the frequency, and a term quadratic in k is sufficient to obtain a reliable fit for the imaginary part up to fairly large values of $B \approx 8$. While we show the evolution of velocities and attenuations for $\gamma = 3/2 < \gamma_c$ in fig. 3.9, we have checked that their behavior does not change significantly when we perform the same calculation for $\gamma = 5 > \gamma_c$.

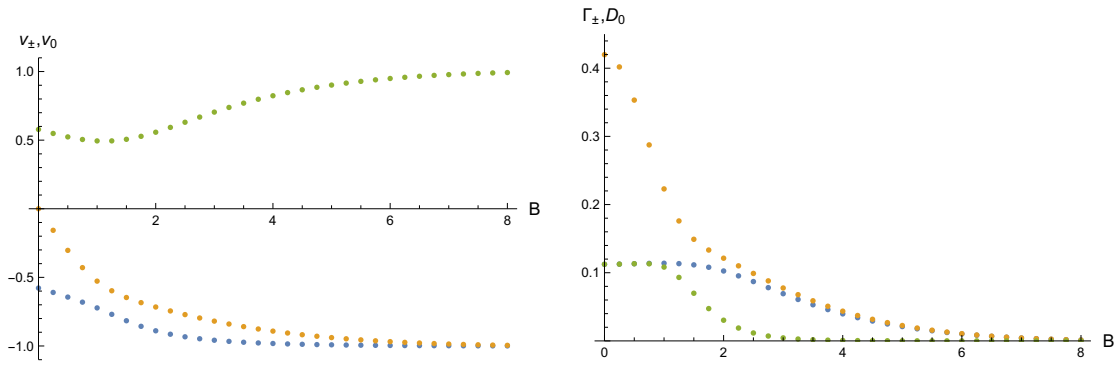

Fig. 3.9.: The velocities v_0 (orange), v_+ (green), v_- (blue) and the attenuation coefficients D_0 (orange), Γ_+ (green), Γ_- (blue) for the three hydrodynamic modes in the helicity-0 sector as a function of B and with a Chern-Simons coupling $\gamma = 3/2 < \gamma_c$.

One of the helicity-0 modes (the former charge diffusion mode) turns into a chiral magnetic wave mode [122][10] with velocity v_0 and attenuation D_0 displayed from zero to large B in fig. 3.9. At large magnetic field the chiral magnetic wave velocity

[10] [122] works with an axial and a vector current, defining the chiral magnetic wave as an excitation that involves a coupling between axial and electric charge. In this present work we have only one current and thus only one charge, namely the axial one. Nevertheless, the hydrodynamic dispersion relations of the relevant excitations are identical as can be seen from sec. 3.5.

asymptotes to $v_0 = 1$, i.e. to the magnitude of the speed of light. This is particularly intriguing as that same chiral magnetic wave QNM shows Landau level behavior at large magnetic field, i.e. the real part of the frequency is proportional to $\sqrt{B}$ and the imaginary part asymptotes to zero. This provides evidence at strong coupling for the relation between Landau level occupation and the large B behavior of v_0. That relation was proposed by Kharzeev and Yee in [122] based on weak coupling reasoning. This can also be understood as supporting Kharzeev and Yee's conjecture that the form of the chiral magnetic velocity is valid at arbitrary B.

Long-lived modes: Landau Levels in the helicity-0 sector

Besides the hydrodynamic modes, we find other modes which are long-lived in particular for large magnetic fields. These modes behave similarly to Landau levels, as discussed in [127] for a similar model. As in the helicity-1 sector, we identify QNMs whose real part scales as $\sqrt{B}$ for large magnetic fields as can be seen from the left panel of fig. 3.10. In particular, we find that for $\mu = 0.01$, the real part of the dispersion relation of the two next-to-lowest Landau levels may be fitted by $\mathrm{Re}(\omega) \sim \pm 1.8\sqrt{B}$ and $\mathrm{Re}(\omega) \sim \pm 2.2\sqrt{B}$ for large magnetic fields B.

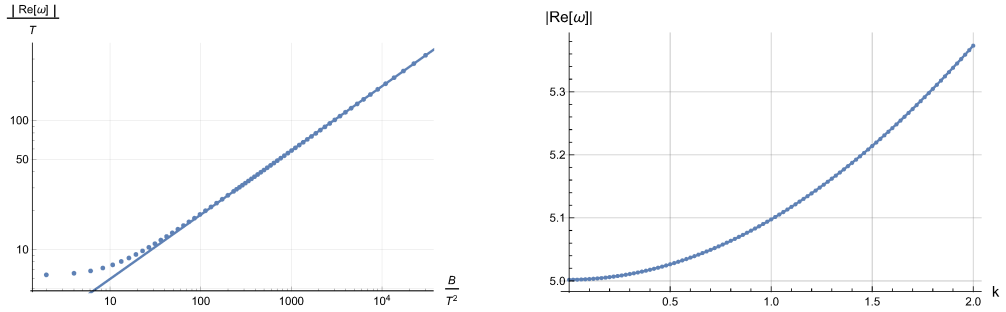

Fig. 3.10.: Left panel: real part of dispersion relation versus $\tilde{B}$ for $\mu = 0.01$. We can identify the expected $\sqrt{B}$ behaviour; Right panel: k dependence of the real part of ω for $B = 7.4$ for the next-to-lowest Landau level. The numerical data is fitted best by $\mathrm{Re}(\omega) = 0.98\sqrt{(5.1)^2 + k^2}$.

In the left panel of fig. 3.10 we investigated the k-dependence of the next-to-lowest Landau level. In particular, we fixed the magnetic field $B = 7.4$ and the chemical potential $\mu = 0.01$, and plotted the real part of the dispersion relation as a function of k, the momentum along the magnetic field. The numerical data is best fitted by $\mathrm{Re}(\omega) = 0.98\sqrt{(5.1)^2 + k^2}$, the expected k-dependence for Landau levels if we extrapolate the dispersion-relation at weak coupling.

Moreover, we investigated the influence of finite charge density on the dispersion

relation of the Landau levels. Again, the characteristic $\sqrt{B}$-behaviour of the real part of the frequency for large magnetic fields is unchanged. This is to be expected since for $\mu \ll \sqrt{B}$ the behaviour due to the magnetic field dominates. However, as displayed in fig. 3.11, the chemical potential modifies the real and imaginary part of the dispersion relation for small magnetic fields.

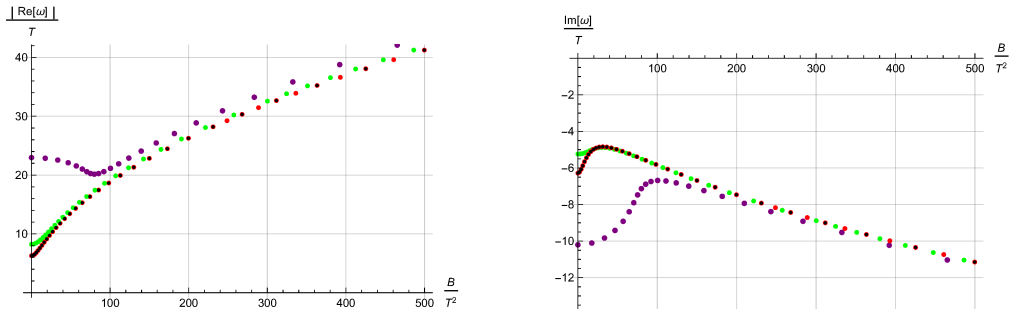

Fig. 3.11.: Left panel: Real part of dispersion relation versus $\tilde{B}$ for $\gamma = 3/2$ and different chemical potential μ: $\mu = 0$ black dots, $\mu = 0.01$ red dots and $\mu = 1$ green dots, $\mu = 2$ purple dots. Right panel: Imaginary part versus $\tilde{B}$ with the same colour coding.

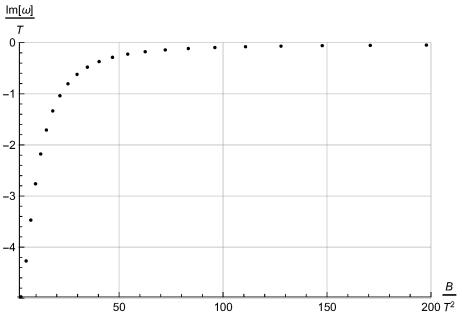

Fig. 3.12.: Imaginary part of next-to-lowest Landau level as a function of $\tilde{B}$ for $\gamma = 5 > \gamma_c$.

As in the case of the helicity-1 sector, the anomaly coefficient γ plays an important role whether the modes are long-lived. For $\gamma < \gamma_c \approx 4$, the imaginary part seems to diverge, and hence the QNM is not long-lived. In particular, the imaginary part of the dispersion relation is fitted best by $\mathrm{Im}(\omega) \sim -\sqrt{B}$. However, as displayed in fig. 3.12 for $\gamma > \gamma_c \approx 4$, the QNMs, corresponding to the next-to-lowest Landau levels, approach the real axis and hence are long-lived excitations for large magnetic fields.

3.6.4. Instabilities

We find one QNM with positive imaginary part for very low temperatures $\bar{T} = 0.01$ in the helicity-1 sector for finite k [130]. This mode corresponds to the helical charged magnetic phase [66], discussed in the next chapter. We find the instability exactly in the k-range where the helical phase exists, see fig. 3.13.

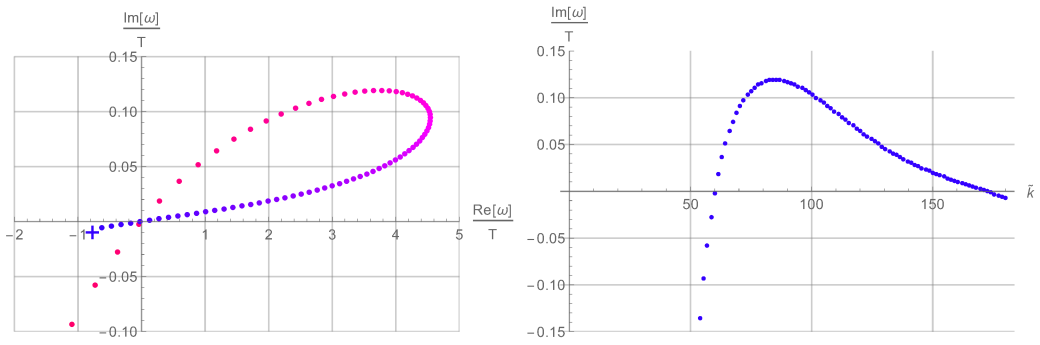

Fig. 3.13.: QNM with positive imaginary part in the helicity-1 sector indicate an instability (left). We find the helical instability in the range of $\tilde{k} = 60 - 173$ (right) for $\bar{T} = 0.01$, $B = 2, \tilde{B} = 69.44$, $\tilde{k}_{max} = 180$.

4. Helical charged magnetic branes

So far we have studied charged magnetic branes, where we have found an instability towards a spatially modulated phase. Here we construct and study this novel phase. As shown in [130, 131] for $\gamma > \gamma_c \approx 1.158$, the electrically charged AdS-RN black brane is unstable against spatial modulation below a critical temperature, suggesting that the system is in a spatially modulated phase in which the current acquires a helical order. The corresponding backreacted solution for zero magnetic field was presented in [66]. In this chapter we find numerical evidence that the helical structure at zero magnetic field persists at finite magnetic field, at least in some part of the phase diagram. This chapter is based on and heavily draws from [82].

The remainder of the chapter is organised as follows. In sec. 4.1 we summarize the holographic setup used here. First, we present our coordinate ansatz in the gravitational theory which exhibits Bianchi VII_0 symmetry implying that the corresponding equations of motion are ordinary differential equations. Then, we briefly state the asymptotic expansions close to the horizon and conformal boundary and discuss how to extract the thermodynamic observables of the dual CFT from the gravitational theory.

In sec. 4.4 we numerically construct asymptotically AdS_5 black brane solutions with non-trivial electric charge density and magnetic field breaking translational invariance spontaneously. In particular, we determine the phase diagram at finite temperature, chemical potential and magnetic field. Moreover, we characterise the new phase by identifying the order parameters and critical exponents close the phase transition. Finally, we explicitly show that the entropy density vanishes in the limit of zero temperature.

More details concerning the equations of motion, thermodynamics, special cases and numerics are given in the appendices. Note that in app. A.2 some techniques are presented to improve the numerical accuracy, specifically at low temperatures, which may be relevant also for other holographic setups.

4.1. Holographic setup

Bianchi VII_0 symmetry

We like to construct electrically and magnetically charged black branes with (reduced) Bianchi VII_0 symmetry, which give rise to the helical order in the currents and energy-momentum tensor. The Bianchi VII_0 symmetry is manifest using the one-forms ω_i defined by

$$\begin{aligned} \omega_1 &= \cos(k\,x_3)\,\mathrm{d}x_1 - \sin(k\,x_3)\,\mathrm{d}x_2\,, \\ \omega_2 &= \sin(k\,x_3)\,\mathrm{d}x_1 + \cos(k\,x_3)\,\mathrm{d}x_2\,, \\ \omega_3 &= \mathrm{d}x_3\,. \end{aligned} \tag{4.1}$$

Note that $\omega_1 \wedge \omega_2 = \mathrm{d}x_1 \wedge \mathrm{d}x_2$ as well as $\mathrm{d}\omega_1 = k\,\omega_2 \wedge \omega_3$, $\mathrm{d}\omega_2 = -k\,\omega_1 \wedge \omega_3$ and $\mathrm{d}\omega_3 = 0$. The meaning of the differential forms ω_i, or to be precise their dual tangent vectors, is apparent from fig. 4.1.

Using the differential forms (4.1) we assume[1] that the helical structure is parallel to the magnetic field B, i.e. ω_3 is aligned along the magnetic field. The differential forms ω_1 and ω_2 span the plane of the spatial directions perpendicular to the magnetic fields, i.e. the (x_1,x_2)-plane.

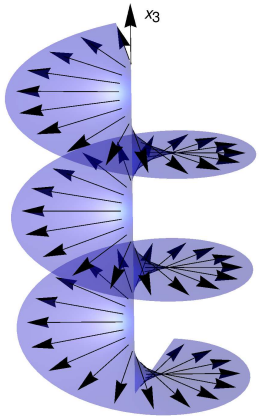

Fig. 4.1.: Helical structure displaying the tangent vectors dual to ω_i.

[1] This assumption is justified a posteriori since the new black brane solution will have zero entropy density for $T \to 0$ and hence we speculate that this is the true ground state of the system.

Ansatz

We aim to determine the phase diagram at finite magnetic field, chemical potential and temperature of the new helical phase. In particular, we use the following ansatz

$$\begin{aligned} \mathrm{d}s^2 &= \frac{1}{z^2}\left(\frac{\mathrm{d}z^2}{u(z)} - u(z)\,\mathrm{d}t^2 + v(z)^2\,\alpha(z)^{-2}\,\omega_2^2 + w(z)^2\,(\omega_3 + c(z)\,\mathrm{d}t)^2\right. \\ &\quad \left. + v(z)^2\,\alpha(z)^2\,(\omega_1 + g(z)\,\omega_3 + q(z)\,\mathrm{d}t)^2\right) \end{aligned} \tag{4.2}$$

for the metric and

$$F = e(z)\,\mathrm{d}t \wedge \mathrm{d}z + B\,\omega_1 \wedge \omega_2 + p(z)\,\mathrm{d}z \wedge \omega_3 + b'(z)\,\mathrm{d}z \wedge \omega_1 + b(z)\,\mathrm{d}\omega_1 \tag{4.3}$$

for the field strength tensor $F = \mathrm{d}A$. Note that B has to be independent of z in order to satisfy the Bianchi identitiy $dF = 0$. The ansatz specified by (4.2) and (4.3) respects the Bianchi VII_0 symmetry mentioned above. The field strength tensor may be obtained from a gauge field A of the form

$$A = -E(z)\,\mathrm{d}t\; - B\,x_2\,\mathrm{d}x_1\; + b(z)\,\omega_1 + P(z)\,\omega_3\,, \tag{4.4}$$

where $A_t(z)$ is related to the electric field $e(z)$ by $E'(z) = e(z)$. Moreover, $P'(z) = p(z)$, where $'$ denotes the derivative with respect to z.

We have chosen the specific form of the metric ansatz (4.2) such that we can explicitly calculate the square root

$$\sqrt{-\det(g)} = \frac{v(z)^2 w(z)}{z^5}\,, \tag{4.5}$$

which greatly simplifies the analytical structure of the EOM.

Limiting cases

Note that the ansatz (4.2)–(4.4) generalises the charged magnetic branes [63] and the charged helical brane [66]:

On the one hand we obtain the original D'Hoker and Kraus background [63] for

$$\alpha(z) = 1, \quad b(z) = 0, \quad Q(z) = 0, \quad g(z) = 0, \quad k = 0\,. \tag{4.6}$$

In ch. 3 we studied this solution in Eddington-Finkelstein coordinates, while here

we work in Poincare coordinates. On the other hand we obtain a setup equivalent to Donos and Gauntlett [66], as discussed in sec. 4.4.1, in the limiting case

$$c(z) = 0, \quad p(z) = 0, \quad g(z) = 0, \quad B = 0\,. \tag{4.7}$$

Note that we have to allow for an additional function $g(z)$, which was not present in both limiting cases. This was found with the method outlined in sec. 3.1.1 for $c(z)$: Without $g(z)$ in the ansatz the constraints are not consistent. As a result the ϵ expansion shows that $g_{\omega_1\omega_3}$ has to be non zero.

Equations of Motion

Inserting the ansatz (4.2) and (4.3) into the Einstein equations (2.94), we obtain nine differential equations, i.e. seven second order differential equations for the metric functions $u(z)$, $v(z)$, $w(z)$, $q(z)$, $c(z)$, $\alpha(z)$ and $g(z)$ as well as two constraints, denoted by CON_1 and CON_2, which contain only first derivatives of the metric fields. Moreover, there are three independent equations of motion (2.95) for the gauge fields. While $b(z)$ has to satisfy a second order differential equation, the fields $p(z)$ and $e(z)$ satisfy first order equations of motion which can be recasted in the form

$$B\,\gamma\,e(z) + \partial_z E^*(z) = 0 \quad \text{and} \quad B\,\gamma\,p(z) + \partial_z P^*(z) = 0, \tag{4.8}$$

with

$$\begin{aligned} E^*(z) &= \frac{v^2}{z\,w}\left(c\,w^2\,(q\,b' + e) + (g\,b' - p)\left(u - c^2 w^2\right)\right), \\ P^*(z) &= \frac{v^2\,w}{z}\left((c\,g - q)\,b' - c\,p - e\right) + \frac{1}{2}\gamma\,k\,b^2\,, \end{aligned} \tag{4.9}$$

where we have omitted the argument "(z)" on the metric functions for clearness. The full form of the remaining equations of motion is not very enlightening. For these reasons, we do not display them here (see app. A.1 for more details).

Moreover, we explicitly checked that the two constraints are consistent, as outlined in sec. 2.5. To be precise, using the EOM of the metric and gauge fields we showed that the constraints satisfy the following differential equations

$$\partial_z\left(\mathrm{CON}_1(z)\right) + f(z)\,\mathrm{CON}_1(z) = 0 \qquad \partial_z\left(\mathrm{CON}_2(z)\right) + \tilde{f}(z)\,\mathrm{CON}_2(z) = 0 \tag{4.10}$$

for some functions $f(z)$ and $\tilde{f}(z)$. Accordingly, we impose the constraints only at the boundaries.

4.1.1. Asymptotic expansions

In order to solve the equations of motion numerically, we first need the asymptotic expansion of the metric and gauge fields at the boundaries. A detailed derivation of the boundary expansion is presented in app. A.1. Imposing asymptotically AdS at the conformal boundary $z = 0$

$$u'(0) = 0, \quad v(0) = 1, \quad w(0) = 1, \quad \alpha(0) = 1, \quad c(0) = 0, \quad q(0) = 0, \quad g(0) = 0,$$

$$A_t(0) = -E(0) = \mu, \quad e'(0) = \rho, \quad P(0) = 0, \quad b(0) = 0,$$

we obtain for the metric functions

$$\begin{aligned}
u(z) &= 1 + z^4\left[\mathbf{u}_4 + \mathcal{O}(z^2)\right] + z^4\ln(z)\left[\frac{B^2}{6} + \mathcal{O}(z^2)\right], \\
v(z) &= 1 + z^4\left[-\frac{\mathbf{w}_4}{2} + \mathcal{O}(z^2)\right] + z^4\ln(z)\left[-\frac{B^2}{24} + \mathcal{O}(z^2)\right], \\
w(z) &= 1 + z^4\left[\mathbf{w}_4 + \mathcal{O}(z^2)\right] + z^4\ln(z)\left[\frac{B^2}{12} + \mathcal{O}(z^2)\right], \\
\alpha(z) &= 1 + z^4\left(\mathbf{a}_4 + \mathcal{O}(z^2) + z^4\ln(z)\left[-\frac{B^2}{2304}\left(B^2 + 192\mathbf{a}_4\right) + \mathcal{O}(z^2)\right]\right), \\
c(z) &= z^4\left(\mathbf{c}_4 + \mathcal{O}(z^2) + z^4\ln z\left[-\frac{B^2}{12}\mathbf{c}_4 + \mathcal{O}(z^2)\right]\right), \\
g(z) &= z^4\left(\frac{B}{2k}\mathbf{b}_2 + \mathcal{O}(z^2) + z^4\ln(z)\left[\mathcal{O}(1)\right]\right), \\
q(z) &= z^4\left(\mathbf{q}_4 + \mathcal{O}(z^2) + z^4\ln(z)\left[\frac{B^2}{24}\mathbf{q}_4 + \mathcal{O}(z^2)\right]\right),
\end{aligned} \tag{4.11}$$

while the gauge field functions read

$$\begin{aligned}
E(z) &= -\boldsymbol{\mu} + \frac{\boldsymbol{\rho}}{2}z^2 + \frac{\gamma B\mathbf{p}_1}{8}z^4 + \mathcal{O}(z^6), & e(z) &= z\left(\boldsymbol{\rho} + \frac{B\gamma}{2}\mathbf{p}_1 z^2 + \mathcal{O}(z^4)\right), \\
P(z) &= z^2\left(\frac{\mathbf{p}_1}{2} + \frac{\gamma B\boldsymbol{\rho}}{8}z^2 + \mathcal{O}(z^4)\right), & p(z) &= z\left(\mathbf{p}_1 + \frac{B\gamma}{2}\boldsymbol{\rho}z^2 + \mathcal{O}(z^4)\right), \\
b(z) &= z^2\left(\mathbf{b}_2 + \mathcal{O}(z^2) + z^4\ln(z)\left[-\frac{\mathbf{b}_2}{12}B^2 + \mathcal{O}(z^2)\right]\right).
\end{aligned} \tag{4.12}$$

Using diffeomorphisms, we can shift the horizon to $z = 1$. The event horizon condition imposes that $u(1) = 0$. Then, it follows from the regularity conditions that $c(1) = q(1) = 0$. Therefore, the expansion around $z = 1$ assumes the following structure for the metric functions

$$\begin{aligned} u(z) &= (1-z)\left[\bar{\mathbf{u}}_{\mathbf{1}} + \mathcal{O}(1-z)\right], & c(z) &= (1-z)\left[\bar{\mathbf{c}}_{\mathbf{1}} + \mathcal{O}(1-z)\right], \\ q(z) &= (1-z)\left[\bar{\mathbf{q}}_{\mathbf{1}} + \mathcal{O}(1-z)\right], & w(z) &= \bar{\mathbf{w}}_{\mathbf{0}} + \mathcal{O}(1-z), \\ g(z) &= \bar{\mathbf{g}}_{\mathbf{0}} + \mathcal{O}(1-z), & v(z) &= \bar{\mathbf{v}}_{\mathbf{0}} + \mathcal{O}(1-z), \\ \alpha(z) &= \bar{\mathbf{a}}_{\mathbf{0}} + \mathcal{O}(1-z). \end{aligned} \tag{4.13}$$

Furthermore, we also impose regularity for A_t at the horizon, i.e. $E(1) = 0$. In turn, we obtain for the gauge field functions

$$\begin{aligned} E(z) &= (1-z)\left[-\bar{\mathbf{e}}_{\mathbf{0}} + \mathcal{O}(1-z)\right], & e(z) &= \bar{\mathbf{e}}_{\mathbf{0}} + \mathcal{O}(1-z), \\ P(z) &= \bar{\mathbf{P}}_{\mathbf{0}} + \mathcal{O}(1-z), & p(z) &= \bar{p}_0 + \mathcal{O}(1-z), \\ b(z) &= \bar{\mathbf{b}}_{\mathbf{0}} + \mathcal{O}(1-z). \end{aligned} \tag{4.14}$$

The boldface letters in (4.11)–(4.14) denote quantities that are not determined by the expansion, i.e. their values are obtained only after a global solution is found.

In the ansatz for the gauge field (4.4) the functions $E(z)$ and $P(z)$ appear. By integrating (4.8) we can determine $P(z)$ and $E(z)$. For $\gamma B \neq 0$, the function $E(z)$ is given by

$$E(z) = -\frac{E^*(z)}{B\gamma}. \tag{4.15}$$

Since we identify $E(0)$ with the chemical potential μ, i.e. $A_t(0) = -E(0) = \mu$, we can use (4.9) and (4.15) as well as the asymptotic expansion (4.12) to obtain

$$p_1 = -B\,\gamma\,\mu\,. \tag{4.16}$$

Similarly, we can solve the equation (4.8) to determine $P(z)$. Note that in this case, we only have to demand regularity at the horizon and hence we cannot fix $P(1)$. However, we only want to study systems where we do not allow for a source term of the operator dual to $P(z)$ and hence we have to demand $P(0) = 0$.

4.2. Thermodynamics

Next we describe how to extract further thermodynamic information from our solutions which describe thermal equilibrium states in the dual CFT. We will work in the grand canonical ensemble in which the chemical potential μ is fixed.

Wick rotation

In order to analyse the thermodynamical properties of the black brane solution, we have to analytically continue to a Euclidean time $\tau = t_{(E)}$ by a Wick rotation of the form $\tau = i\,t$. Since the metric and the vector field should be real in Euclidean signature, we also have to introduce $q_{(E)} = -i\,q, c_{(E)} = -i\,c$ as well as $e_{(E)} = -i\,e$. The leading order coefficients for $q_{(E)}$, $c_{(E)}$ and $e_{(E)}$ at the horizon, see (4.13) and (4.14), are denoted by $\bar{q}_{1(E)}, \bar{c}_{1(E)}$ and $\bar{e}_{0(E)}$ respectively. Hence the Euclidean metric and the field strength tensor of the gauge field near the horizon $z = 1$ are given by

$$\begin{aligned} \mathrm{d}s^2_{(E)} &= \frac{1}{z^2}\left(\frac{\mathrm{d}z^2}{u(z)} + u(z)\,\mathrm{d}\tau^2 + v(z)^2\,\alpha(z)^{-2}\,(\omega_2)^2 + w(z)^2\,\left(\omega_3 + c_E(z)\,\mathrm{d}\tau\right)^2\right. \\ &\qquad \left. + v(z)^2\alpha(z)^2\,\Big(\omega_1 + g(z)\omega_3 + q_{(E)}(z)\,\mathrm{d}\tau\Big)^2\right) \\ &\approx \frac{\mathrm{d}z^2}{\bar{u}_1\,(1-z)} + \bar{u}_1\,(1-z)\,\mathrm{d}\tau^2 + \bar{v}_0^2\,\bar{a}_0^{-2}\,(\omega_2)^2 + \bar{w}_0^2\,\Big(\omega_3 - \bar{c}_{1(E)}\,(1-z)\,\mathrm{d}\tau\Big)^2 \\ &\qquad + \bar{v}_0^2\,\bar{a}_0^2\,\Big(\omega_1 + \bar{g}_0\,\omega_3 - \bar{q}_{1(E)}\,(1-z)\,\mathrm{d}\tau\Big)^2 \end{aligned} \tag{4.17}$$

as well as

$$\begin{aligned} F_{(E)} &= e_{(E)}(z)\,\mathrm{d}\tau\wedge\mathrm{d}z + B\,\omega_1\wedge\omega_2 + p(z)\,\mathrm{d}z\wedge\omega_3 + b'(z)\,\mathrm{d}z\wedge\omega_1 + b(z)\,d\omega_1\,, \\ F_{(E)} &\approx \bar{e}_{0(E)}\,\mathrm{d}\tau\wedge\mathrm{d}z + B\,\omega_1\wedge\omega_2 + \bar{p}_0\,\mathrm{d}z\wedge\omega_3 + \bar{b}_1\,\mathrm{d}z\wedge\omega_1 + \bar{b}_0\,d\omega_1\,. \end{aligned} \tag{4.18}$$

In the last lines of (4.17) and of (4.18) we kept only the leading terms in the near horizon limit.

We can read off the temperature T and the entropy density s of the black brane solution using (2.127) and (2.131), respectively. In particular, we find that the temperature and entropy density is given by

$$T = \frac{|\bar{u}_1|}{4\pi}\,, \qquad s = 4\pi\,\bar{v}_0^2\,\bar{w}_0\,. \tag{4.19}$$

Euclidean action

In order to determine the total Euclidean action $S_{(E)tot}$,

$$S_{(E)tot} = S_{(E)grav} + S_{(E)bdy}\,, \tag{4.20}$$

we first perform the Wick-rotation on the action S as given by (2.93) (including its boundary terms (2.98)), and denote the result by $\bar{S}_{grav}$ and $\bar{S}_{bdy}$, respectively. Then the corresponding Euclidean actions $S_{(E)grav}$ and $S_{(E)bdy}$ are given by $S_{(E)grav} = -i\bar{S}_{grav}$ and $S_{(E)bdy} = -i\bar{S}_{bdy}$. Note that $S_{(E)tot} = -S_{tot}$. We will use the action S_{tot} in Minkowski signature from now on. Hence the grand-canonical potential is given by

$$\Omega = T\, S^{o.s.}_{(E)tot} = -T\, S^{o.s.}_{tot}\,, \tag{4.21}$$

where *o.s.* indicates that we have to evaluate the total action on-shell. The total Euclidean on-shell action is displayed in sec. 4.3. Using the boundary and horizon expansions (4.11)–(4.14), we obtain for the density of the grand canonical potential (which we also denote by Ω to keep the notation simple)

$$\Omega = -\bar{u}_1\,\bar{v}_0^2\,\bar{w}_0 - 3\,u_4 - \mu\,\rho + \frac{1}{3}\,B\,\gamma\int_0^1 \mathrm{d}z\,E(z)\,p(z)\,. \tag{4.22}$$

EM-Tensor and Current

Using (2.101), we can extract the energy-momentum tensor of the dual conformal field theory.[2] The non-vanishing components of the energy-momentum tensor are given by

$$\begin{aligned}
\langle T_{tt}\rangle &= -3\,u_4\,,\\
\langle T_{t\omega_1}\rangle = \langle T_{\omega_1 t}\rangle &= 4\,q_4\,,\\
\langle T_{tx_3}\rangle = \langle T_{x_3 t}\rangle &= 4\,c_4\,,\\
\langle T_{\omega_1\omega_1}\rangle &= -\frac{B^2}{4} + 8\,a_4 - u_4 - 4\,w_4\,,\\
\langle T_{\omega_2\omega_2}\rangle &= -\frac{B^2}{4} - 8\,a_4 - u_4 - 4\,w_4\,,\\
\langle T_{\omega_1 x_3}\rangle = \langle T_{x_3\omega_1}\rangle &= \frac{2\,B\,b_2}{k}\,,\\
\langle T_{x_3x_3}\rangle &= 8\,w_4 - u_4\,.
\end{aligned} \tag{4.23}$$

[2]Recall that we set $2\kappa^2 \equiv 1$ from the beginning.

In particular, the trace of the energy momentum tensor is given by

$$\langle T^{\mu}{}_{\mu} \rangle = -\frac{B^2}{2} = -\frac{1}{4} F_{\mu\nu} F^{\mu\nu} \,. \tag{4.24}$$

Similarly, we can also read off the expectation value of the current in the dual field theory using (2.102). The non-zero components of the current are given for our ansatz by

$$\langle J_t \rangle = -\rho \,, \qquad \langle J_{\omega_1} \rangle = -2\, b_2 \,, \qquad \langle J_{x_3} \rangle = p_1 \,. \tag{4.25}$$

Hence we can write Ω in the form

$$\Omega = U - s\,T - \mu \left\langle J^t \right\rangle + \frac{1}{3} B\, \gamma \int_0^1 \mathrm{d}z\, E(z)\, p(z) \,, \tag{4.26}$$

where we have assumed that $u'(0) < 0$ and hence $\bar{u}_1 > 0$, which is the case for our numerical results. Moreover, the charge density reads $\langle J^t \rangle = \rho$, while the energy density is given by $U = \langle T^{tt} \rangle = -3\, u_4$.

Note that for $\gamma = 0$, the grand canonical potential (4.26) reduces to its standard form $\Omega = U - sT - \mu \langle J^t \rangle$. If both γ and B are non-vanishing we obtain an additional contribution to the grand canonical potential due to the chiral anomaly.

4.3. More on thermodynamics

Calculating thermodynamic properties requires the evaluation of the on-shell action, which in principle is an integral over the numerically determined solutions. It is more enlightening to have an analytic expression in which only boundary values of the solution have to be inserted. In this section we show how to rewrite (part of) the on-shell Lagrangian as a total derivative. This is usually also used to get Smarr Type formulas, for example see [132, 133]. We present here systematically how to do this step by step. First by taking the trace of the Einstein equations,

$$\begin{aligned} R_{mn} &= -4 g_{mn} + T_{mn} \,, & R &= -20 + T \,, \\ T_{mn} &= \frac{1}{2}\left(F_{mo} F_n{}^o - \frac{1}{6} g_{mn} F_{op} F^{op} \right) \,, & T &= \frac{1}{12} F_{mn} F^{mn} \,, \end{aligned} \tag{4.27}$$

we can reformulate the Einstein-Maxwell part of the Lagrangian as

$$\mathcal{L}_{EM} = R + 12 - \frac{1}{4} F_{mn} F^{mn} = -8 - \frac{1}{6} F_{mn} F^{mn} \,. \tag{4.28}$$

The equations of motion (4.27) may be written in the following form

$$2\,R_t{}^t = -8 + 2\,T^t{}_t = -8 + 2\,\tilde{T}^t{}_t - \frac{1}{6}F_{mn}F^{mn}\,, \tag{4.29}$$

where $\tilde{T}_m{}^n = F_{mo}\,F^{no}/2$. Hence we obtain for $\mathcal{L}_{EM}$

$$\mathcal{L}_{EM} = 2\,R^t{}_t - 2\,\tilde{T}^t{}_t\,. \tag{4.30}$$

In order to rewrite $\sqrt{-g}\,\mathcal{L}_{EM}$ as a total derivative we have to massage $R^t{}_t$ and $\tilde{T}^t{}_t$.

Let us start with $R^t{}_t$ by using the identity $R^m_n\,\xi^n = \nabla_m\nabla_n\xi^n$ for an arbitrary Killing vector ξ (with components ξ^m). If the metric depends only on the radial coordinate z the identity can be expressed as a total derivative

$$\sqrt{-g}\,R^m_n\,\xi^n = -\partial_z\left(\sqrt{-g}\nabla^z\xi^m\right)\,. \tag{4.31}$$

In particular $\sqrt{-g}R^t{}_t$ reads

$$\begin{aligned}\sqrt{-g}R^t_t &= -\partial_z\left(\sqrt{-g}\nabla^z\xi^t\right)\,, \\ &= -\partial_z\left(\frac{v^2\,w\,(z\,(c\,(\alpha^2\,q\,v^2\,g' - w^2\,c') - \alpha^2\,q\,v^2\,q' + u') - 2\,u)}{2z^4}\right)\,.\end{aligned} \tag{4.32}$$

In order to rewrite $\sqrt{-g}\,\tilde{T}^t{}_t$ as a total derivative we analyse the Maxwell equations

$$d*F + \frac{\gamma}{2}F\wedge F = 0 \tag{4.33}$$

in the following systematic way: The $F\wedge F$ term has a rather simple structure

$$\begin{aligned}\frac{\gamma}{2}F\wedge F \;&= -\gamma\;(k\,b(z)\,b'(z) + B\,p(z)) && \mathrm{d}x_1\wedge\mathrm{d}x_2\wedge\mathrm{d}x_3\wedge\mathrm{d}z \\ &\quad + \gamma\,k\,b(z)\,e(z)\sin(k\,x_3) && \mathrm{d}t\wedge\mathrm{d}x_1\wedge\mathrm{d}x_3\wedge\mathrm{d}z \\ &\quad + \gamma\,k\,b(z)\,e(z)\cos(k\,x_3) && \mathrm{d}t\wedge\mathrm{d}x_2\wedge\mathrm{d}x_3\wedge\mathrm{d}z \\ &\quad + B\,\gamma\,e(z) && \mathrm{d}t\wedge\mathrm{d}x_1\wedge\mathrm{d}x_2\wedge\mathrm{d}z\end{aligned} \tag{4.34}$$

while the term $d*F$ is a sum of total derivatives of z and x_3

$$d*F = \left(\frac{\partial(*F)_{mnp}}{\partial z}\,\mathrm{d}z + \frac{\partial(*F)_{mnp}}{\partial x_3}\,\mathrm{d}x_3\right)\wedge\mathrm{d}x^m\wedge\mathrm{d}x^n\wedge\mathrm{d}x^p\,. \tag{4.35}$$

The relevant parts of $*F$ are those, without either $\mathrm{d}z$ or $\mathrm{d}x_3$. This gives three

independent equations of motion. By comparing to the remainder $\tilde{T}^t{}_t$ given by

$$-2\sqrt{-g}\,\tilde{T}^t{}_t = e(z)\,M_{1d}(z), \tag{4.36}$$

with $M_{1d}(z)$ defined by[3]

$$\begin{aligned} M_{1d}(z) &= \frac{\gamma\,k\,b(z)^2}{2} - P^*(z) \\ &= \frac{v(z)^2\,w(z)}{z}\left(c(z)\left(p(z) - g(z)\,b'(z)\right) + q(z)\,b'(z) + e(z)\right), \end{aligned} \tag{4.37}$$

we see that the Maxwell equation with legs $\mathrm{d}x_1 \wedge \mathrm{d}x_2 \wedge \mathrm{d}x_3 \wedge \mathrm{d}z$ corresponds to equation relating $p(z)$ and $P^*(z)$ in (4.8). For convenience, we rewrite it here in the form

$$\frac{\partial}{\partial z} M_{1d}(z) = \gamma\,R_1(z) \quad \text{with} \quad R_1(z) = B\,p(z) + k\,b(z)\,b'(z). \tag{4.38}$$

Now, in order to rewrite $-2\sqrt{-g}\,\tilde{T}^t{}_t$ as a total derivative, we multiply $M_{1d}(z)$ by $E(z)$ and substract again the additional term of $\partial_z(E(z)\,M_{1d}(z))$.

Finally, we also have to consider the Chern-Simons term

$$-\frac{\gamma}{6} A \wedge F \wedge F = \mathcal{C}(z, x_3, x_2)\,\mathrm{d}t \wedge \mathrm{d}x_1 \wedge \mathrm{d}x_2 \wedge \mathrm{d}x_3 \wedge \mathrm{d}z \tag{4.39}$$

plus the remaining term $E(z)\,R_1(z)$,

$$\begin{aligned} E(z)\,R_1(z) + \mathcal{C}(z, x_3, x_2) &= \gamma\,k\,b(z)\,\mathrm{E}(z)\,b'(z) - B\,\gamma\,\mathrm{E}(z)\,p(z) \\ &\quad -\mathrm{E}(z)\,\gamma\,(B\,p(z) - k\,b(z)\,b'(z)) + \ldots\,. \end{aligned} \tag{4.40}$$

The absent terms in (4.40) are proportional to $x_2\cos(kx_3)$ and vanish when we integrate over any symmetric interval with respect to x_2. The expression (4.40) can be reformulated in terms of the following two total derivatives

$$\frac{\partial}{\partial z}\left(\frac{1}{3}\gamma\,k\,b(z)^2\,\mathrm{E}(z)\right), \qquad \frac{\partial}{\partial z}\left(-\frac{1}{3}B\,\gamma\,\mathrm{E}(z)\,P(z)\right), \tag{4.41}$$

plus the remaining term $\frac{1}{3}\,B\,\gamma\,E(z)\,p(z)$. Collecting everything we end up with the

[3] $P^*(z)$ was first introduced in eq. (4.9).

action density s, defined by $S = \text{vol}(\mathbb{R}^{3,1})\, s$,

$$s = \int dz \quad \left[2\sqrt{-g} R^t{}_t + \frac{\partial}{\partial z}\left(M_{1d}(z)\, E(z) \right) \right. \\ \left. - \frac{\gamma}{3}\frac{\partial}{\partial z}\left(k\, b(z)^2\, E(z) + B\, E(z)\, P(z) \right) - \frac{\gamma}{3} B\, E(z)\, p(z) \right] . \quad (4.42)$$

Finally, we have to insert the boundary and horizon expansions (4.11) – (4.14)

$$s = \bar{u}_1\, \bar{v}_0^2\, \bar{w}_0 + \frac{B^2}{6} + 2\, u_4 - \frac{2}{z^4} + \mu\rho + \frac{1}{3} B^2\, \log(z) - \frac{1}{3} B\, \gamma \int \mathrm{E}(z)\, p(z)\, dz\, . \quad (4.43)$$

The divergent parts are canceled by appropriate counterterms given by (2.98). Hence the final result for the on-shell action density reads

$$s = \bar{u}_1\, \bar{v}_0^2\, \bar{w}_0 + 3\, u_4 + \mu\rho - \frac{1}{3} B\, \gamma \int_0^1 dz\, \mathrm{E}(z)\, p(z)\, . \quad (4.44)$$

Note that the final result still contains an integral and hence the Lagrangian does not seem to reduce to a total derivative. However, the integral expression is actually a boundary term in x_2 direction. We checked this explicitly by computing the Noether charges along the lines of [134, 135].

4.4. Numerical solutions

We present now the results describing our magnetic helical black brane solution. We provide more details on the numerical techniques employed here in app. A.2.

As described in [66], for $\bar{B} = 0$ one expects to construct the spatially modulated black brane solutions provided the Chern-Simons coupling be $\gamma > 1.158$. As representative examples, we focus ourselves on the results with $\gamma = 1.5$. Besides, as a generalisation of the particular results from [66], we also comment on some specific features of the case $\gamma = 1.7$.

We first address the question in which region of the parameter space $\{\bar{k}, \bar{B}\}$ we expect new solutions. Then we construct these solutions and single out the thermodynamically preferred ones. Following this we discuss thermodynamic properties of these solutions, with particular emphasis on the behaviour of near the critical temperature and in the low temperature limit.

4.4.1. The special case $B = 0$

In our coordinates the helical black brane solution [66] corresponds to the choice of

$$B = P(z) = c(z) = g(z) = 0. \tag{4.45}$$

In this case, the line element (4.2), the field strength tensor (4.3) and the gauge field (4.4) read

$$\begin{aligned} \mathrm{d}s^2 &= \frac{1}{z^2}\left(\frac{\mathrm{d}z^2}{u(z)} - u(z)\,\mathrm{d}t^2 + v(z)^2\,\alpha(z)^{-2}\,\omega_2^2 + v(z)^2\,\alpha(z)^2\,\left(\omega_1 + q(z)\,\mathrm{d}t\right)^2 + w(z)^2\,\omega_3^2\right), \\ F &= e(z)\,\mathrm{d}t\wedge\mathrm{d}z + b'(z)\,\mathrm{d}z\wedge\omega_1 + b(z)\,d\omega_1\,, \\ A &= -E(z)\,\mathrm{d}t + b(z)\,\omega_1. \end{aligned} \tag{4.46}$$

Note that our ansatz differs slightly from the one presented in [66]: first we compactify r by $r = 1/z$ with $z \in [0,1]$, second we re-label the one-forms: $\omega_{1\text{ here}} = \omega_{2\text{ DG}}, \omega_{2\text{ here}} = \omega_{3\text{ DG}}$ and $\omega_{3\text{ here}} = \omega_{1\text{ DG}}$ and third we use a slightly different metric ansatz which is closer to the one used by D'Hoker and Kraus (see sec. 3.3). In particular, while in [66] the metric components in terms of z satisfy $z^4\,g_{tt}g_{zz} = -f(z)^2$, we choose an ansatz such that $z^4\,g_{tt}g_{zz} = -1$ and $z^4 g_{\omega_2\omega_2}\,g_{\omega_1\omega_1} = v(z)^4$. Finally, the authors of [66] use scaling freedom of the coordinates to set $\mu = 1$, while the coordinate location of the event horizon is not known a priori. In contrast, we fix the horizon to be located at $z = 1$, and hence we are not allowed to set μ to one.

Our numerics pass an important check: We can reproduce all their results down to temperatures of order $\bar{T} \approx 10^{-5}$. The authors of [66] reported some difficulties in studying the behaviour of the solutions in the regime of very low temperatures, $\bar{T} \to 0$. In this regime, some functions develop strong gradients around the horizon.

An example is depicted in fig. 4.2 for the results shown in sec. 4.4.3 ($\gamma = 1.5$). As we drop the temperature, the function $\tilde{q}(z)$ becomes steeper around $z = 1$. Numerically, the solution must be obtained either by a massive increase in the number of grid points or by the development of specific techniques adapted to this drawback. In this chapter, we use the so called analytical mesh-refinements [136, 137], described in app. A.2 to circumvent these problems.

4.4.2. The phase boundary

The magnetic helical black brane solution is described by the existence of a function $b(z) \neq 0$. As described in sec. 3.3, in the limiting case $b(z) = 0$, one obtains the

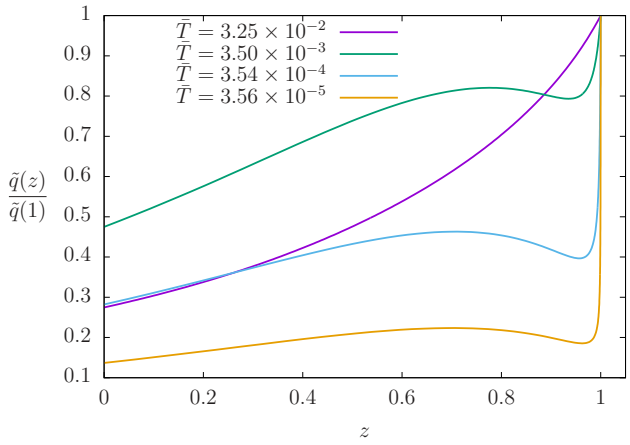

Fig. 4.2.: Function $\tilde{q}(z)$ normalised by its value on $z = 1$. In the regime $\bar{T} \to 0$, the function develops very strong gradients around the horizon. The numerical solution requires higher resolution and, eventually, specific techniques must be employed (such as the analytical mesh-refinement - see app. A.2).

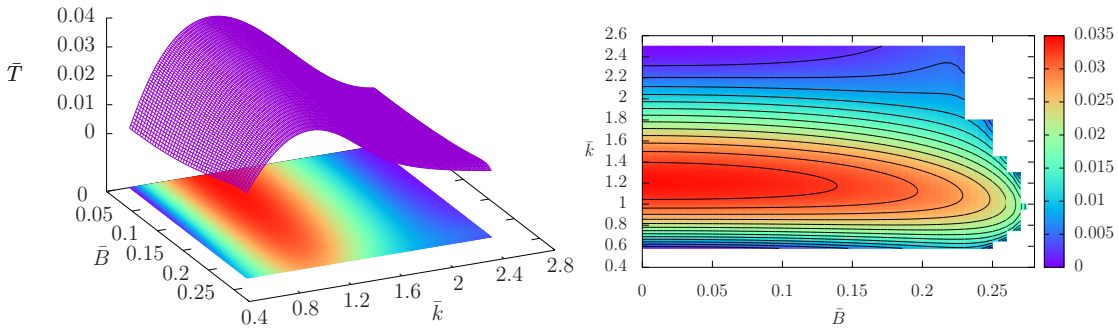

Fig. 4.3.: Left panel: temperature $\bar{T}(\bar{k}, \bar{B})$ below which we find new magnetic helical black brane solution. Right panel: contour plot of isothermals in the $(\bar{k}, \bar{B})$-plane. The highest temperature for which the magnetic helical black brane exists decreases as the magnetic field $\bar{B}$ is increased. The results are shown for $\gamma = 1.5$.

electrically charged RN black brane with $\bar{B} = 0$ or the electrically and magnetically charged brane for $\bar{B} \neq 0$. The boundary between the two regimes is therefore naturally defined as the region for which $b(z) \approx 0$.[4]

In the left panel of fig. 4.3, the highest temperature $\bar{T}$ for which the magnetic helical black brane exists is plotted as a function of $\bar{k}$ and $\bar{B}$. In other words, above the surface only the RN black brane exists while below the surface both the RN

[4]Numerically, the boundary is characterised by $b_2 \approx 10^{-9}$ as introduced in (4.11), see discussion in app. A.2.

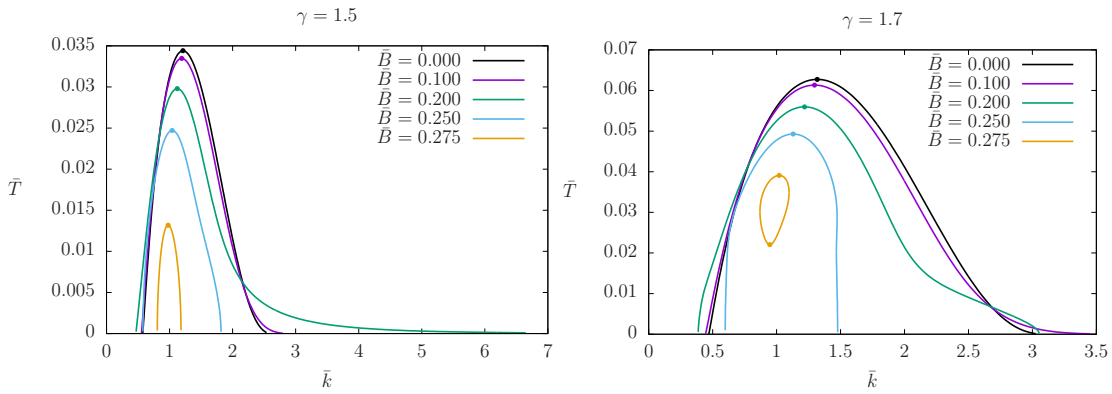

Fig. 4.4.: Slices of $\bar{B}$ =constant in the $(\bar{T}, \bar{k})$-plane. Left panel: results for $\gamma = 1.5$. The range of $\bar{k}$ for which magnetic helical black brane solutions exist first increases with increasing $\bar{B}$, reaching value as high as $\bar{k} \approx 6.5$, and then shrinks again. Right panel: results for $\gamma = 1.7$. For $\bar{B} \gtrsim 0.274$ the new phase lies entirely within a closed curve.

black brane as well as the magnetic helical black brane solution coexist. Projecting the surface onto the $\bar{B} = 0$ plane, we reproduce[5] the expected profile showed in [66] and the contour plot in the right panel of the same figure highlights the isothermal curves on the $(\bar{k}, \bar{B})$-plane.

To appreciate this property, in fig. 4.4 we restrict ourselves to the $(\bar{T}, \bar{k})$-plane with $\bar{B}$ = constant. The left panel corresponds to the same results as in the previous figure, i.e. with $\gamma = 1.5$. It becomes evident that the critical temperature $\bar{T}_{\rm C}(\bar{B}) = \max_{\bar{k}}[\bar{T}(\bar{k}, \bar{B})]$ decreases for increasing $\bar{B}$.

It is worth mentioning the equivalent results for $\gamma = 1.7$, depicted in the right panel of fig. 4.4. For values $\bar{B} \gtrsim 0.274$, we observe that the magnetic helical phase lies entirely within a closed curve. In the particular example with $\bar{B} = 0.275$ displayed here, phase transitions occur at both $\bar{T}_{\rm C} \approx 0.03909$ and $\bar{T}_{\rm C} \approx 0.022061$.

After identifying the critical temperature in the $(\bar{T}, \bar{k})$-plane, we study the dependence of $\bar{T}_{\rm C}$ on the magnetic field $\bar{B}$ and present the results in fig. 4.5. Here again, it is evident that there exists a value $\bar{B}_0$ as $\bar{T}_{\rm C} \to 0$, which limits the region where the magnetic helical solution is expected to be found. For the particular examples treated here, these values are $\bar{B}_0 \approx 0.279$ ($\gamma = 1.5$) and $\bar{B}_0 \approx 0.274$ ($\gamma = 1.7$). We also identify in the same figure the quantum critical point $\bar{B}_{\rm C}$ as found in [63] (see also the discussion in sec. 3.3). In particular, the critical values are $\bar{B}_C \approx 0.185$ and $\bar{B}_C \approx 0.220$ for $\gamma = 1.7$ and $\gamma = 1.5$, respectively. It is interesting to notice that $\bar{B}_{\rm C}$

[5]The results shown in fig. 4.3 are for $\gamma = 1.5$ while the results explicitly shown in [66] are for $\gamma = 1.7$.

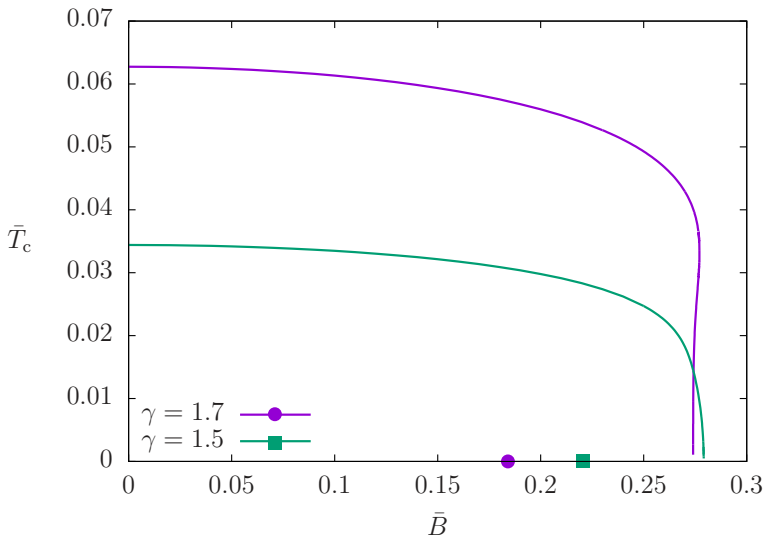

Fig. 4.5.: Boundary of the magnetic helical phase in the $(\bar{T}, \bar{B})$ phase diagram. There exist a maximum value $\bar{B}_0$ limiting the region where the new solution exists. For $\gamma = 1.5$ and $\gamma = 1.7$, we find $\bar{B}_0 \approx 0.279$ and $\bar{B}_0 \approx 0.274$, respectively. The corresponding quantum critical points are also displayed at $\bar{B}_C \approx 0.185$ ($\gamma = 1.7$) and $\bar{B}_C \approx 0.220$ ($\gamma = 1.5$). They lie within the new magnetic helical phase.

lies within the new phase region, meaning that the phase transition should occur before the system reaches the quantum critical point.

The important question that arises now is what happens to the system as we lower the temperature and move inside the new phase along curves of constant $\bar{B}$. Of particular interests is the region $\bar{B} < \bar{B}_C$ and the behaviour of the entropy $\bar{s}$ in the low temperature regime. We address this issue and discuss further details about the thermodynamics in the next section.

4.4.3. Thermodynamic results

For fixed $\bar{B}$ and for fixed temperature $\bar{T}$ we construct the solutions for different values of $\bar{k}$. The solution corresponding to the physical state minimizes the grand canonical potential $\bar{\Omega}(\bar{k})$. The corresponding value for $\bar{k}$ is denoted by $\bar{k}_*$. For fixed $\bar{B}$ we repeat this procedure for smaller temperatures $\bar{T}$ and hence obtain a trajectory $\bar{k}_*(\bar{T})$ in the $(\bar{T}, \bar{k})$-plane of thermodynamically preferred solutions. This trajectory is shown in fig. 4.6 for the values $\bar{B} = 0.200 < \bar{B}_C$ and $\bar{B} = 0.250 > \bar{B}_C$. In both cases, note that when lowering the temperature $\bar{T}$, the wave-number $\bar{k}_*(\bar{T})$ decreases and hence the pitch $\bar{p}_* = 2\pi/\bar{k}_*$ increases.

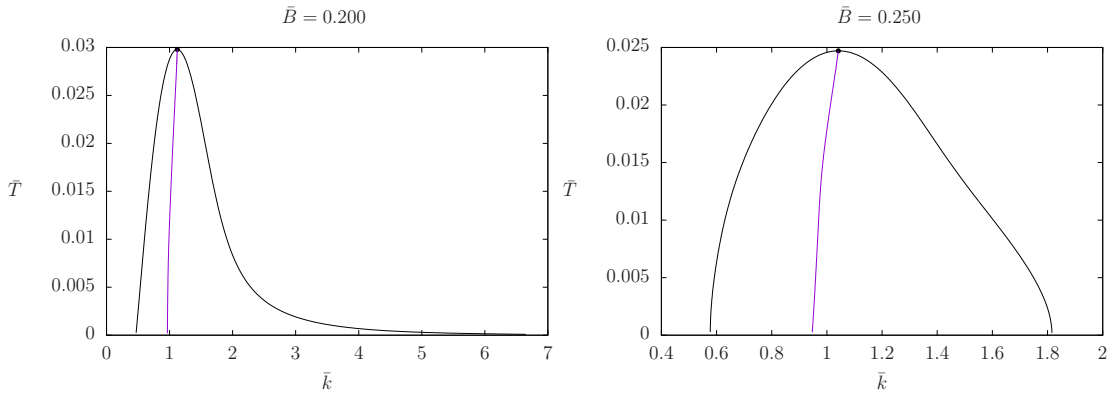

Fig. 4.6.: Diagram of the $(\bar{T}, \bar{k})$-plane for fixed $\bar{B} = 0.200 < \bar{B}_{\mathrm{C}}$ (left panel) and $\bar{B} = 0.250 > \bar{B}_{\mathrm{C}}$ (right panel). The thermodynamically most favourable physical states are found along the curve $\bar{k}_*(\bar{T})$ for which the grand canonical potential $\bar{\Omega}$ is minimised.

Along such trajectories of thermodynamically preferred solutions, we evaluate the observables derived in sec. 4.2 and compare them to the corresponding values from the charged magnetic solution. In all the following figures, a continuous line represents a result within the new magnetic helical phase, whereas the dashed lines depict the results of [63] (see sec. 3.3 for more details).

First, in fig. 4.7 we present the entropy density $\bar{s}$ as a function of $\bar{T}$. Let us

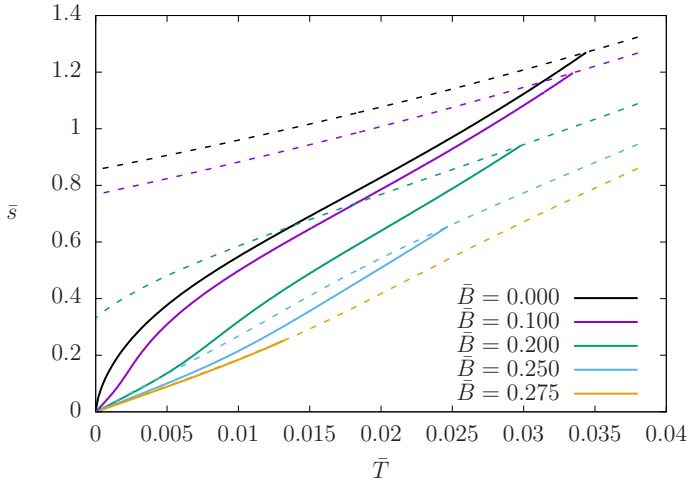

Fig. 4.7.: Low temperature behaviour of entropy $\bar{s}$. The dashed lines are the charged magnetic results. For $\bar{B} < \bar{B}_{\mathrm{C}}$ the entropy does not vanish as $\bar{T} \to 0$. In the new magnetic helical phase (continuous line), $\bar{s}$ goes to zero for $\bar{T} \to 0$, regardless of the value of the magnetic field.

first concentrate on the dahsed lines corresponding to the charged magnetic black brane. For $\bar{B} < \bar{B}_{\mathrm{C}}$ the entropy goes to a non-vanishing constant as $\bar{T} \to 0$ in agreement with the results of [63]. However, for the new helical magnetic black brane constructed in this thesis, we observe that $\bar{s} \to 0$ as $\bar{T} \to 0$ regardless of the value of $\bar{B}$. Due to the vanishing entropy density we are confident that the magnetic helical black brane is dual to the true ground state of the CFT. Moreover, for fixed $\bar{B}$ the entropy is continuous close to the phase transition, i.e. for $\bar{T} \lesssim \bar{T}_C(\bar{B})$. Hence the phase transition is second order.

Next, we turn to the non-vanishing components of the energy-momentum tensor $\left\langle \bar{T}_{\mu\nu} \right\rangle$ and the current $\left\langle \bar{J}_{\mu} \right\rangle$ of the dual field theory. Fig. 4.8 depicts the components $\left\langle \bar{T}_{tt} \right\rangle$, $\left\langle \bar{T}_{\omega_1\omega_1} \right\rangle + \left\langle \bar{T}_{\omega_2\omega_2} \right\rangle$, $\left\langle \bar{T}_{x_3x_3} \right\rangle$ and $\left\langle \bar{J}_{t} \right\rangle$. In all cases there are expected small deviations between the helical magnetic black brane and the charge magnetic black brane.

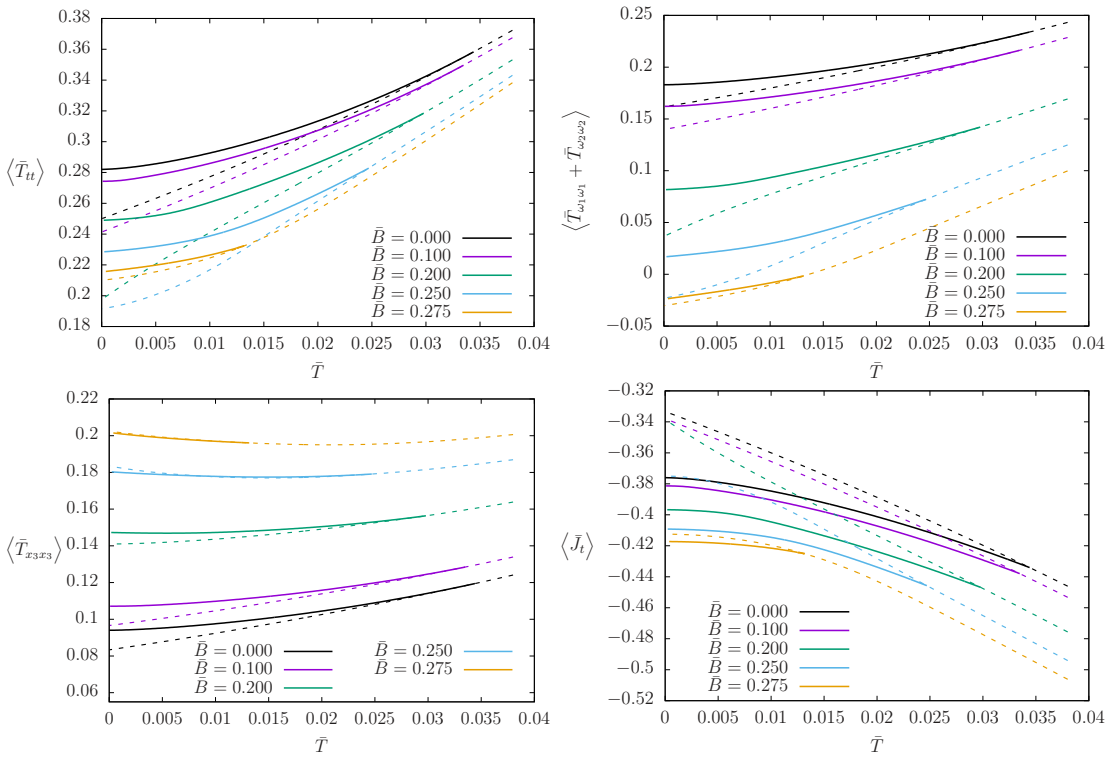

Fig. 4.8.: Components $\left\langle \bar{T}_{tt} \right\rangle$, $\left\langle \bar{T}_{\omega_1\omega_1} \right\rangle + \left\langle \bar{T}_{\omega_2\omega_2} \right\rangle$, $\left\langle \bar{T}_{x_3x_3} \right\rangle$ of the energy momentum tensor and $\left\langle \bar{J}_{t} \right\rangle$ of the current. Note that $\langle J_t \rangle = -\rho$ where ρ is the charge density. The dashed lines are the charged magnetic results, while the continuous lines correspond to the values in the magnetic helical phase.

Moreover, from (3.12) and the normalisation (2.134) it is clear that $\left\langle \bar{J}_{x_3} \right\rangle = -\gamma\, \bar{B}$ is a constant. Furthermore, we also confirm that (3.13) holds numerically, i.e. in terms of dimensionless quantities $\left\langle \bar{T}_{tx_3} \right\rangle = \frac{1}{2}\gamma \bar{B}$. Note that the relation (3.13) is also satisfied for the charged magnetic black brane [63], which we explicitly demonstrate in sec. 3.3.

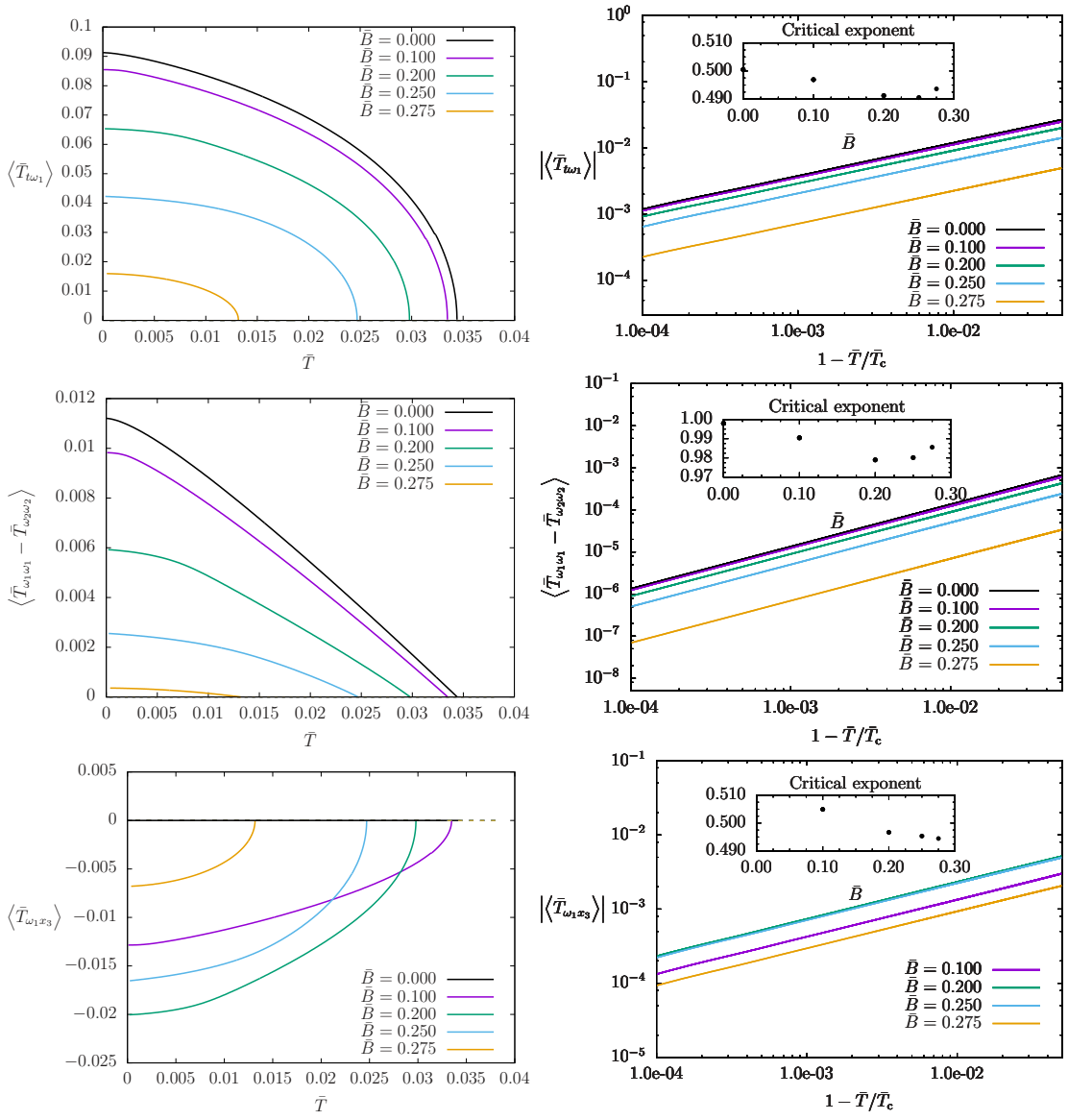

Fig. 4.9.: Components $\left\langle \bar{T}_{t\omega_1} \right\rangle$, $\left\langle \bar{T}_{\omega_1\omega_1} \right\rangle - \left\langle \bar{T}_{\omega_2\omega_2} \right\rangle$, $\left\langle \bar{T}_{\omega_1 x_3} \right\rangle$ of the energy momentum tensor. Left panel: these observables vanishes as $\bar{T} \to \bar{T}_C$. Right panel: Behaviour in terms of $\left|1 - \frac{\bar{T}}{\bar{T}_C}\right|$. From the double logarithmic scale we infer the critical exponents depicted in the inset. We observe no systematic dependence on $\bar{B}$.

Finally, we display the results for the components $\left\langle \bar{T}_{t\omega_1} \right\rangle$, $\left\langle \bar{T}_{\omega_1\omega_1} \right\rangle - \left\langle \bar{T}_{\omega_2\omega_2} \right\rangle$, $\left\langle \bar{T}_{\omega_1 x_3} \right\rangle$ in fig. 4.9 and $\left\langle \bar{J}_{\omega_1} \right\rangle$ in fig. 4.10. As one can see in the left panels of fig. 4.9, and fig. 4.10, these components vanish as $\bar{T} \to \bar{T}_{\rm C}$. Hence these components are candidates for the order parameter. The right panels show the same observables against $\left|1 - \frac{\bar{T}}{\bar{T}_{\rm C}}\right|$ in a double logarithmic scale. The critical exponents are displayed in the inset of those figures. Within the interval range $\left|1 - \frac{\bar{T}}{\bar{T}_{\rm C}}\right| \in [10^{-4}, 10^{-2}]$, we do not observe any systematic dependency on the magnetic field $\bar{B}$ since the deviations are within the expected range of numerical errors. The critical exponents are those expected from mean field, i.e.

$$\begin{aligned} \left\langle \bar{T}_{t\omega_1} \right\rangle &\sim \left|1 - \frac{\bar{T}}{\bar{T}_{\rm C}}\right|^{1/2}, & \left\langle \bar{T}_{\omega_1 x_3} \right\rangle &\sim \left|1 - \frac{\bar{T}}{\bar{T}_{\rm C}}\right|^{1/2}, \\ \left\langle \bar{J}_{\omega_1} \right\rangle &\sim \left|1 - \frac{\bar{T}}{\bar{T}_{\rm C}}\right|^{1/2}, & \left[\left\langle \bar{T}_{\omega_1\omega_1} \right\rangle - \left\langle \bar{T}_{\omega_2\omega_2} \right\rangle\right] &\sim \left|1 - \frac{\bar{T}}{\bar{T}_{\rm C}}\right|^{1}. \end{aligned} \tag{4.47}$$

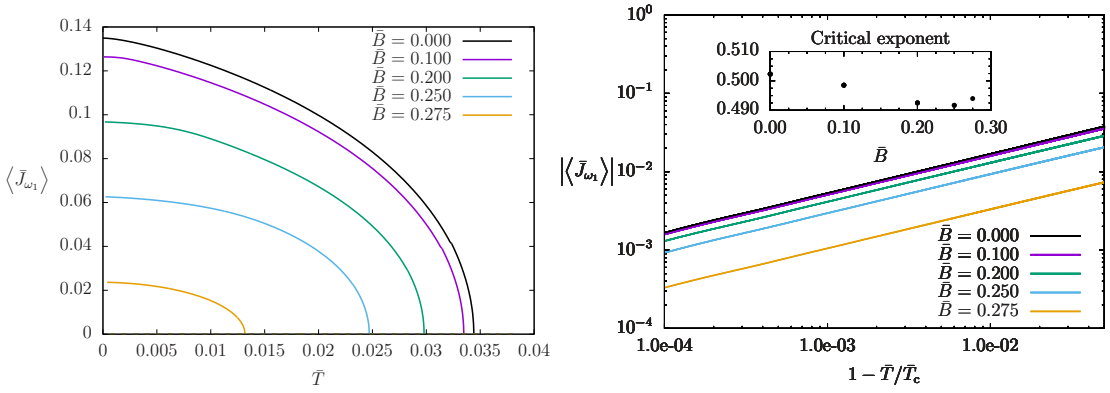

Fig. 4.10.: Component $\left\langle \bar{J}_{\omega_1} \right\rangle$ of the current. Left panel: these observables vanishes as $\bar{T} \to \bar{T}_{\rm C}$. Right panel: Behaviour in terms of $\left|1 - \frac{\bar{T}}{\bar{T}_{\rm C}}\right|$. From the double logarithmic scale we infer the critical exponents depicted in the inset. We observe no systematic dependence on $\bar{B}$.

5. Conclusion

5.1. Summary

We studied strongly coupled four dimensional CFTs with chiral anomaly, whose gravitational description is given in terms of Einstein-Maxwell-Chern-Simons theory in asymptotically AdS spacetime. For a particular value of the Chern-Simons coupling, the action is a consistent truncation of type IIB supergravity, and the dual field theories are well-known, including $\mathcal{N} = 4$ SYM.

Transport and QNM

First, we have investigated transport and dissipation in this thermal plasma in a magnetic field of arbitrary strength at strong coupling. In the dual gravitational calculation we have evaluated and analyzed quasinormal modes (QNMs) of Einstein-Maxwell-Chern-Simons theory in the asymptotically AdS charged magnetic black brane background. We have investigated the effects of having a finite temperature T, chemical potential μ and a non-zero external magnetic field B on the QNMs. We have chosen the momentum of the QNMs k, to be (anti-)parallel to B.

Hydrodynamics

In parallel to the holographic calculation, we have computed the weak B hydrodynamic description of our system. The five (formerly) hydrodynamic poles were computed at nonzero B. We extend previous treatments keeping our derivation general and providing expressions for the various velocities and attenuations. At leading order in derivatives, we have also worked out an expression for the energy momentum tensor and axial current containing polarization effects (2.42). The hydrodynamic results are collected in sec. 3.5.

QNM results

In a systematic study of all metric and gauge field fluctuations propagating along the magnetic field, we investigated QNMs both within and outside the hydrodynamic regime. We find that some of the QNMs are long-lived and show characteristic behavior known from Landau levels, see figs. 3.10–3.12.

The helicity-2 QNMs do not exhibit any hydrodynamic modes. However, some of these QNMs appear to have vanishing real part in the limit of large B, see fig. 3.4. There are five hydrodynamic modes in total.

Two of those modes at vanishing B are momentum diffusion modes appearing in the helicity-1 sector. At nonzero B these modes acquire a complex gap and can not be considered hydrodynamic modes according to our previous definition. However, they are still well described by the hydrodynamic dispersion relation (3.31) at intermediate values of B. The remaining three hydrodynamic modes appear in the helicity-0 sector. At $B = 0$ they reduce to the charge diffusion pole and the two sound poles, see the dispersion relation (3.23), (3.26)–(3.28) and fig. 3.9. These are hydrodynamic modes (ungapped) even at $B \neq 0$, as can be seen from the dispersion relations (3.23).

One of the helicity-0 modes (the former charge diffusion mode) turns into a chiral magnetic wave mode with velocity v_0 and attenuation D_0 displayed from zero to large B in fig. 3.9. At large magnetic field the chiral magnetic wave velocity asymptotes to $v_0 = -1$, i.e. to the magnitude of the speed of light. This is particularly intriguing as that same chiral magnetic wave QNM shows Landau level behavior at large magnetic field, i.e. the real part of the frequency is proportional to $\sqrt{B}$ and the imaginary part asymptotes to zero. This provides evidence at strong coupling for the relation between Landau level occupation and the large B behavior of v_0.

Chiral magnetic wave

The present work extends [122] to fully backreacted geometry and a solution valid at arbitrary B. We further provide a hydrodynamic and holographic calculation of the chiral magnetic wave attenuation D_0, as well as the velocities $v_\pm$ and attenuations $\Gamma_\pm$ of the former sound modes. Remarkably, all of these velocities obtain contributions from the anomaly, as seen explicitly e.g. in (3.26) and (3.27).

This is also true for the two helicity-1 modes, see e.g. (3.20). Dispersion relations for all five hydrodynamic modes are provided in the thermodynamic frame, see sec. 3.5.

Helical phase

In the second part, we investigated the phase diagram at finite temperature, chemical potential and magnetic field and found a new spatially modulated phase for low temperatures and small magnetic fields. This is dual to asymptotically AdS_5 black brane solutions with non-trivial electric charge density and magnetic field spontaneously acquiring a helical current which we construct numerically. Note that this helical phase is supposed to exist only for large enough coefficient γ of the chiral anomaly. In this thesis we presented results mainly for $\gamma = 1.5$.

The new spatially modulated phase has interesting features. First, the quantum critical point at $B = B_C$ is hidden in this new phase, at least for the values of γ studied here. Second, the phase transition is second order with mean field exponents. Third, our numerical results indicate that the entropy density vanishes in the limit of zero temperature supporting our speculations that this is the true ground state of the system. Fourth, we have extracted how the wave-number of the helical structure changes with the parameters of the phase diagram. Finally, during the course of this work, as a side product we developed new numerical techniques which may be also useful for other holographic systems.

5.2. Outlook

For the future, it would be interesting to relax the restriction of having the QNM momentum k parallel to the external magnetic field B; see [88] for a field theory discussion of a related system. This would allow many more modes to arise, and thus even richer phenomenology. But this is technically challenging since the classification in accordance to $SO(2)$ in sec. 3.4.1 breaks down and all 16 fluctuations generically couple. In addition, the parameter space is greatly enlarged from $\{k_3\}$ to $\{k_1, k_2, k_3\}$.

A similar question arises for the helical phase. Are the states with helical structure aligned to the magnetic field really thermodynamically favoured? Answering this question will require to solve partial differential equations on the gravity side.

Moreover, it will be worthwhile to explore if there exists a simple relation between the location of the quantum critical point, given by $B = B_C$, and the location of the phase boundary $B = B_0$ at zero temperature. Note that both, the new phase and the quantum critical point, are controlled by the chiral anomaly coefficient and hence such a relation may exist although it is not obvious in terms of the dual field theory. In addition, it will be very interesting to further analyse the phase diagram

change for other values of the chiral anomaly coefficient.

An apparent future direction is to study transport coefficients and quasi-normal modes within the new helical phase extending the results of this thesis and [53].

Additionally, the results presented here can be generalised to models with an anomaly structure closer to the one of QCD and Weyl semimetals. It would also be interesting to have two U(1) gauge fields in the gravity theory [138], i.e. introducing an axial and a conserved vector current in the dual field theory. In particular, the interplay between a magnetic field and chemical potentials for the vector/axial charge may be interesting. This is relevant for testing some predictions for chiral magnetic waves and for Weyl semimetals and their surface states, see [57–61].

Furthermore, it would be interesting to include mixed gauge-gravity anomalies and study their effects on the QNMs, see for example [139] in which a mixed anomaly appears to lead to a phase transition.

In this thesis we have only considered hydrodynamics in the regime of weak external gauge fields but QNM for large magnetic fields. It would be very interesting to work out the hydrodynamics in the case where the gauge fields are strong building on [96] and [94]. Lastly, it would be desirable to extend our setup systematically to magnetohydrodynamics as viewed from a modern perspective [140].

A. Appendix

This appendix provides details on the equations of motion and the numerics used in this thesis.

We start with a detailed discussion of the boundary expansion at the conformal boundary and the horizon, respectively. We discuss the helical charged magnetic brane solutions of ch. 4 in Poincare coordinates. The boundary expansions for the charged magnetic brane solutions in Eddington-Finkelstein coordinates as well as the boundary expansion for the linearized QNM equations can be obtained in the same way.

We then briefly introduce spectral methods and present their implementation to get the solutions of ch. 4. This is fully realized in the programming language C. We stress out numerical difficulties arising in our setup. More details on spectral methods can be found in [141, 142] as well as in the specialised reviews [143, 144].

Finally we present the numerics of ch. 3. The background and QNM solutions of ch. 3 are again obtained with a spectral method. As we will discuss, the behaviour of the QNM solutions requires higher numerical accuracy. However, the system of EOM is smaller and hence the solutions are numerical less expensive in terms of computing time. We therefore use Mathematica instead of C which allows us to use arbitrary precision numerics.

A.1. Equations of motion

In this section we give some details on the non-linear equations of motions for the background solutions and, in particular, how we treat them as a boundary value problem. We discuss here the more general solutions of the helical charged magnetic brane ansatz (4.2)–(4.4), since the charged magnetic brane solutions of sec. 3 are included in this more general ansatz.

For convenience, let us reproduce here (2.94) and (2.97) and define them as

$$\begin{aligned}\mathcal{E}_{mn} &= R_{mn} + 4g_{mn} - \frac{1}{2}\left(F_{mo}F_n{}^o - \frac{1}{6}g_{mn}F_{op}F^{op}\right), \\ \mathcal{M} &= \mathrm{d}\star F + \frac{\gamma}{2}F\wedge F.\end{aligned}$$

Furthermore, we complete the one-forms (4.1) with $\omega_0 = \mathrm{d}t$ and $\omega_4 = \mathrm{d}z$ and express the equations of motion in terms of the tetrad basis $\omega^a = \omega^a{}_m dx^m$, i.e. we look specifically at[1]

$$\mathcal{E}^{ab} = \omega^a{}_m\,\omega^b{}_n\,\mathcal{E}^{mn}\,, \tag{A.1}$$

$$\mathcal{M}^{abcd} = \omega^a{}_m\,\omega^b{}_n\,\omega^c{}_o\,\omega^d{}_p\,\mathcal{M}^{mnop}\,. \tag{A.2}$$

The non-zero components $\{\mathcal{E}^{00}, \mathcal{E}^{01}, \mathcal{E}^{03}, \mathcal{E}^{11}, \mathcal{E}^{13}, \mathcal{E}^{22}, \mathcal{E}^{24}, \mathcal{E}^{33}, \mathcal{E}^{44}\}$ and $\{\mathcal{M}^{1234}, \mathcal{M}^{1245}, \mathcal{M}^{2345}\}$ form a system of 12 ordinary differential equations (ODE) for our 10 field variables: the components of the metric (7 functions) and gauge field (3 functions).

In spite of being overdetermined, this system of ODE is consistent as already shown in sec. 4.1. Therefore, we must solve 10 out of 12 equations and ensure that the remaining 2 are satisfied for at least one value of z. Yet, we must assure that the chosen equations are independent of each other.

The first point to notice is that the second derivatives appearing in each of the Maxwell-Chern-Simons equations involve only one of each gauge field function. In other words, the equations $\mathcal{M}^{1234}$, $\mathcal{M}^{1245}$ and $\mathcal{M}^{2345}$ can be regarded individually as equations for $E(z)$, $P(z)$ and $b(z)$, respectively. Next, we observe that $\mathcal{E}^{24}$ contains only first order derivatives. Finally, one can work the second derivates out of the remaining $\mathcal{E}^{ab}$ and obtain equations for each one of the metric fields $u(z)$, $c(z)$, $v(z)$, $w(z)$, $\alpha(z)$, $g(z)$ or $q(z)$. This procedure leaves us with 7 second order ODEs and one additional first order ODE (apart from $\mathcal{E}^{24}$).

By sorting out the second derivatives, we can associate for each one of the fields its respective ODE. In this way, we need boundary values at both $z = 0$ and $z = 1$. The only exception is the function $g(z)$, for which we work with the first order ODE $\mathcal{E}^{24}$ and therefore we are only allowed to fix the value at one of the surfaces. To exemplify the structure of the system of equations, let us collect the field variables

[1] In the tetrad basis, the equations do not present any trigonometric term related to $\cos(k\,x_3)$ or $\sin(k\,x_3)$.

and the equations of motion into the vector notation

$$\vec{x} = \begin{bmatrix} u(z) \\ c(z) \\ w(z) \\ v(z) \\ \alpha(z) \\ g(z) \\ q(z) \\ E(z) \\ P(z) \\ b(z) \end{bmatrix}, \quad \vec{f}(\vec{x}; z) = \begin{bmatrix} f_u(u'', \vec{x}', \vec{x}; z) \\ f_c(c'', \vec{x}', \vec{x}; z) \\ f_w(w'', \vec{x}', \vec{x}; z) \\ f_v(v'', \vec{x}', \vec{x}; z) \\ f_\alpha(\alpha'', \vec{x}', \vec{x}; z) \\ f_g(\vec{x}', \vec{x}; z) \\ f_q(q'', \vec{x}', \vec{x}; z) \\ f_E(E'', \vec{x}', \vec{x}; z) \\ f_P(P'', \vec{x}', \vec{x}; z) \\ f_b(b'', \vec{x}', \vec{x}; z) \end{bmatrix}. \tag{A.3}$$

The boundary values are a mixture of regularity conditions imposed by the equations of motion and physical assumptions ensuring the surfaces $z = 0$ and $z = 1$ to represent the AdS boundary and the event horizon, respectively.

For example, at $z = 1$ the horizon condition tells us that $u(1) = 0$. Moreover due to regularity, we have to impose $E(1) = 0$. By imposing such conditions on the remaining equations, we are left with regularity conditions involving the value of fields and their first derivatives at $z = 1$ (Robin boundary conditions). In some specific cases, the conditions are rather simple and reduce to $q(1) = 0$, $c(1) = 0$.

The next step is to study the asymptotic expansion around the AdS boundary $z = 0$. In its most generic form, the expansions read

$$\begin{aligned}
u(z) &= 1 + u_2 z^2 + \mathbf{u}_4 z^4 + \mathcal{O}(z^6) + z^4 \ln(z) \left[\hat{u}_4 + \mathcal{O}(z^2)\right] \\
&\quad + \mathbf{u}_1 z \left(1 + u_5 z^4 + \mathcal{O}(z^6) + z^4 \ln(z) \left[\hat{u}_5 + \mathcal{O}(z^2)\right]\right), \\
v(z) &= \mathbf{v}_0 + v_2 z^2 + v_4 z^4 + \mathcal{O}(z^6) + z^4 \ln(z) \left[\hat{v}_4 + \mathcal{O}(z^2)\right] \\
&\quad + \mathbf{u}_1 z \left(v_1 + v_3 z^2 + \mathcal{O}(z^2) + z^4 \ln(z) \left[\hat{v}_5 + \mathcal{O}(z^2)\right]\right), \\
w(z) &= \mathbf{w}_0 + w_2 z^2 + \mathbf{w}_4 z^4 + \mathcal{O}(z^6) + z^4 \ln(z) \left[\hat{w}_4 + \mathcal{O}(z^2)\right] \\
&\quad + \mathbf{u}_1 z \left(w_1 + w_3 z^2 + \mathcal{O}(z^2) + z^4 \ln(z) \left[\hat{w}_5 + \mathcal{O}(z^2)\right]\right), \\
\alpha(z) &= \mathbf{a}_0 + a_2 z^2 + \mathbf{a}_4 z^4 + \mathcal{O}(z^6) + z^4 \ln(z) \left[\hat{a}_4 + \mathcal{O}(z^2)\right] \\
&\quad + \mathbf{u}_1 z \left(a_3 z^2 + a_5 z^4 + \mathcal{O}(z^6) + z^4 \ln(z) \left[\hat{a}_5 + \mathcal{O}(z^2)\right]\right),
\end{aligned} \tag{A.4}$$

as well as

$$\begin{aligned}
c(z) &= \mathbf{c}_0 + c_2 z^2 + \mathbf{c}_4 z^4 + \mathcal{O}(z^6) + z^4 \ln(z) \left[\hat{a}_4 + \mathcal{O}(z^2)\right] \\
&\quad + \mathbf{u}_1 z \left(c_3 z^2 + c_5 z^4 + \mathcal{O}(z^6) + z^4 \ln(z) \left[\hat{a}_5 + \mathcal{O}(z^2)\right]\right) , \qquad \text{(A.5)} \\
g(z) &= \mathbf{g}_0 + g_2 z^2 + g_4 z^4 + \mathcal{O}(z^6) + z^4 \ln(z) \left[\hat{a}_4 + \mathcal{O}(z^2)\right] \\
&\quad + \mathbf{u}_1 z \left(g_3 z^2 + g_5 z^4 + \mathcal{O}(z^6) + z^4 \ln(z) \left[\hat{a}_5 + \mathcal{O}(z^2)\right]\right) , \\
q(z) &= \mathbf{q}_0 + q_2 z^2 + \mathbf{q}_4 z^4 + \mathcal{O}(z^6) + z^4 \ln(z) \left[\hat{q}_4 + \mathcal{O}(z^2)\right] \\
&\quad + \mathbf{u}_1 z \left(q_3 z^2 + q_5 z^4 + \mathcal{O}(z^6) + z^4 \ln(z) \left[\hat{q}_5 + \mathcal{O}(z^2)\right]\right) , \\
E(z) &= \mathbf{E}_0 + \left(\mathbf{E}_2 z^2 + E_3 z^3 + \mathcal{O}(z^4) + z^2 \ln(z) \left[\hat{E}_2 + \hat{E}_4 z^2 + \mathcal{O}(z^4)\right]\right) , \\
&\quad + \mathbf{u}_1 z^3 \left(E_3 + E_5 z^2 + \mathcal{O}(z^4) + \ln(z) \left[\hat{E}_3 + \hat{E}_4 z^2 + \mathcal{O}(z^4)\right]\right) , \\
P(z) &= \mathbf{P}_0 + \left(\mathbf{P}_2 z^2 + P_3 z^3 + \mathcal{O}(z^4) + z^2 \ln(z) \left[\hat{P}_2 + \hat{P}_4 z^2 + \mathcal{O}(z^4)\right]\right) , \\
&\quad + \mathbf{u}_1 z^3 \left(P_3 + P_5 z^2 + \mathcal{O}(z^4) + \ln(z) \left[\hat{P}_3 + \hat{P}_4 z^2 + \mathcal{O}(z^4)\right]\right) , \\
b(z) &= b_0 + \mathbf{b}_2 z^2 + b_4 z^4 + \mathcal{O}(z^6) + z^2 \ln(z) \left[\hat{b}_2 + \hat{b}_4 z^2 \mathcal{O}(z^4)\right] \\
&\quad + \mathbf{u}_1 z \left(b_3 z^2 + b_5 z^4 + \mathcal{O}(z^6) + z^2 \ln(z) \left[\hat{b}_3 + \hat{b}_5 z^2 + \mathcal{O}(z^2)\right]\right) .
\end{aligned}$$

The quantities in boldface are free parameters, which can not be determined by the series expansion. All the other terms are fixed by them if one considers *all* equations of motion (including here the two first order differential equations). For example, we find that

$$(B\, g_0 + k\, b_0)(1 - w_0^2\, c_0^2) + B\, w_0^2\, c_0\, q_0 = 0\,. \qquad \text{(A.6)}$$

Asymptotically AdS solutions require

$$v_0 = 1, \quad w_0 = 1, \quad \alpha_0 = 1, \quad c_0 = 0, \quad g_0 = 0, \quad q_0 = 0\,,$$

and thus $b_0 = 0$ from (A.6).

In our numerics we demand $u_1 = 0$ in order to fix all remaining diffeomorphisms. For the gauge field functions, we fix the chemical potential[2] $E_0 = -\mu$. Moreover, we do not allow for a source term for operators dual to $P(z)$. Hence we impose $P_0 = 0$. With this conditions, the expansions around $z = 0$ take the much simpler form given by (4.11).

Once the solution is available, the thermodynamic observables (see sec. 4.3) require the knowledge of some coefficients related to higher derivatives, such as u_4, w_4, a_4, c_4 and q_4. Not only do we lose accuracy by calculating them numerically,

[2]From the ODE point of view, we could also prescribe $E_2 = \rho/2$ instead of E_0.

but there are also some cases in which the derivative might not even exist due to the presence of terms $z^4\ln(z)$. In order to get access to all the needed coefficients with a reliable high accuracy, we incorporate the boundary conditions into our variables and introduce auxiliary fields via

$$\begin{aligned}
u(z) &= 1+\frac{B^2}{6}z^4\ln(z)+z^4\left[-1+(1-z)\tilde{u}(z)\right], & \alpha(z) &= 1+z^4\tilde{\alpha}(z),\\
v(z) &= 1-\frac{B^2}{24}z^4\ln(z)+z^4\tilde{v}(z), & c(z) &= z^4(1-z)\tilde{c}(z),\\
w(z) &= 1+\frac{B^2}{12}z^4\ln(z)+z^4\tilde{w}(z), & q(z) &= z^4(1-z)\tilde{q}(z),\\
E(z) &= (1-z)\tilde{E}(z), & g(z) &= z^4\tilde{g}(z),\\
P(z) &= z^2\tilde{P}(z)), & b(z) &= z^2\tilde{b}(z). \qquad \text{(A.7)}
\end{aligned}$$

After substituting (A.7) into the equations of motion (A.3), we factor out powers of z and $(1-z)$ and impose the resulting equations in the entire interval $z\in[0,1]$, i.e. as $z\to 0$ and $z\to 1$, the boundary conditions follow automatically from the limiting values of the the equations of motion written in terms of the auxiliary variables. The equations are then solved numerically with a spectral method, described in app. A.2.

A.2. Numerical details

As mentioned before, the system of equations (A.3) expressed in terms of the auxiliary variables (A.7) is solved numerically by means of a spectral method. In this section, we elaborate further on this topic and we give more details on the numerics involved.

Spectral methods are best applied to differential equations whose solutions are known to be analytic. In such a case, the error coming from the numerics decays exponentially as one increases the grid resolution. On the other hand, the presence of logarithmic terms spoils this properties, rendering a merely algebraic convergence rate. Yet, the introduction of the auxiliary variables (A.7) removed the leading $z^4\ln(z)$ terms and we verify that our solutions show typically a rather efficient convergence rate, even for large values of $\bar{B}$.

In addition to the high accuracy, spectral methods are also flexible enough to deal with other unknown parameters apart from the field functions. In order to fix these parameters, one needs to specify extra conditions together with the equations of motion. As a global scheme, the method makes no distinction between the unknown

functions and parameters and solves the system of all variables at once. In the context of gauge/gravity dualities, it is possible to address the low temperature behaviour within spectral methods. In addition, spectral methods also allow to include singular points and hence the equations of motion can be solved in the whole domain.

A.2.1. Spectral Methods

Let n_{fields} be the total number of unknown functions X^I (with $I = 1, \ldots, n_{\text{fields}}$) defined on the domain $z \in [0, 1]$. Let us also assume the existence of n_{par} unknown real parameters χ^A (with $A = 1, \ldots, n_{\text{par}}$). Moreover, we consider the following system of equations

$$\begin{cases} F_0^I(X'^I, X^I; \chi^A) = 0 & \text{for} \quad z = 0\,, \\ F^I(X''^I, X'^I, X^I, z; \chi^A) = 0 & \text{for} \quad 0 < z < 1\,, \\ F_1^I(X'^I, X^I; \chi^A) = 0 & \text{for} \quad z = 1\,, \\ \Phi^A(X''^I, X'^I, X^I; \chi^A) = 0\,. \end{cases} \tag{A.8}$$

Here, X'^I and X''^I are, respectively, the first and second derivative of the functions $X^I(z)$. F_0^I and F_1^I are the boundary conditions, whereas F^I represent the equations of motions. Finally, Φ^A stand for the extra conditions that fix the unknown parameters.

In order to solve numerically the system of equations (A.8), we first provide a numerical resolution N and expand the functions $X^I(z)$ as

$$X^I(z) = \sum_{k=0}^{N} c^I{}_k \, T_k(2z - 1) + R^I(z). \tag{A.9}$$

In the expansion above, the basis functions are the Chebyshev polynomials of first kind $T_k(\xi) = \cos[k \arccos(\xi)]$, $\xi \in [-1, 1]$, while $R^I(z)$ are the residual functions. To determine the Chebyshev coefficients $c^I{}_k$, we specify a set of grid points z_i (with $i = 0, \ldots, N$) and impose that the residual function vanishes exactly at the grid points, i.e. $R(z_i) = 0$. In other words, at the grid points, the unknown functions are given exactly by the spectral representation

$$X^I(z_i) = \sum_{k=0}^{N} c^I{}_k \, T_k(2z_i - 1). \tag{A.10}$$

The Chebyshev coefficients are then obtained after the inversion of (A.10). From the

${c^I}_k$, we can obtain the coefficients ${c'^I}_k$ and ${c''^I}_k$ describing the spectral representation of the derivatives $X'^I(z)$ and $X''^I(z)$ as in (A.9). In this thesis, we work with the Chebyshev-Lobatto grid points

$$z_i = \frac{1}{2}\left[1 + \cos\left(\pi \frac{i}{N}\right)\right], \qquad i = 0, \ldots, N. \tag{A.11}$$

Now we can combine the function values ${X^I}_i := X^I(z_i)$ and the parameters χ^A into the single vector $\vec{X}$ of length $n_{\text{total}} = (N+1)n_{\text{Fields}} + n_{\text{par}}$

$$\vec{X}^{\mathrm{T}} = \left(X^1_0, \ldots, X^1_N, \ldots X^{n_{\text{Fields}}}_0, \ldots X^{n_{\text{Fields}}}_N | \chi^1, \ldots, \chi^{n_{\text{par}}}\right) \tag{A.12}$$

from which we can also form the vectors $\vec{X}'$ and $\vec{X}''$ representing the discrete spectral derivatives with respect to z. These vectors are finally used to evaluate the system of equations (A.8) at the grid points (A.11), giving us a non-linear algebraic system

$$\vec{F}(\vec{X}) = 0 \tag{A.13}$$

to be solved for the components of the vector $\vec{X}$. The solution of the algebraic system (A.13) is obtained by a Newton-Raphson method, i.e. given an initial guess $\vec{X}_0$, the solution is iteratively approximated by

$$\vec{X}_{n+1} = \vec{X}_n + \delta\vec{X}_n, \quad \text{with} \quad \delta\vec{X}_n = -\left[\hat{J}(\vec{X}_n)\right]^{-1} \vec{F}(\vec{X}_n). \tag{A.14}$$

The inversion of the Jacobian matrix $\hat{J}(\vec{X}) = \partial\vec{F}/\partial\vec{X}$ is performed with a LU decomposition. One can show that the Newton-Rapshon scheme always converges, providing the initial guess $\vec{X}_0$ is sufficiently close to a solution.

A.2.2. Numerical solution: illustration

To illustrate the solutions, we show in fig. A.1 the results for the auxiliary metric and gauge field functions with $\gamma = 1.5$ for the following two configurations:

$$\begin{aligned} &\{\bar{B} = 0, \qquad \bar{k} = 1.21, \bar{T} = 3.25 \times 10^{-2}\}, \\ &\{\bar{B} = 0.275, \bar{k} = 0.98, \bar{T} = 1.25 \times 10^{-2}\}, \end{aligned} \tag{A.15}$$

giving respectively $\mu = 2.172$ and $\mu = 2.982$ for the chemical potential.

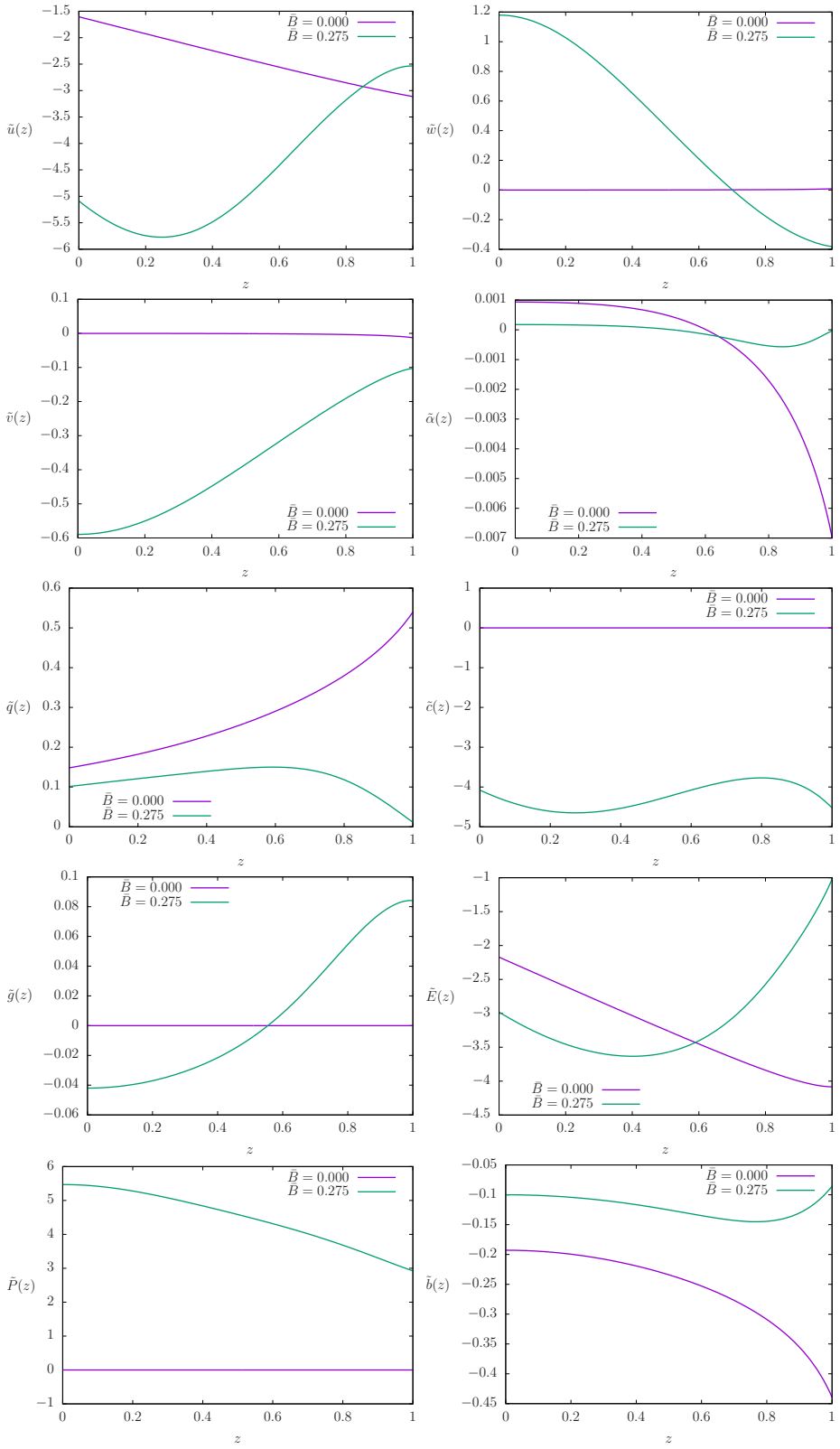

Fig. A.1.: Solutions for the metric functions $\tilde{u}(z)$, $\tilde{w}(z)$, $\tilde{v}(z)$, $\tilde{\alpha}(z)$, $\tilde{q}(z)$, $\tilde{c}(z)$ and the gauge field functions $\tilde{E}(z)$, $\tilde{P}(z)$, $\tilde{b}(z)$ for $\{\bar{B} = 0, \bar{k} = 1.21, \bar{T} = 3.25 \times 10^{-2}\}$ and $\{\bar{B} = 0.275, \bar{k} = 0.98, \bar{T} = 1.25 \times 10^{-2}\}$.

A.2.3. Numerical solution: the initial guess

We are looking for the numerical solution of the $n_{\text{Fields}} = 10$ metric and gauge field functions. If $\bar{B} = 0$, the electrically charged Reissner-Nordstroem black brane (2.106) is always a solution, regardless of $\bar{k}$ and γ. Similarly, for $\bar{B} \neq 0$ one always obtains charged magnetic black brane as trivial solution. The interesting cases are those values of γ and $\bar{k}$ for which a non-trivial solution with $b(z) \neq 0$ and $q(z) \neq 0$ also exists.

Unfortunately, our first experiences showed that, for a given boundary value $\tilde{E}(0) = -\mu$, the Newton-Raphson method always converged to a trivial solution of the non-linear algebraic system (A.13), regardless of the initial guess $\vec{X}_0$. In order to obtain the new solution describing the condensed phase, an extremely careful fine-tuning to the initial guess $\vec{X}_0$ seems to be needed.

To solve this issue, we consider the parameter μ as a further unknown variable (thus $n_{\text{par}} = 1$) and impose the extra condition $\tilde{b}(0) = b_2 = \varepsilon$. By fixing a value $\varepsilon \neq 0$, we enforce that the Newton-Raphson scheme will necessarily converge to the non-trivial solution.

For a given $\bar{k}$, γ, we start with $\bar{B} \sim 0$, and $\varepsilon \sim 0$. Then, the new solution should be just a small perturbation of the AdS Reissner-Nordstroem spacetime. Therefore, our initial-guess constitutes of (2.118) and (2.119), with the slight modification $\tilde{b}(z) = \varepsilon$. Besides, we must also provide an initial-guess for the variable μ. In all our experiments, the value $\mu = 2$ was sufficient for the convergence of the Newton-Raphson scheme. Once a solution is available, we can use it as initial-guess for a modified set of parameters $\left\{\gamma, \bar{B}, \bar{k}, \varepsilon\right\}$.

From the numerical point of view, fixing $\left\{\gamma, \bar{B}, \bar{k}, \varepsilon\right\}$ is an efficient method to find the non-trivial solution. However, from the physical perspective, a system with a constant temperature $\bar{T}$, i.e. specified by $\left\{\gamma, \bar{B}, \bar{k}, \bar{T}\right\}$ is what one really wants to describe. Note that, as an alternative to the extra condition $\tilde{b}(0) = b_2 = \varepsilon$, we can indeed impose $\bar{T} =$ constant. This corresponds to looking for the value of μ leading to a solution with a fixed value $\tilde{u}(1)$.

Unfortunately, this approach does not guarantee that the method will give us the non-trivial solution. Depending on how far the initial-guess is from the trivial solution, the Newton-Rapshon scheme might converge to the charged magnetic black brane solution (with $\tilde{b}(z) = 0$). Therefore, for a fixed $\{\gamma, \bar{B}\}$, our algorithm is a combination of both possibilities and can be divided into three stages:

I) Phase boundary: we set $\varepsilon = 10^{-9}$ and scan the values of $\bar{k} \in [\bar{k}_0, \bar{k}_1]$ to get the phase boundary[3]. With the knowledge of $\bar{T}(\bar{k})$ we find the point $\{\bar{k}_{\rm C}, \bar{T}_{\rm C}\}$ for which $\bar{T}_{\rm C} = \bar{T}(\bar{k}_{\rm C})$ is at a maximum.

II) Condensed phase: we then keep $\bar{k} = \bar{k}_{\rm C}$ fixed and find new solutions inside the phase by slowly increasing the values of ε until a given $0 < \bar{T}_0 < \bar{T}_{\rm C}$ is achieved. Typically, we set $\bar{T}_0 = 0.95\,\bar{T}_{\rm C}$.

III) Constant temperature: with the solution inside the phase provided by step II as initial guess, we no longer need to keep ε fixed. We now solve at surfaces of constant $\bar{T} \in [\bar{T}_{\rm min}, \bar{T}_0] \cup [\bar{T}_0, \bar{T}_{\rm C}]$ in a given interval $\bar{k} \in [\bar{k}_0(\bar{T}), \bar{k}_1(\bar{T})]$ and find the physical state $\bar{k}_*(\bar{T})$ for which the grand canonical potential $\bar{\Omega}_* = \bar{\Omega}(\bar{k}_*)$ is at a minimum.

A.2.4. Numerical error

Finally, we discuss the accuracy of our method. Given a high resolution $N_{\rm max}$, we consider a reference solution $\left\{X^I(z; N_{\rm max}), \rho(N_{\rm max})\right\}$ and define, for a lower resolution $N < N_{\rm max}$, the numerical error of the solution $\left\{X^I(z; N), \mu(N)\right\}$ by

$$\epsilon^I(N) = \max_{z\in[0,1]} \left|X^I(z; N) - X^I(z; N_{\rm max})\right|, \qquad \epsilon^\mu(N) = \left|\mu(N) - \mu(N_{\rm max})\right| . \tag{A.16}$$

Fig. A.2 displays the error for the configurations mentioned in the previous section. The left panel shows the case $\bar{B} = 0$ and we see the typical exponential convergence provided by the spectral method. The right panel depicts the case $\bar{B} = 0.275$. Despite the presence of logarithmic terms, the convergence rate is very efficient and we do not observe a significant influence of an algebraic decay within the machine limits imposed by round off errors.

Even though the method provides a high accuracy solution for moderate values of $\bar{T}$, we note that the small temperature regime requires a massive increase in resolution. This feature becomes evident in fig. A.3, where we compare the convergence rate (for instance for μ) at different temperatures. As already mentioned in app. 4.4.1 and illustrated in fig. 4.2, the main reason is the presence of strong gradients around the horizon $z = 1$.

[3]For some values of $\{\gamma, \bar{B}\}$ one might find returning points, i.e. there might exist values of $\bar{k}$ with two different solutions $\bar{T}(\bar{k})$. In such cases, we employed the methods described in [144] to scan the whole parameter range.

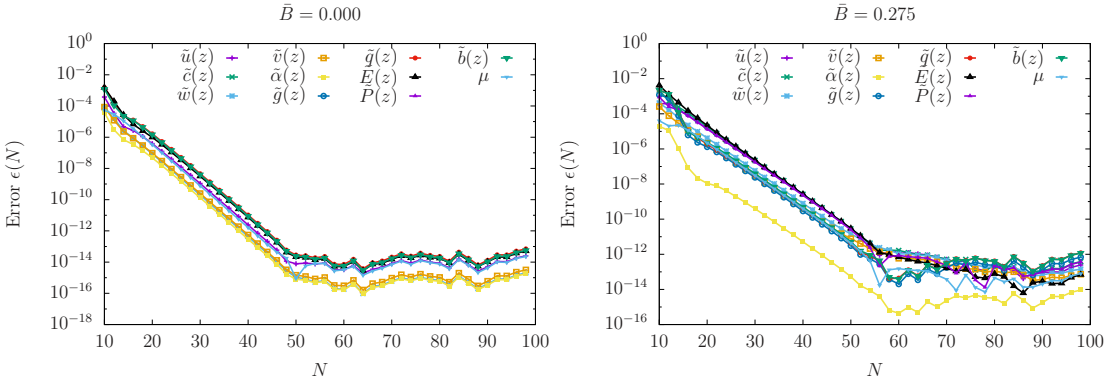

Fig. A.2.: Numerical errors for the two configurations $\{\bar{B} = 0, \bar{k} = 1.21, \bar{T} = 3.25 \times 10^{-2}\}$ (left panel) and $\{\bar{B} = 0.275, \bar{k} = 0.98, \bar{T} = 1.25 \times 10^{-2}\}$ (right panel). For $\bar{B} = 0$ we obtain the expected exponential convergence rate. For $\bar{B} \neq 0$ one expects a merely algebraic decay due to the logarithmic terms. Its contribution, however, enters only within the machine precision.

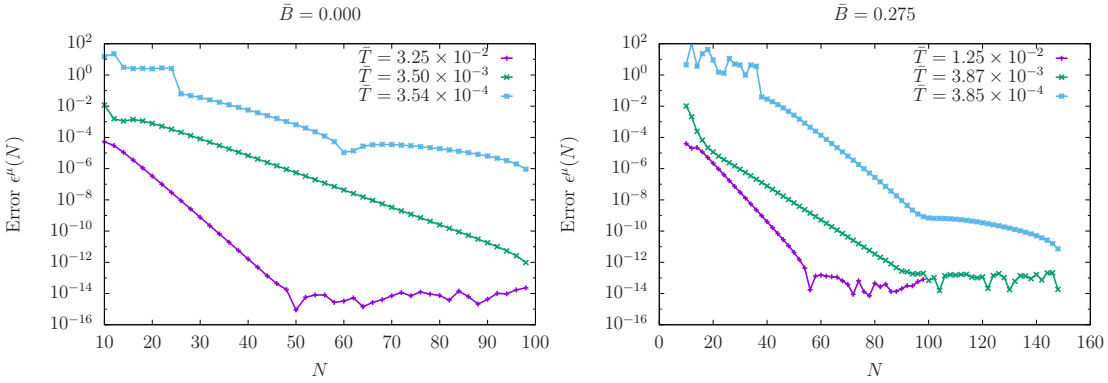

Fig. A.3.: Numerical error for low temperatures. Despite the exponential convergence rate, the method becomes less efficient as the temperature decreases due to the presence of strong gradients near $z = 1$ (see fig. 4.2). A reliable highly accurate solution requires a massive increase in the numerical resolution.

One technique to deal with such strong gradients is the so called analytical mesh-refinement, described in [136, 137]. It consists of mapping the coordinate $z \in [0, 1]$ into $\zeta \in [0, 1]$ via

$$z = 1 - \frac{\sinh[\lambda(1 - \zeta)]}{\sinh \lambda}. \tag{A.17}$$

By choosing an adequate parameter λ, the mapping increases the number of grid points around $z = 1$ and smoothens out the solution. In our case we set $\lambda = \left|b_2 \ln(\bar{T})\right|$. In fig. A.4 one sees the significant improvement of the convergence rate,

specially in the case $\bar{B} = 0$. For $\bar{B} \neq 0$, the method is still effective at low temperatures, but it also intensifies the algebraic decay rate introduced by logarithmic terms. Even though the analytical mesh-refinement provides the necessary tools to study the low temperature limit within the scope of this work, we note that there are still possibilities for enhancing the accuracy of the $\bar{B} \neq 0$ case.[4]

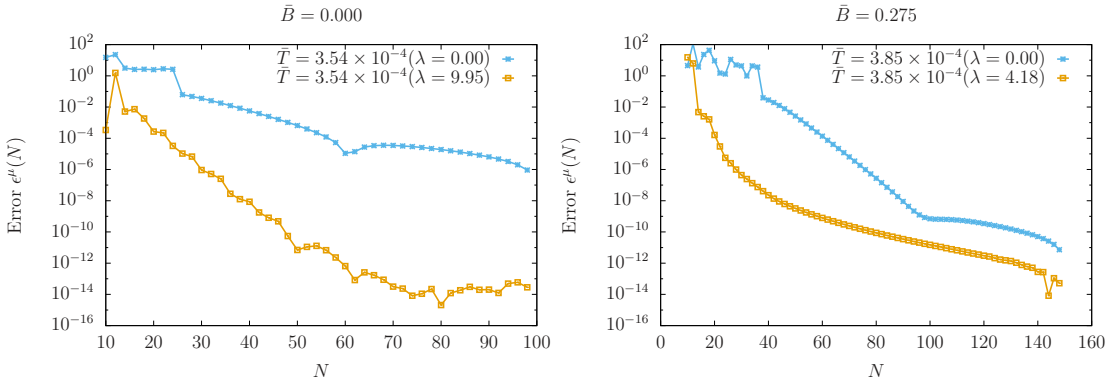

Fig. A.4.: Numerical error for low temperatures with the analytical mesh-refinement. Left panel: for $\bar{B} = 0$ the convergence rate is significantly improved and we achieve the machine precision with a moderate number of grid points. Right panel: for $\bar{B} \neq 0$ we still obtain a better convergence rate, though the method worsens the algebraic decay due to the logarithmic terms.

A.3. Numerical methods for QNMs & charged branes

Let us now discuss the numerics for the background and the QNM of ch. 3. The equations of motion for the background and the equations of motion for the fluctuations on the corresponding background are given by (2.94) and (2.95) using the ansatz (3.1)-(3.3) or (3.15),(3.16) respectively. The equations obtained are solved numerically with spectral methods. In this section, we briefly discuss the numerics for the nonlinear background equations as well as the nonlinear generalized eigenvalue problem for the QNMs in detail. The whole numerics is set up in Mathematica. This enforces us to use several performance optimizations, which we will discuss for the background and the QNMs.

[4] An option is to use a multi-domain code with another coordinate map to remove the logarithmic terms [145, 146].

A.3.1. Background

The equations of motion (2.94) and (2.95) for the background are given by six nonlinear ordinary differential equations and one constraint equation for the six unknown functions, $u(z), v(z), w(z), c(z)$ and $A_v(z), P(z)$. The constraint is again incorporated in the boundary conditions. For this project we also subtract the leading logarithms as previously introduced (A.7) and calculate all background data with 100 gridpoints, which we justify in the following discussion on QNMs.

To be able to use large gridsizes and to get high precision results we use the following advanced techniques in our numerical code. In the first step we carefully make sure to keep the equations of motion in a very short form, in particular after extracting the logarithms, terms like e.g. $u(z)^2 = (1 + z^4 u_4 + z^4 \ln(z) B^2/6)^2$ should not be expanded, which can be the case when using Simplify[ ] in Mathematica.

We than replace the functions $f(z) = \{u(z), v(z), w(z), c(z), A_v(z), P(z)\}$ by symbolic quantities by $f = \{u, v, w, c, A_v, P\}$. Instead of replacing derivatives of f by their spectral representation, we also replace $f'(z)$ by $df = \{du, dv, dw, dc, dA_v, dP\}$ and their second derivatives by $d^2 f$. This has the advantage, that numerical values for the derivatives are calculated only once in each step using spectral differentiation matrices, such that e.g. the numerical value of the symbol du is calculated once and then replaced everywhere it appears in the equations of motion or in the Jacobian. The replacement is done with a faster Dispatch-rule in Mathematica instead of a trivial replacement-rule.

In addition we calculate the Jacobian only in the first step of the Newton-Raphson iteration symbolically and store it for the further iterations. The Jacobian is calculated using the chain rule, i.e. calculating

$$\frac{\partial (EoM)_i}{\partial (f)_j} + \frac{\partial (EoM)_i}{\partial (df)_l} \frac{\partial (df)_l}{\partial (f)_j} + \frac{\partial (EoM)_i}{\partial (d^2 f)_l} \frac{\partial (d^2 f)_l}{\partial (f)_j} \,, \tag{A.18}$$

where $\frac{\partial (df)_l}{\partial (f)_j}$ and $\frac{\partial (d^2 f)_l}{\partial (f)_j}$ are given by a block matrix of the spectral differentiation matrix.

Moreover to calculate backgrounds with constant $\bar{T}$ and varying $\bar{B}$ or constant $\bar{B}$ and varying $\bar{T}$, we replace the boundary condition $A_v(0) = \mu$ at the conformal boundary by a condition for the temperature $u'(1) = 4\pi\mu\bar{T}$. This is equivalent to promoting μ to an extra parameter and implementing $u'(1) = 4\pi\mu\bar{T}$ as an extra condition.

A.3.2. Quasinormal Modes

The fluctuation equations are discretized in the same way, where we now have to insert the numerical values for the previously calculated background. We use the second order differential equations to formulate the eigenvalue problem and include the constraints in the boundary conditions. The QNMs are determined as solution of a generalized eigenvalue problem

$$(A - \omega\, B)\, \vec{x} = 0\,, \tag{A.19}$$

with respect to the right boundary conditions, see sec. 3.4.2. The vector $\vec{x}$ contains the values of all fields evaluated at the gridpoints, which represents our numerical solution for the QNM functions. We force the boundary value of all fluctuations to be zero by factorizing out proper powers of z

$$h_{ij}(z) = z^4 \tilde{h}_{ij}(z)\,, \qquad a_i(z) = z^2 \tilde{a}_i(z)\,. \tag{A.20}$$

Despite being in Eddington Finkelstein coordinates, the helicity-0 sector has a quadratic ω dependence, giving a nonlinear eigenvalue problem. This arises from additional ω contributions in the determinant of the metric. The helicity-1 and helicity-2 sectors are still linear in ω. The quadratic eigenvalue problem can be reduced to a linear eigenvalue problem by doubling the number of fields, introducing $h_{ij}^{new}(z) = \omega\, h_{ij}(z)$.

In addition to the numerical techniques for the background, we replace the derivatives of the background and the fluctuations again symbolically and calculate their values only once. Moreover we use the background equations of motion to eliminate all second derivatives of background fields in our QNM equations. For interpolation we use the fast and accurate Clenshaw algorithm. The linear eigenvalue problems are solved with Mathematica Eigenvalue/Eigensystem, to get the QNM and the eigenfunctions, respectively. All QNM data in this project are calculated also with 100 gridpoints and 60 digits precision, which means solving a 100×100 matrix for helicity-2, two 300×300 matrices for helicity-1 and a 800×800 matrix for helicity-0 sector.

By plugging back the eigenvalue and the eigenfunctions into the equation of motion, we check if we have a true solution of the full system including constraints. In our analysis QNMs appear, that converge and fulfil the equations of motion, but not the constraint(s). It happens that those QNMs additionally do not change with k. Accordingly these QNMs are identified as numerical artefacts and are rejected

for the analysis. We refer them as fake QNMs which also show up in the continued fraction method [147, 148]. In particular, the fake QNMs may be traced back to a degeneracy of the ingoing/outgoing horizon conditions in the Poincare chart. At the horizon, ingoing and outgoing modes have a term of the form $(1-z)^{\pm i\omega/u_1}$, which for $\omega = -i\,n\,u_1/2$, with $n \in \mathbb{N}$, is degenerate from the power series in $1-z$. Taking into account $u_1 = 4\pi T$, the fake QNMs lie at $\omega = -2\pi i\,T\,n$ with $n \in \mathbb{N}$, as expected.

A.3.3. Helicity-2 sector

The helicity-2 sector is described by two decoupled equations of motion. The convergence in helicity-2 sector is slow due to logarithms in the background and logarithms in the QNM eigenfunctions. It further shows an even/odd gridsize oscillation, meaning that the QNM value for even/odd gridsizes approaches the correct value from above and below respectively.

Therefore we have to introduce a $z \mapsto z^2$ mapping. This moves the logarithms to higher orders

$$z^n \log(z) \mapsto 2\, z^{2n} \log(z)\,, \tag{A.21}$$

which improves the convergence. The coordinate mapping (A.21) is more practical in this case, compared to mapping (A.17), as it leaves the simple algebraic structure of the EOMs unchanged. This is more important in Mathematica compared to a C-implementation. Interestingly we find that this allows to use simplified boundary conditions at $z = 0$. In principle one has to specify the new boundary condition $f'(z) = 0$ for all fields f as well as the boundary condition before the mapping. In our case the condition $f'(z) = 0$ was sufficient to reproduce the results before the mapping, since our boundary conditions are solely given by the equations of motion. All calculations, and in particular the convergence plots shown below, are obtained with this mapping. With the z^2 mapping we already obtain good results with 40 gridpoints, see fig. A.5.

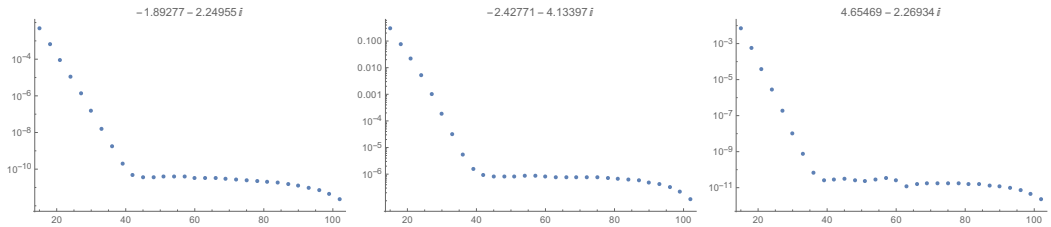

Fig. A.5.: Convergence test for three helicity-2 modes at $\tilde{k} = 20$, $\tilde{B} = 65$, $\bar{T} = 0.1$.

A.3.4. Helicity-1 and helicity-0 sector

Helicity-1 is given by two decoupled subsectors, helicity-$1^{\pm}$. Each subsector consists of three equations of motion and one constraint and has to be solved separately. We exemplary show the lowest eigenmodes and the error in the constraint in table A.1 for helicity-1^{-}. The error is obtained by plugging the corresponding eigenvector, which is the numerical solution for the fluctuations evaluated at the gridpoints, into the constraint equations and taking the norm. For example, the QNM $\omega = 0. - 2.20477\, i$ in table A.1 does not fulfil the constraint and does also not change from $\tilde{k} = 0$ to $\tilde{k} = 20$. This mode is identified as a fake QNM.

QNM ω, $\tilde{k} = 0$	Δ constraint	QNM ω, $\tilde{k} = 20$	Δ constraint
0.829152 - 0.0843573 i	$3. \times 10^{-14}$	0. - 2.20477 i	31.
-0.0933396 - 1.36129 i	$4. \times 10^{-12}$	-1.68677 - 1.54155 i	$4. \times 10^{-11}$
0. - 2.20477 i	14.	3.41168 - 0.845203 i	$3. \times 10^{-12}$
1.84644 - 1.34191 i	$7. \times 10^{-12}$	-2.23184 - 3.36554 i	$2. \times 10^{-8}$
-0.267106 - 3.58127 i	$5. \times 10^{-8}$	0. -4.40955 i	43.

Table A.1.: Error in the constraint for $k = 0$ and $\tilde{k} = 20$, $\tilde{B} = 65$, $\bar{T} = 0.1$ in the helicity-1^{-} sector, where we plug the numerical QNM frequency and QNM eigenfunctions into the constraint equation.

This mode also appears in helicity-1^{+}. Despite being a fake mode, it converges nicely, as shown in fig. A.6. In fig. A.7 we show the slower convergence for larger $\tilde{B}$ and $\tilde{k}$.

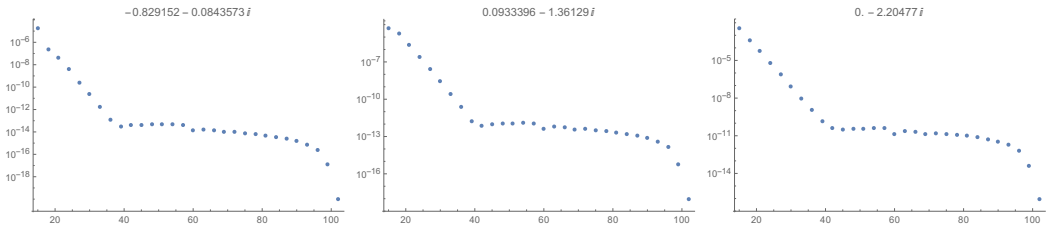

Fig. A.6.: Convergence test for three helicity-1^{+} modes at $\tilde{k} = 0$, $\tilde{B} = 65$, $\bar{T} = 0.1$.

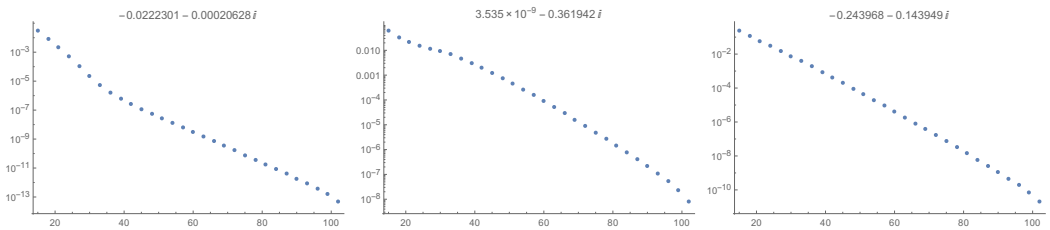

Fig. A.7.: Convergence test for three helicity-1^{+} modes at $\tilde{k} = 20$, $\tilde{B} = 65$, $\bar{T} = 0.1$.

Comparing the convergence at the same point in parameter space $\tilde{B} = 65$, $\bar{T} = 0.1$ for $\tilde{k} = 0$, shown in fig. A.6, and $\tilde{k} = 20$, shown in fig. A.7, reveals the slowing down of the convergence for larger $\tilde{k}$, which requires to use large gridsizes.

The helicity-0 sector is given by six equations of motion and four constraints. It is in addition quadratically in ω, therefore we introduce two additional fields, known as doubling trick, to get a linear system again. Convergence does not pose a problem in the helicity-0 sector, however calculations are time consuming due to very large matrices in the eigenvalue problem compared to helicity-1 and helicity-2.

B. Bibliography

[1] W. Pauli. "Über das Wasserstoffspektrum vom Standpunkt der neuen Quantenmechanik". *Zeitschrift für Physik* 36.5 (1926), p. 336.

[2] S. Elitzur. "Impossibility of Spontaneously Breaking Local Symmetries". *Phys. Rev.* D12 (1975), p. 3978.

[3] S. L. Adler. "Axial vector vertex in spinor electrodynamics". *Phys. Rev.* 177 (1969), p. 2426.

[4] J. S. Bell and R. Jackiw. "A PCAC puzzle: pi0 –> gamma gamma in the sigma model". *Nuovo Cim.* A60 (1969), p. 47.

[5] G. M. Newman. "Anomalous hydrodynamics". *JHEP* 01 (2006), p. 158. arXiv: hep-ph/0511236 [hep-ph].

[6] J. Erdmenger, M. Haack, M. Kaminski, and A. Yarom. "Fluid dynamics of R-charged black holes". *JHEP* 01 (2009), p. 055. arXiv: 0809.2488 [hep-th].

[7] D. T. Son and P. Surowka. "Hydrodynamics with Triangle Anomalies". *Phys. Rev. Lett.* 103 (2009), p. 191601. arXiv: 0906.5044 [hep-th].

[8] D. E. Kharzeev and H.-U. Yee. "Anomalies and time reversal invariance in relativistic hydrodynamics: the second order and higher dimensional formulations". *Phys. Rev.* D84 (2011), p. 045025. arXiv: 1105.6360 [hep-th].

[9] D. E. Kharzeev, J. Liao, S. A. Voloshin, and G. Wang. "Chiral magnetic and vortical effects in high-energy nuclear collisions - A status report". *Prog. Part. Nucl. Phys.* 88 (2016), p. 1. arXiv: 1511.04050 [hep-ph].

[10] Q. Li et al. "Observation of the chiral magnetic effect in ZrTe5". *ArXiv e-prints* (2014). arXiv: 1412.6543 [cond-mat.str-el].

[11] C. Shekhar et al. "Large and unsaturated negative magnetoresistance induced by the chiral anomaly in the Weyl semimetal TaP". *ArXiv e-prints* (2015). arXiv: 1506.06577 [cond-mat.mtrl-sci].

[12] C. Zhang et al. "Detection of chiral anomaly and valley transport in Dirac semimetals". *ArXiv e-prints* (2015). arXiv: 1504.07698 [cond-mat.mtrl-sci].

[13] Z. Wang et al. "Helicity protected ultrahigh mobility Weyl fermions in NbP". *ArXiv e-prints* (2015). arXiv: 1506.00924 [cond-mat.mes-hall].

[14] X. Yang, Y. Liu, Z. Wang, Y. Zheng, and Z.-a. Xu. "Chiral anomaly induced negative magnetoresistance in topological Weyl semimetal NbAs". *ArXiv e-prints* (2015). arXiv: 1506.03190 [cond-mat.mtrl-sci].

[15] S. Sachdev. *Quantum phase transitions*. Cambridge University Press, 2001.

[16] A. W. Rost, R. S. Perry, J.-F. Mercure, A. P. Mackenzie, and S. A. Grigera. "Entropy Landscape of Phase Formation Associated with Quantum Criticality in Sr3Ru2O7". *Science* 325.5946 (2009), p. 1360. eprint: http://science.sciencemag.org/content/325/5946/1360.full.pdf.

[17] G. Basar, G. V. Dunne, and D. E. Kharzeev. "Chiral Magnetic Spiral". *Phys. Rev. Lett.* 104 (2010), p. 232301. arXiv: 1003.3464 [hep-ph].

[18] K.-Y. Kim, B. Sahoo, and H.-U. Yee. "Holographic chiral magnetic spiral". *JHEP* 10 (2010), p. 005. arXiv: 1007.1985 [hep-th].

[19] A. Ballon-Bayona, K. Peeters, and M. Zamaklar. "A chiral magnetic spiral in the holographic Sakai-Sugimoto model". *JHEP* 11 (2012), p. 164. arXiv: 1209.1953 [hep-th].

[20] G. W. Gibbons and C. M. Warnick. "The helical phase of chiral nematic liquid crystals as the Bianchi VII(0) group manifold". *Phys. Rev.* E84 (2011), p. 031709. arXiv: 1106.2423 [gr-qc].

[21] *BeautifulChemistry*. URL: http://www.beautifulchemistry.net/liquid-crystals/ (visited on 06/28/2017).

[22] E. Fradkin, S. A. Kivelson, M. J. Lawler, J. P. Eisenstein, and A. P. MacKenzie. "Nematic Fermi Fluids in Condensed Matter Physics". *Annual Review of Condensed Matter Physics* 1 (2010), p. 153. arXiv: 0910.4166 [cond-mat.str-el].

[23] J. M. Maldacena. "The large N limit of superconformal field theories and supergravity". *Adv. Theor. Math. Phys.* 2 (1998), p. 231. arXiv: hep-th/9711200.

[24] M. Ammon and J. Erdmenger. *Gauge/gravity duality*. Cambridge, UK: Cambridge Univ. Pr., 2015.

[25] H. Nastase. *Introduction to the AdS/CFT Correspondence*. Cambridge, UK: Cambridge Univ. Pr., 2015.

[26] J. Zaanen, Y. Liu, Y.-W. Sun, and K. Schalm. *Holographic Duality in Condensed Matter Physics*. Cambridge, UK: Cambridge Univ. Pr., 2016.

[27] S. A. Hartnoll. "Lectures on holographic methods for condensed matter physics". *Class. Quant. Grav.* 26 (2009), p. 224002. arXiv: 0903.3246 [hep-th].

[28] C. P. Herzog. "Lectures on Holographic Superfluidity and Superconductivity". *J. Phys.* A42 (2009), p. 343001. arXiv: 0904.1975 [hep-th].

[29] J. McGreevy. "Holographic duality with a view toward many-body physics". *Adv. High Energy Phys.* 2010 (2010), p. 723105. arXiv: 0909.0518 [hep-th].

[30] J. Casalderrey-Solana, H. Liu, D. Mateos, K. Rajagopal, and U. A. Wiedemann. "Gauge/String Duality, Hot QCD and Heavy Ion Collisions" (2011). arXiv: 1101.0618 [hep-th].

[31] M. Ammon. "Gauge/gravity duality applied to condensed matter systems". *Fortschritte der Physik* 58.11-12 (2010), p. 1123.

[32] S. A. Hartnoll, C. P. Herzog, and G. T. Horowitz. "Building a Holographic Superconductor". *Phys. Rev. Lett.* 101 (2008), p. 031601. arXiv: 0803.3295 [hep-th].

[33] S. S. Gubser and S. S. Pufu. "The gravity dual of a p-wave superconductor". *JHEP* 11 (2008), p. 033. arXiv: 0805.2960 [hep-th].

[34] M. Ammon, J. Erdmenger, M. Kaminski, and P. Kerner. "Superconductivity from gauge/gravity duality with flavor". *Phys. Lett.* B680 (2009), p. 516. arXiv: 0810.2316 [hep-th].

[35] M. Ammon, J. Erdmenger, M. Kaminski, and P. Kerner. "Flavor Superconductivity from Gauge/Gravity Duality". *JHEP* 10 (2009), p. 067. arXiv: 0903.1864 [hep-th].

[36] M. Ammon, J. Erdmenger, V. Grass, P. Kerner, and A. O'Bannon. "On Holographic p-wave Superfluids with Back-reaction". *Phys. Lett.* B686 (2010), p. 192. arXiv: 0912.3515 [hep-th].

[37] H. Liu, J. McGreevy, and D. Vegh. "Non-Fermi liquids from holography". *Phys. Rev.* D83 (2011), p. 065029. arXiv: 0903.2477 [hep-th].

[38] M. Ammon, J. Erdmenger, M. Kaminski, and A. O'Bannon. "Fermionic Operator Mixing in Holographic p-wave Superfluids". *JHEP* 05 (2010), p. 053. arXiv: 1003.1134 [hep-th].

[39] J. Erdmenger, C. Hoyos, A. O'Bannon, and J. Wu. "A Holographic Model of the Kondo Effect". *JHEP* 12 (2013), p. 086. arXiv: 1310.3271 [hep-th].

[40] J. Erdmenger, M. Flory, C. Hoyos, M.-N. Newrzella, and J. M. S. Wu. "Entanglement Entropy in a Holographic Kondo Model". *Fortsch. Phys.* 64 (2016), p. 109. arXiv: 1511.03666 [hep-th].

[41] J. Erdmenger et al. "Holographic impurities and Kondo effect". *Fortsch. Phys.* 64 (2016), p. 322. arXiv: 1511.09362 [hep-th].

[42] J. Erdmenger, M. Flory, M.-N. Newrzella, M. Strydom, and J. M. S. Wu. "Quantum Quenches in a Holographic Kondo Model". *JHEP* 04 (2017), p. 045. arXiv: 1612.06860 [hep-th].

[43] C. Hoyos-Badajoz, K. Jensen, and A. Karch. "A Holographic Fractional Topological Insulator". *Phys. Rev.* D82 (2010), p. 086001. arXiv: 1007.3253 [hep-th].

[44] A. Karch, J. Maciejko, and T. Takayanagi. "Holographic fractional topological insulators in 2+1 and 1+1 dimensions". *Phys. Rev.* D82 (2010), p. 126003. arXiv: 1009.2991 [hep-th].

[45] M. Ammon and M. Gutperle. "A supersymmetric holographic dual of a fractional topological insulator". *Phys. Rev.* D86 (2012), p. 025018. arXiv: 1204.2217 [hep-th].

[46] J. L. Davis, P. Kraus, and A. Shah. "Gravity Dual of a Quantum Hall Plateau Transition". *JHEP* 11 (2008), p. 020. arXiv: 0809.1876 [hep-th].

[47] A. Gynther, K. Landsteiner, F. Pena-Benitez, and A. Rebhan. "Holographic Anomalous Conductivities and the Chiral Magnetic Effect". *JHEP* 1102 (2011), p. 110. arXiv: 1005.2587 [hep-th].

[48] P. K. Kovtun and A. O. Starinets. "Quasinormal modes and holography". *Phys. Rev.* D72 (2005), p. 086009. arXiv: hep-th/0506184 [hep-th].

[49] D. T. Son and A. O. Starinets. "Minkowski space correlators in AdS / CFT correspondence: Recipe and applications". *JHEP* 09 (2002), p. 042. arXiv: hep-th/0205051 [hep-th].

[50] M. P. Heller, D. Mateos, W. van der Schee, and M. Triana. "Holographic isotropization linearized". *JHEP* 09 (2013), p. 026. arXiv: 1304.5172 [hep-th].

[51] A. Buchel, M. P. Heller, and R. C. Myers. "Equilibration rates in a strongly coupled nonconformal quark-gluon plasma". *Phys. Rev. Lett.* 114.25 (2015), p. 251601. arXiv: 1503.07114 [hep-th].

[52] J. F. Fuini and L. G. Yaffe. "Far-from-equilibrium dynamics of a strongly coupled non-Abelian plasma with non-zero charge density or external magnetic field". *JHEP* 07 (2015), p. 116. arXiv: 1503.07148 [hep-th].

[53] S. Janiszewski and M. Kaminski. "Quasinormal modes of magnetic and electric black branes versus far from equilibrium anisotropic fluids" (2015). arXiv: 1508.06993 [hep-th].

[54] R. A. Janik, J. Jankowski, and H. Soltanpanahi. "Quasinormal modes and the phase structure of strongly coupled matter". *JHEP* 06 (2016), p. 047. arXiv: 1603.05950 [hep-th].

[55] M. Attems et al. "Thermodynamics, transport and relaxation in non-conformal theories". *JHEP* 10 (2016), p. 155. arXiv: 1603.01254 [hep-th].

[56] A. Nunez and A. O. Starinets. "AdS / CFT correspondence, quasinormal modes, and thermal correlators in N=4 SYM". *Phys. Rev.* D67 (2003), p. 124013. arXiv: hep-th/0302026 [hep-th].

[57] K. Landsteiner and Y. Liu. "The holographic Weyl semi-metal". *Phys. Lett.* B753 (2016), p. 453. arXiv: 1505.04772 [hep-th].

[58] K. Landsteiner, Y. Liu, and Y.-W. Sun. "Quantum phase transition between a topological and a trivial semimetal from holography". *Phys. Rev. Lett.* 116.8 (2016), p. 081602. arXiv: 1511.05505 [hep-th].

[59] C. Copetti, J. Fernández-Pendás, and K. Landsteiner. "Axial Hall effect and universality of holographic Weyl semi-metals" (2016). arXiv: 1611.08125 [hep-th].

[60] M. Ammon, M. Heinrich, A. Jimenez-Alba, and S. Moeckel. "Surface States in Holographic Weyl Semimetals" (2016). arXiv: 1612.00836 [hep-th].

[61] G. Grignani, A. Marini, F. Pena-Benitez, and S. Speziali. "AC conductivity for a holographic Weyl Semimetal" (2016). arXiv: 1612.00486 [cond-mat.str-el].

[62] P. Hosur and X. Qi. "Recent developments in transport phenomena in Weyl semimetals". *Comptes Rendus Physique* 14 (2013), p. 857. arXiv: 1309.4464 [cond-mat.str-el].

[63] E. D'Hoker and P. Kraus. "Holographic Metamagnetism, Quantum Criticality, and Crossover Behavior". *JHEP* 05 (2010), p. 083. arXiv: 1003.1302 [hep-th].

[64] E. D'Hoker and P. Kraus. "Magnetic Field Induced Quantum Criticality via new Asymptotically AdS5 Solutions". *Class. Quant. Grav.* 27 (2010), p. 215022. arXiv: 1006.2573 [hep-th].

[65] E. D'Hoker and P. Kraus. "Quantum Criticality via Magnetic Branes". *Lect. Notes Phys.* 871 (2013), p. 469. arXiv: 1208.1925 [hep-th].

[66] A. Donos and J. P. Gauntlett. "Black holes dual to helical current phases". *Phys. Rev.* D86 (2012), p. 064010. arXiv: 1204.1734 [hep-th].

[67] A. Donos. "Striped phases from holography". *JHEP* 05 (2013), p. 059. arXiv: 1303.7211 [hep-th].

[68] B. Withers. "Holographic Checkerboards". *JHEP* 09 (2014), p. 102. arXiv: 1407.1085 [hep-th].

[69] O. Domenech, M. Montull, A. Pomarol, A. Salvio, and P. J. Silva. "Emergent Gauge Fields in Holographic Superconductors". *JHEP* 08 (2010), p. 033. arXiv: 1005.1776 [hep-th].

[70] S. Bolognesi and D. Tong. "Monopoles and Holography". *JHEP* 01 (2011), p. 153. arXiv: 1010.4178 [hep-th].

[71] M. Ammon, J. Erdmenger, P. Kerner, and M. Strydom. "Black Hole Instability Induced by a Magnetic Field". *Phys. Lett.* B706 (2011), p. 94. arXiv: 1106.4551 [hep-th].

[72] A. Almuhairi and J. Polchinski. "Magnetic AdS x R2: Supersymmetry and stability" (2011). arXiv: 1108.1213 [hep-th].

[73] Y.-Y. Bu, J. Erdmenger, J. P. Shock, and M. Strydom. "Magnetic field induced lattice ground states from holography". *JHEP* 03 (2013), p. 165. arXiv: 1210.6669 [hep-th].

[74] S. Cremonini and A. Sinkovics. "Spatially Modulated Instabilities of Geometries with Hyperscaling Violation". *JHEP* 01 (2014), p. 099. arXiv: 1212.4172 [hep-th].

[75] M. Montull, O. Pujolas, A. Salvio, and P. J. Silva. "Magnetic Response in the Holographic Insulator/Superconductor Transition". *JHEP* 04 (2012), p. 135. arXiv: 1202.0006 [hep-th].

[76] A. Salvio. "Holographic Superfluids and Superconductors in Dilaton-Gravity". *JHEP* 09 (2012), p. 134. arXiv: 1207.3800 [hep-th].

[77] A. Salvio. "Transitions in Dilaton Holography with Global or Local Symmetries". *JHEP* 03 (2013), p. 136. arXiv: 1302.4898 [hep-th].

[78] N. Bao, S. Harrison, S. Kachru, and S. Sachdev. "Vortex Lattices and Crystalline Geometries". *Phys. Rev.* D88.2 (2013), p. 026002. arXiv: 1303.4390 [hep-th].

[79] N. Jokela, M. Jarvinen, and M. Lippert. "Gravity dual of spin and charge density waves". *JHEP* 12 (2014), p. 083. arXiv: 1408.1397 [hep-th].

[80] A. Donos and J. P. Gauntlett. "Minimally packed phases in holography" (2015). arXiv: 1512.06861 [hep-th].

[81] M. Ammon, M. Kaminski, R. Koirala, J. Leiber, and J. Wu. "Quasinormal modes of charged magnetic black branes & chiral magnetic transport". *JHEP* 04 (2017), p. 067. arXiv: 1701.05565 [hep-th].

[82] M. Ammon, J. Leiber, and R. P. Macedo. "Phase diagram of 4D field theories with chiral anomaly from holography". *JHEP* 03 (2016), p. 164. arXiv: 1601.02125 [hep-th].

[83] J. A. Harvey. "TASI 2003 lectures on anomalies". In: 2005. arXiv: hep-th/0509097 [hep-th].

[84] K. Landsteiner. "Notes on Anomaly Induced Transport". *Acta Phys. Polon.* B47 (2016), p. 2617. arXiv: 1610.04413 [hep-th].

[85] M. N. Chernodub, A. Cortijo, A. G. Grushin, K. Landsteiner, and M. A. H. Vozmediano. "Condensed matter realization of the axial magnetic effect". *Phys. Rev.* B89.8 (2014), p. 081407. arXiv: 1311.0878 [hep-th].

[86] M. Rangamani. "Gravity and Hydrodynamics: Lectures on the fluid-gravity correspondence". *Class. Quant. Grav.* 26 (2009), p. 224003. arXiv: 0905.4352 [hep-th].

[87] P. Kovtun. "Lectures on hydrodynamic fluctuations in relativistic theories". *J. Phys.* A45 (2012), p. 473001. arXiv: 1205.5040 [hep-th].

[88] N. Abbasi, D. Allahbakhshi, A. Davody, and S. F. Taghavi. "Collective Excitations in QCD Plasma" (2016). arXiv: 1612.08614 [nucl-th].

[89] K. Jensen, M. Kaminski, P. Kovtun, R. Meyer, A. Ritz, et al. "Parity-Violating Hydrodynamics in 2+1 Dimensions". *JHEP* 1205 (2012), p. 102. arXiv: 1112.4498 [hep-th].

[90] K. Jensen, M. Kaminski, P. Kovtun, R. Meyer, A. Ritz, et al. "Towards hydrodynamics without an entropy current". *Phys.Rev.Lett.* 109 (2012), p. 101601. arXiv: 1203.3556 [hep-th].

[91] K. Landsteiner, E. Megias, and F. Pena-Benitez. "Gravitational Anomaly and Transport". *Phys.Rev.Lett.* 107 (2011), p. 021601. arXiv: 1103.5006 [hep-ph].

[92] K. Landsteiner, E. Megias, L. Melgar, and F. Pena-Benitez. "Holographic Gravitational Anomaly and Chiral Vortical Effect". *JHEP* 09 (2011), p. 121. arXiv: 1107.0368 [hep-th].

[93] I. Amado, K. Landsteiner, and F. Pena-Benitez. "Anomalous transport coefficients from Kubo formulas in Holography". *JHEP* 05 (2011), p. 081. arXiv: 1102.4577 [hep-th].

[94] X.-G. Huang, A. Sedrakian, and D. H. Rischke. "Kubo formulae for relativistic fluids in strong magnetic fields". *Annals Phys.* 326 (2011), p. 3075. arXiv: 1108.0602 [astro-ph.HE].

[95] W. Israel. "The Dynamics of Polarization". *Gen. Rel. Grav.* 9 (1978), p. 451.

[96] P. Kovtun. "Thermodynamics of polarized relativistic matter". *JHEP* 07 (2016), p. 028. arXiv: 1606.01226 [hep-th].

[97] K. Jensen, R. Loganayagam, and A. Yarom. "Anomaly inflow and thermal equilibrium". *JHEP* 05 (2014), p. 134. arXiv: 1310.7024 [hep-th].

[98] D. Tong. "String Theory" (2009). arXiv: 0908.0333 [hep-th].

[99] B. Zwiebach. *A first course in string theory*. Cambridge University Press, 2006.

[100] A. V. Ramallo. "Introduction to the AdS/CFT correspondence". *Springer Proc. Phys.* 161 (2015), p. 411. arXiv: 1310.4319 [hep-th].

[101] P. H. Ginsparg. "APPLIED CONFORMAL FIELD THEORY". In: *Les Houches Summer School in Theoretical Physics: Fields, Strings, Critical Phenomena Les Houches, France, June 28-August 5, 1988*. 1988, p. 1. arXiv: hep-th/9108028 [hep-th].

[102] R. Blumenhagen and E. Plauschinn. "Introduction to conformal field theory". *Lect. Notes Phys.* 779 (2009), p. 1.

[103] P. Breitenlohner and D. Z. Freedman. "Stability in Gauged Extended Supergravity". *Annals Phys.* 144 (1982), p. 249.

[104] E. Witten. "Anti-de Sitter space and holography". *Adv. Theor. Math. Phys.* 2 (1998), p. 253. arXiv: hep-th/9802150.

[105] A. Buchel and J. T. Liu. "Gauged supergravity from type IIB string theory on Y**p,q manifolds". *Nucl. Phys.* B771 (2007), p. 93. arXiv: hep-th/0608002 [hep-th].

[106] J. P. Gauntlett, E. O Colgain, and O. Varela. "Properties of some conformal field theories with M-theory duals". *JHEP* 02 (2007), p. 049. arXiv: hep-th/0611219 [hep-th].

[107] J. P. Gauntlett and O. Varela. "Consistent Kaluza-Klein reductions for general supersymmetric AdS solutions". *Phys. Rev.* D76 (2007), p. 126007. arXiv: 0707.2315 [hep-th].

[108] E. O. Colgáin, M. M. Sheikh-Jabbari, J. F. Vázquez-Poritz, H. Yavartanoo, and Z. Zhang. "Warped Ricci-flat reductions". *Phys. Rev.* D90.4 (2014), p. 045013. arXiv: 1406.6354 [hep-th].

[109] S. de Haro, S. N. Solodukhin, and K. Skenderis. "Holographic reconstruction of space-time and renormalization in the AdS / CFT correspondence". *Commun. Math. Phys.* 217 (2001), p. 595. arXiv: hep-th/0002230 [hep-th].

[110] K. Skenderis. "Lecture notes on holographic renormalization". *Class.Quant.Grav.* 19 (2002), p. 5849. arXiv: hep-th/0209067 [hep-th].

[111] M. Henningson and K. Skenderis. "The Holographic Weyl anomaly". *JHEP* 07 (1998), p. 023. arXiv: hep-th/9806087 [hep-th].

[112] V. Balasubramanian and P. Kraus. "A Stress tensor for Anti-de Sitter gravity". *Commun. Math. Phys.* 208 (1999), p. 413. arXiv: hep-th/9902121 [hep-th].

[113] M. Taylor. "More on counterterms in the gravitational action and anomalies" (2000). arXiv: hep-th/0002125 [hep-th].

[114] E. D'Hoker and P. Kraus. "Charged Magnetic Brane Solutions in AdS (5) and the fate of the third law of thermodynamics". *JHEP* 03 (2010), p. 095. arXiv: 0911.4518 [hep-th].

[115] S. W. Hawking. "Particle Creation by Black Holes". *Commun. Math. Phys.* 43 (1975). [,167(1975)], p. 199.

[116] J. D. Bekenstein. "Black holes and entropy". *Phys. Rev.* D7 (1973), p. 2333.

[117] E. D'Hoker and P. Kraus. "Magnetic Brane Solutions in AdS". *JHEP* 10 (2009), p. 088. arXiv: 0908.3875 [hep-th].

[118] E. D'Hoker and P. Kraus. "Charge Expulsion from Black Brane Horizons, and Holographic Quantum Criticality in the Plane". *JHEP* 09 (2012), p. 105. arXiv: 1202.2085 [hep-th].

[119] S. I. Finazzo, R. Critelli, R. Rougemont, and J. Noronha. "Momentum transport in strongly coupled anisotropic plasmas in the presence of strong magnetic fields". *Phys. Rev.* D94.5 (2016), p. 054020. arXiv: 1605.06061 [hep-ph].

[120] R. Critelli, S. I. Finazzo, M. Zaniboni, and J. Noronha. "Anisotropic shear viscosity of a strongly coupled non-Abelian plasma from magnetic branes". *Phys. Rev.* D90.6 (2014), p. 066006. arXiv: 1406.6019 [hep-th].

[121] T. Kalaydzhyan and E. Murchikova. "Thermal chiral vortical and magnetic waves: new excitation modes in chiral fluids" (2016). arXiv: 1609.00024 [hep-th].

[122] D. E. Kharzeev and H.-U. Yee. "Chiral Magnetic Wave". *Phys. Rev.* D83 (2011), p. 085007. arXiv: 1012.6026 [hep-th].

[123] B. Sahoo and H.-U. Yee. "Holographic chiral shear waves from anomaly". *Phys. Lett.* B689 (2010), p. 206. arXiv: 0910.5915 [hep-th].

[124] Y. Matsuo, S.-J. Sin, S. Takeuchi, and T. Tsukioka. "Magnetic conductivity and Chern-Simons Term in Holographic Hydrodynamics of Charged AdS Black Hole". *JHEP* 04 (2010), p. 071. arXiv: 0910.3722 [hep-th].

[125] J. Hur, K. K. Kim, and S.-J. Sin. "Hydrodynamics with conserved current from the gravity dual". *JHEP* 0903 (2009), p. 036. arXiv: 0809.4541 [hep-th].

[126] Y. Matsuo, S.-J. Sin, S. Takeuchi, T. Tsukioka, and C.-M. Yoo. "Sound Modes in Holographic Hydrodynamics for Charged AdS Black Hole". *Nucl. Phys.* B820 (2009), p. 593. arXiv: 0901.0610 [hep-th].

[127] M. Ammon, S. Grieninger, A. Jimenez-Alba, R. P. Macedo, and L. Melgar. "Holographic quenches and anomalous transport". *JHEP* 09 (2016), p. 131. arXiv: 1607.06817 [hep-th].

[128] M. Edalati, J. I. Jottar, and R. G. Leigh. "Shear Modes, Criticality and Extremal Black Holes". *JHEP* 1004 (2010), p. 075. arXiv: 1001.0779 [hep-th].

[129] M. Edalati, J. I. Jottar, and R. G. Leigh. "Holography and the sound of criticality". *JHEP* 1010 (2010), p. 058. arXiv: 1005.4075 [hep-th].

[130] S. Nakamura, H. Ooguri, and C.-S. Park. "Gravity Dual of Spatially Modulated Phase". *Phys. Rev.* D81 (2010), p. 044018. arXiv: 0911.0679 [hep-th].

[131] H. Ooguri and C.-S. Park. "Holographic End-Point of Spatially Modulated Phase Transition". *Phys. Rev.* D82 (2010), p. 126001. arXiv: 1007.3737 [hep-th].

[132] J. Bhattacharya, S. Bhattacharyya, and S. Minwalla. "Dissipative Superfluid dynamics from gravity". *JHEP* 04 (2011), p. 125. arXiv: 1101.3332 [hep-th].

[133] A. Donos, J. P. Gauntlett, and C. Pantelidou. "Competing p-wave orders". *Class. Quant. Grav.* 31 (2014), p. 055007. arXiv: 1310.5741 [hep-th].

[134] M. Rogatko. "First Law of Black Rings Thermodynamics in Higher Dimensional Chern-Simons Gravity". *Phys. Rev.* D75 (2007), p. 024008. arXiv: hep-th/0611260 [hep-th].

[135] N. V. Suryanarayana and M. C. Wapler. "Charges from Attractors". *Class. Quant. Grav.* 24 (2007), p. 5047. arXiv: 0704.0955 [hep-th].

[136] R. Meinel, M. Ansorg, A. Kleinwächter, G. Neugebauer, and D. Petroff. *Relativistic figures of equilibrium*. Cambridge University Press, 2008.

[137] R. P. Macedo and M. Ansorg. "Axisymmetric fully spectral code for hyperbolic equations". *J. Comput. Phys.* 276 (2014), p. 357. arXiv: 1402.7343 [physics.comp-ph].

[138] A. Jimenez-Alba and L. Melgar. "Anomalous Transport in Holographic Chiral Superfluids via Kubo Formulae". *JHEP* 10 (2014), p. 120. arXiv: 1404.2434 [hep-th].

[139] Y. Liu and F. Pena-Benitez. "Spatially modulated instabilities of holographic gauge-gravitational anomaly" (2016). arXiv: 1612.00470 [hep-th].

[140] S. Grozdanov, D. M. Hofman, and N. Iqbal. "Generalized global symmetries and dissipative magnetohydrodynamics" (2016). arXiv: 1610.07392 [hep-th].

[141] J. P. Boyd. *Chebyshev and Fourier Spectral Methods (Second Edition, Revised)*. New York: Dover Publications, 2001.

[142] C. Canuto, M. Hussaini, A. Quarteroni, and T. Zang. *Spectral Methods: Fundamentals in Single Domains*. Berlin: Springer, 2006.

[143] P. M. Chesler and L. G. Yaffe. "Numerical solution of gravitational dynamics in asymptotically anti-de Sitter spacetimes". *JHEP* 07 (2014), p. 086. arXiv: 1309.1439 [hep-th].

[144] O. J. C. Dias, J. E. Santos, and B. Way. "Numerical Methods for Finding Stationary Gravitational Solutions" (2015). arXiv: 1510.02804 [hep-th].

[145] M. Kalisch and M. Ansorg. "Highly Deformed Non-uniform Black Strings in Six Dimensions". In: *14th Marcel Grossmann Meeting*. 2015. arXiv: 1509.03083 [hep-th].

[146] M. Kalisch and M. Ansorg. "Pseudo-spectral construction of non-uniform black string solutions in five and six spacetime dimensions". *Class. Quant. Grav.* 33.21 (2016), p. 215005. arXiv: 1607.03099 [gr-qc].

[147] A. O. Starinets. "Quasinormal modes of near extremal black branes". *Phys. Rev.* D66 (2002), p. 124013. arXiv: hep-th/0207133 [hep-th].

[148] S. Janiszewski. "Perturbations of Moving Membranes in AdS_7". *JHEP* 09 (2012), p. 093. arXiv: 1112.0085 [hep-th].

C. Ehrenwörtliche Erklärung

Ich erkläre hiermit ehrenwörtlich, dass ich die vorliegende Arbeit selbstständig, ohne unzulässige Hilfe Dritter und ohne Benutzung anderer als der angegebenen Hilfsmittel und Literatur angefertig habe. Die aus anderen Quellen direkt oder indirekt übernommenen Daten und Konzepte sind unter Angabe der Quelle gekennzeichnet.

Bei der Auswahl und Auswertung des Materials haben mir die nachstehend aufgeführten Personen unentgeltlich geholfen:

1. J.Prof. Dr. Martin Ammon
2. Dr. Rodrigo P. Macedo (Publikation [82])
3. Prof. Dr. M. Kaminski, Dr. J. Wu, R. Koirala (Publikation [81])

Weitere Personen waren an der inhaltlich-materiellen Erstellung der vorliegenden Arbeit nicht beteiligt. Insbesondere habe ich hierfür nicht die entgeltliche Hilfe von Vermittlungs- bzw. Beratungsdiensten (Promotionsberater oder andere Personen) in Anspruch genommen. Niemand hat von mir unmittelbar oder mittelbar geldwerte Leistungen für Arbeiten erhalten, die im Zusammenhang mit dem Inhalt der vorgelegten Dissertation stehen.

Die Arbeit wurde bisher weder im In- noch im Ausland in gleicher oder ähnlicher Form einer anderen Prüfungsbehörde vorgelegt.

Die geltende Promotionsordnung der Physikalisch-Astronomischen Fakultät ist mir bekannt.

Ich versichere ehrenwörtlich, dass ich nach bestem Wissen die reine Wahrheit gesagt und nichts verschwiegen habe.

Ort, Datum Unterschrift d. Verfassers